

Preoperative diagnosis of mesial temporal lobe epilepsy subtypes
with in vivo MRI

by

Trevor Adam Steve

A thesis submitted in partial fulfillment of the requirements for the degree of

Doctor of Philosophy

in

EXPERIMENTAL MEDICINE

Department of Medicine
University of Alberta

© Trevor Adam Steve, 2018

Abstract

Approximately 50 million people worldwide suffer from epilepsy, a chronic neurological disorder characterized by recurrent seizures. While most patients with epilepsy will respond to anticonvulsant medications, approximately one third are found to have drug resistant epilepsy. Mesial temporal lobe epilepsy (MTLE) is the most common clinical syndrome associated with intractable seizures.

Pathological studies suggest that MTLE consists of multiple disease subtypes which have distinct clinical features and prognoses for surgical cure. However, MTLE subtypes currently can only be diagnosed postoperatively following surgical resection of the hippocampus. This method of characterizing MTLE subtypes has several limitations including incomplete evaluation of the symptomatic hippocampus, inability to assess the contralateral hippocampus, and analysis of subtypes at only one time point (the time of surgical resection). Therefore, our current understanding of MTLE subtypes remains incomplete. In vivo MRI holds the potential to improve our knowledge of MTLE subtypes by enabling preoperative diagnosis of these disease variants.

The human hippocampus consists of multiple discrete regions (termed 'subfields') which have different histological features, synaptic connectivities,

and putative functions. Several lines of evidence (including animal models and human neuropathology series) support the hypothesis that MTLE is a subfield-specific neurological disorder. While qualitative neuropathological studies suggest that MTLE is characterized by selective involvement of certain hippocampal subfields, it remains unclear whether quantifiable differences exist. We therefore conducted a systematic review and meta-analysis of the current literature in order to quantify subfield involvement in patients with MTLE. We found the greatest magnitude of neuronal loss in CA1 and relative sparing of the CA2 subfield, as suggested by the qualitative neuropathological literature.

MTLE subtypes are currently diagnosed on the basis of neuronal density measurements from specific hippocampal subfields (CA1 and CA4). Despite advances in MRI spatial resolution, neuronal densities cannot be directly measured with this modality. In vivo MRI studies therefore use hippocampal subfield volumes (or areas) as a surrogate marker for subregional densities. We therefore examined the relationship between neuronal densities and subfield areas in our cohort of cadaveric hippocampi. Interestingly, our analysis did not reveal any correlation between neuronal densities and histology-defined subfield areas in control subjects. While our results suggest a complex relationship between these two measurements in normal hippocampi, several

studies have demonstrated a positive correlation between neuronal densities and subfield areas in surgical specimens resected from patients with MTLE.

Recent work has demonstrated the feasibility of mapping histologically defined hippocampal subfields onto ex vivo MR Images, but this has only been described in a single subject. In this thesis, we sought to determine if histological measurements from multiple cadaveric hippocampi could be used to develop a histologically validated segmentation protocol for the hippocampal body. We hypothesized that subfield transitions occur at predictable locations as a proportion of an anatomical structure (the stratum lacunosum moleculare, SLM) which is readily visualized with in vivo MRI. We found that the CA1/CA2 and CA2/CA3 subfield transitions could be accurately localized by using the mean proportion of the SLM for these boundaries as measured from histology. These data were used to obtain ex vivo MRI measurements of subfield areas (CA1, CA2, and CA3/CA4/DG) which were strongly correlated with the 'ground truth' histological areas of these same subregions.

Our method is based on anatomical landmarks which are readily visible with in vivo MRI, which allowed us to directly translate this methodology to preoperative MR Images from patients with MTLE. We found that our method provided reliable hippocampal subfield measurements in healthy controls and subjects with MTLE. Hippocampal subfield volume measurements were then

used to determine MTLE subtypes, which were consistent with the gold standard neuropathological subtype diagnoses in three out of five cases. Furthermore, analysis of subfield areas revealed significant variability of MTLE subtypes along the hippocampal long axis in several patients, which is consistent with previous autopsy studies. These results collectively suggest that our novel method can be reliably applied to determine disease subtypes in subjects with MTLE.

In summary, our results support the hypothesis that MTLE subtypes can be accurately characterized with preoperative in vivo MRI. Further studies are required to explore the clinical correlates of these findings in a larger cohort of subjects and to evaluate the prognostic significance of these findings for patients with MTLE.

Preface

Chapter 7 of this thesis has been published as: *Steve, T. A., J. D. Jirsch, and D. W. Gross. 2014. 'Quantification of subfield pathology in hippocampal sclerosis: a systematic review and meta-analysis', *Epilepsy Res*, 108: 1279-85.*

I was responsible for the data collection and analysis as well as the manuscript composition. J.D. Jirsch provided useful guidance on the meta-analytic technique. D.W. Gross was the supervisory author and was involved with concept formation and manuscript composition. Sandy Campbell assisted with the search strategy and Ben Vandermeer assisted with conducting the meta-analyses.

Chapter 9 of this thesis has been published as: *Steve, T. A., C. L. Yasuda, R. Coras, M. Lail, I. Blumcke, D. J. Livy, N. Malykhin, and D. W. Gross. 2017. 'Development of a histologically validated segmentation protocol for the hippocampal body', *NeuroImage*, 157: 219-32.*

I was responsible for the data collection and analysis as well as the manuscript composition. C.L. Yasuda performed the anatomical resections of hippocampi from the cerebral hemispheres. R. Coras assisted with histological data acquisition and analysis. C.L. Yasuda and M. Lail assisted with inter-rater reliability experiments for histology and ex vivo MRI respectively. D.W. Gross was the supervisory author and was involved with concept formation and manuscript composition.

This thesis is an original work by Trevor Adam Steve. All figures were created by the Author. The work described in Chapter 9 received research ethics approval from the University of Alberta Research Ethics Board, Project

Name “Correlation of human ex vivo MRI with histology”, Pro00072245. The work described in Chapter 10 received research ethics approval from the University of Alberta Research Ethics Board, Project Name “High resolution imaging in epilepsy”, Pro00002937.

Dedication

This work is dedicated to my wife, Brynne Anderson, for her support and encouragement over the years. It is also dedicated to my children: Aria, Willem, and Isla - who are a constant source of joy and inspiration.

Acknowledgements

I would like to thank my supervisor, Don Gross, for his mentorship over the last several years. This work has been the beneficiary of his superb vision for our projects, meticulous approach to our experiments, and extensive comments on our manuscripts. I appreciate his focus on developing the independence of his research trainees. My approach to scientific problems, data analysis, and manuscript composition has improved under his guidance. I look forward to benefiting from his expertise in future collaborative work.

I am thankful to Jack Jhamandas for being a tremendous advocate for my career development. His altruistic support was crucial to the eventual completion of this work. I would also like to thank Doug Zochodne for his career guidance and support, which was likewise essential to the completion of my thesis.

I am grateful for the guidance of my supervisory committee. Dan Livy provided very useful advice regarding the cadaveric hippocampi and histological methods. I am grateful for Nikolai Malykhin, who provided essential critiques on the development of our histology-derived hippocampal subfield segmentation method. I am also thankful for my arms-length examiners, Clayton Dickson and Richard Camicioli, for their helpful questions and comments. I also wish to thank Christian Beaulieu for his helpful comments on many aspects of this work.

A number of individuals at the University of Alberta made this work possible. Jason Papirny and Hugh Barrett from the Anatomical Gifts Program provided assistance with the cadaveric hippocampal specimens. Peter Seres, in particular, was crucial to the success of the project. He provided essential

guidance on imaging of the ex vivo hippocampi and also performed the in vivo scanning.

I am grateful for the funding which made this work possible. The research program was funded by an operating grant held by Don Gross from the Canadian Institutes of Health Research (funding reference number 81083). I was supported by a post-graduate fellowship award from Eisai and the Canadian League Against Epilepsy (CLAE).

I had the pleasure of meeting a number of great people while completing this work. Clarissa Yasuda was a major help with our cadaveric hippocampi, by performing excellent anatomical resections. Roland Coras from the University of Erlangen was instrumental by performing the histological segmentations of the hippocampal specimens. Laura Schmitt provided histopathological classification of HS subtypes and corresponding photomicrographs for our in vivo study. Many thanks to Yasmeen El-Hajj Abdallah, who performed in vivo segmentations of several subjects for this project as well. Ingmar Blumcke from the University of Erlangen was very kind to allow me to work in his laboratory in June 2013. I am also grateful to Tom Nowacki and Cam Elliott for their help with this project over the years.

I am thankful to my parents for always encouraging me to work hard and do my best. They have always been my greatest advocates.

Finally, I wish to express my deep gratitude to my wife and children. They were a major source of inspiration as I completed this work. Thanks so much for your love and support.

Table of Contents

<i>I Introduction</i>	1
Chapter 1 Justification	2
1.1 Background	2
1.2 Hypothesis.....	2
1.3 Research questions	3
1.4 Outline.....	3
Chapter 2 Epileptic activity and the mesial temporal lobe	5
2.1 Gross anatomy.....	5
2.2 Hippocampal cytoarchitecture	8
2.3 Hippocampal connectivity	14
2.4 Epileptic activity	15
Chapter 3 Epilepsy and mesial temporal lobe epilepsy	25
3.1 Definitions.....	25
3.2 Mesial temporal lobe epilepsy	31
3.3 Pathology of MTLE	34
3.4 Etiology of MTLE.....	43
3.5 Clinical aspects.....	49
Chapter 4 Mesial temporal lobe epilepsy subtypes	54
4.1 Pathological characteristics	54
4.2 Prevalence	56
4.3 Clinical features	57
4.4 Limitations of surgical series	65
4.5 Rationale for in vivo diagnosis	68

Chapter 5 In vivo MRI of MTLE	70
5.1 Hippocampal subfield imaging	70
5.2 Manual hippocampal subfield volumetry.....	71
5.3 Automated hippocampal subfield volumetry	74
5.4 Findings in MTLE patients with No HS	75
5.5 Relationship to memory dysfunction	77
5.6 Histological correlates of MRI findings.....	78
5.7 Preoperative diagnosis of MTLE subtypes	79
Chapter 6 Ex vivo MRI	80
6.1 Microscopic anatomy	80
6.2 Methodology	84
6.3 Ex vivo MRI in MTLE.....	88
6.4 Summary	89
<i>II Experiments</i>	90
Chapter 7 Neuronal densities in MTLE	91
7.1 Introduction.....	93
7.2 Methods.....	94
7.3 Results.....	96
7.4 Discussion	102
7.5 Conclusions.....	104
Chapter 8 Neuronal density and subfield areas	105
8.1 Introduction.....	106
8.2 Materials and Methods	107
8.3 Results.....	111
8.4 Discussion	113

8.5	Conclusions.....	116
8.6	Supplementary Methods.....	116
Chapter 9 Histology-derived segmentation of ex vivo MRI118		
9.1	Introduction.....	121
9.2	Materials and Methods.....	123
9.3	Results.....	135
9.4	Discussion.....	146
9.5	Conclusions.....	151
9.6	Appendix.....	153
Chapter 10 In vivo diagnosis of MTLE subtypes164		
10.1	Introduction.....	166
10.2	Materials and Methods.....	168
10.3	Results.....	176
10.4	Discussion.....	185
10.5	Conclusions.....	190
<i>III Discussion..... 191</i>		
Chapter 11 Conclusion.....192		
11.1	Neuronal densities in MTLE (Chapter 7).....	192
11.2	Neuronal density and subfield areas (Chapter 8).....	193
11.3	Histology-derived segmentation of ex vivo MRI (Chapter 9).....	194
11.4	In vivo diagnosis of MTLE subtypes (Chapter 10).....	196
Chapter 12 Limitations.....198		

List of Tables

Table 7.1 - Characteristics of included studies	98
Table 8.1 - Previous studies	114
Table 9.1 - Accuracy of novel method versus previous techniques.....	141
Table 9.2 - Intra- and inter-rater reliability of hippocampal subfield areas	146
Table 9.3 - Accuracy of novel method versus Technique 3.....	159
Table 10.1 - Intra-rater reliability in controls.....	177
Table 10.2 - Intra-rater reliability in hippocampal sclerosis	178

List of Figures

Figure 2.1 - The collateral sulcus.....	6
Figure 2.2 - The parahippocampal gyrus	7
Figure 2.3 - Anatomy of the hippocampal body	9
Figure 2.4 - Delineation of the subiculum/CA1 boundary.....	10
Figure 2.5 - Cytoarchitectonic definition of the CA1/CA2 boundary	11
Figure 2.6 - Distinguishing between areas CA2 and CA3	12
Figure 2.7 - Hippocampal subfields of the end folium	13
Figure 2.8 - Granule cell dispersion.....	21
Figure 3.1 - The surface electroencephalogram (EEG)	28
Figure 3.2 - MRI in the evaluation of a single seizure.....	30
Figure 3.3 - Pathology of hippocampal sclerosis	37
Figure 3.4 - Temporal neocortical low-grade tumor causing epilepsy	39
Figure 3.5 - MRI of focal cortical dysplasia (FCD).....	41
Figure 3.6 - Cavernous angioma	42
Figure 3.7 - Depth electrode implantation	51
Figure 3.8 - Hippocampal sclerosis on MRI	52
Figure 4.1 - Bilateral hippocampal sclerosis.....	66
Figure 7.1 - Literature search and study selection flow diagram.....	97
Figure 7.2 - Neuronal cell counts in hippocampal sclerosis versus control.....	100
Figure 7.3 - Subfield-specific neuronal loss in hippocampal sclerosis.....	101
Figure 8.1 - Cytoarchitectural definitions of subfield boundaries	108
Figure 8.2 - Measurement of hippocampal subfield areas	110
Figure 8.3 - Estimation of neuronal densities in hippocampal subfields	111
Figure 8.4 - Comparison of neuronal densities and subfield areas	112

Figure 9.1 - Histology measurements of subfield boundaries and areas	125
Figure 9.2 - Subfield boundaries according to the novel method	127
Figure 9.3 - Subfield boundaries according to Technique 1	129
Figure 9.4 - Subfield boundaries according to Technique 2	130
Figure 9.5 - Coregistration of ex vivo MRI with histology	131
Figure 9.6 - Subfield area measurements	133
Figure 9.7 - Descriptive statistics.....	136
Figure 9.8 - Segmentation according to the novel method	137
Figure 9.9 - Accuracy of novel method versus previous techniques	138
Figure 9.10 - Histological measurement of subfield boundary distances	140
Figure 9.11 - Direct measurements along the longitudinal axis	142
Figure 9.12 - Effect of hippocampus on direct measurements.....	143
Figure 9.13 - Effect of hippocampus deletion on direct measurements.....	143
Figure 9.14 - Histological and MRI measurements	145
Figure 9.15 - Subfield boundaries according to Technique 3	156
Figure 9.16 - Accuracy of novel method versus Technique 3	158
Figure 9.17 - Histological measures with novel method and Technique 3	160
Figure 9.18 - Subiculum/CA1 boundaries measured in reverse direction.	162
Figure 10.1 - Delineation of the hippocampal body from the head and tail	170
Figure 10.2 - Segmentation of hippocampal subfields using in vivo MRI	171
Figure 10.3 - Hippocampal subfield measurements.....	173
Figure 10.4 - Subtype atrophy patterns along the hippocampal long axis	175
Figure 10.5 - Subfield-specific volume loss in patients with HS.....	180
Figure 10.6 - Assessment of HS subtypes along the hippocampal long axis...181	
Figure 10.7 - Histopathologic classification of ILAE HS subtypes.....	184

I Introduction

Chapter 1 Justification

1.1 Background

Approximately 50 million people worldwide have epilepsy, making it one of the most common neurological disorders (1). In addition, nearly one third of patients with epilepsy do not respond to current anticonvulsant medications (2). Mesial temporal lobe epilepsy (MTLE) is the most common form of drug resistant epilepsy (3). Four distinct subtypes of MTLE have been described in the literature (4). However, MTLE subtypes currently can only be diagnosed pathologically following surgical resection of brain tissue (5). As a result, our current understanding of MTLE subtypes (in terms of etiology, clinical features, and likelihood of surgical cure) remains incomplete (5). Preoperative diagnosis could potentially improve our knowledge of MTLE subtypes and inform the management of patients with MTLE (4, 6, 7).

MTLE subtypes are diagnosed by measuring *neuronal densities* in hippocampal subfields (4, 8). Recent studies have shown that hippocampal subfield *volumes and areas* can be measured in subjects with MTLE using in vivo magnetic resonance imaging (MRI) (9, 10)

1.2 Hypothesis

These studies led us to hypothesize that:

MTLE subtypes can be diagnosed preoperatively with in vivo MRI

1.3 Research questions

In order to test our hypothesis, this thesis will address the following research questions:

- 1) Is specific hippocampal subfield involvement in subjects with MTLE *quantifiable* by measurement of *neuronal densities*? (Chapter 7)
- 2) Are hippocampal subfield *areas* correlated with *neuronal densities* in histological specimens from normal control subjects? (Chapter 8)
- 3) Can subfield *areas* be accurately measured using a histology-derived segmentation protocol applied to *ex vivo MRI*? (Chapter 9)
- 4) Can hippocampal subfield *volume and area* measurements be used to diagnose *MTLE subtypes* with *in vivo MRI*? (Chapter 10)

1.4 Outline

This thesis is organized as follows. The introductory chapters (part I) provide the necessary background information and discuss the previous literature which motivated our experimental work. Chapter 2 provides an introduction to the mesial temporal lobe including gross anatomy, cytoarchitecture and connectivity. In addition, chapter 2 describes the potential mechanisms by which the mesial temporal lobe could generate epileptic activity. Chapter 3 provides an introduction to epilepsy including important definitions, clinical features, and principles of management. Chapter 3 concludes with an overview of MTLE including seizure semiology, pathological features, and potential etiologies. Chapter 4 reviews our current understanding of MTLE subtypes based on clinico-pathologic studies performed to date. Chapter 5 provides a

review of previous *in vivo* MRI studies of hippocampal subfields in subjects with MTLE. The introduction concludes with chapter 6, which describes recent developments in *ex vivo* MRI of the human mesial temporal lobe.

Chapters 7-10 form part II of this thesis, which describes the methodology and results of our experimental work addressing the research questions defined above. Finally, part III provides a summary of the scientific contributions (chapter 11) and limitations (chapter 12) of the experimental work with respect to our hypothesis.

Chapter 2 Epileptic activity and the mesial temporal lobe

Mesial temporal lobe epilepsy is the most common syndrome associated with drug resistant epilepsy (3). Indeed, the mesial temporal lobe (MTL) is predisposed to generate seizures due to its unique anatomy and physiology. In this chapter, we first review the gross anatomy of the MTL and define its constituent parts including the hippocampus. We then discuss the cytoarchitecture of the hippocampus with particular emphasis on the histological definitions of hippocampal subfields. The intra-hippocampal neuronal pathways and connections of the hippocampus with other brain regions are then reviewed. Finally, the presence of intrinsic pacemaker cells and abundant excitatory connectivity is used to explain the propensity of the MTL to generate epileptic activity.

2.1 Gross anatomy

A human cerebral hemisphere consists of four lobes: the frontal, parietal, occipital, and temporal lobes. The sylvian fissure divides each cerebral hemisphere into the frontal lobe (superiorly) and the temporal lobe (inferiorly). The temporal lobe consists of several distinct parts which are recognized by gross anatomical landmarks. First, on the lateral surface of the temporal lobe three large gyri (the superior, middle, and inferior temporal gyri) can be recognized. These are separated from each other by the superior and middle temporal sulci. The inferior temporal sulcus separates the inferior temporal gyrus from the fusiform (occipitotemporal) gyri located on the ventral surface.

The collateral sulcus (1, Figure 2.1) is a major anatomical landmark of the MTL. This large sulcus runs along the ventral surface of the brain, demarcating the parahippocampal gyrus (located mesial to the collateral sulcus - 2, Figure 2.1) from the fusiform gyrus (located lateral to the collateral sulcus). The parahippocampal gyrus extends along the mesial surface of the inferior temporal lobe and demonstrates a mesial enlargement at its anterior tip, which is called the uncus. Furthermore, the entorhinal cortex is identified grossly in the rostral portion of the parahippocampal gyrus by the presence of "verrucae (latin for warts)" (11). These veruccae correspond to "cell islands" identified upon histological examination of the entorhinal cortex (12).

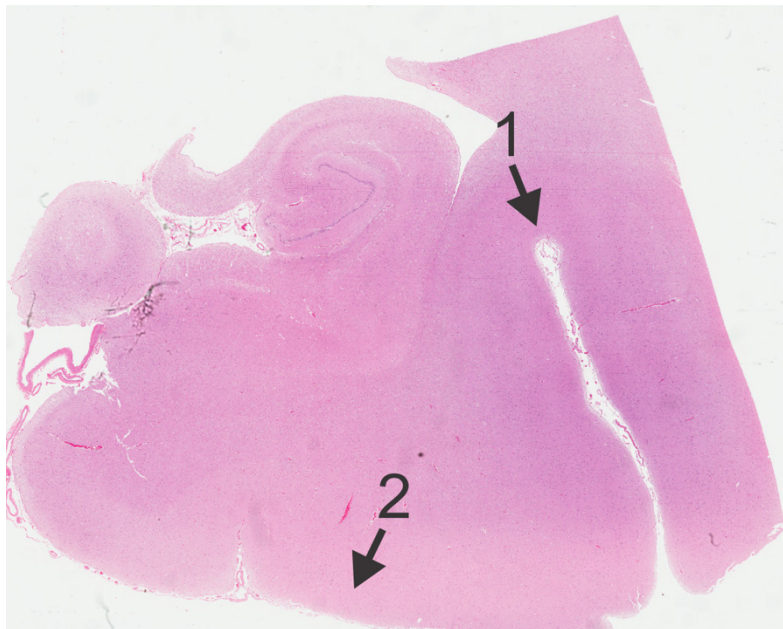


Figure 2.1 - The collateral sulcus

A histological specimen is shown from an autopsy-derived hippocampus. The collateral sulcus (1) is readily identified on the ventral aspect of the mesial temporal lobe. This deep sulcus forms the lateral border of the parahippocampal gyrus (2).

The cortical mantle of the parahippocampal gyrus (1, Figure 2.2), viewed in the coronal plane, begins at the collateral sulcus (2, Figure 2.2). It runs mesially along the tentorium cerebelli (3, Figure 2.2) and reaches its mesial extreme in the ambient cistern (4, Figure 2.2). The cortical mantle then curves laterally and is contiguous with the hippocampus (5, Figure 2.2) (13).

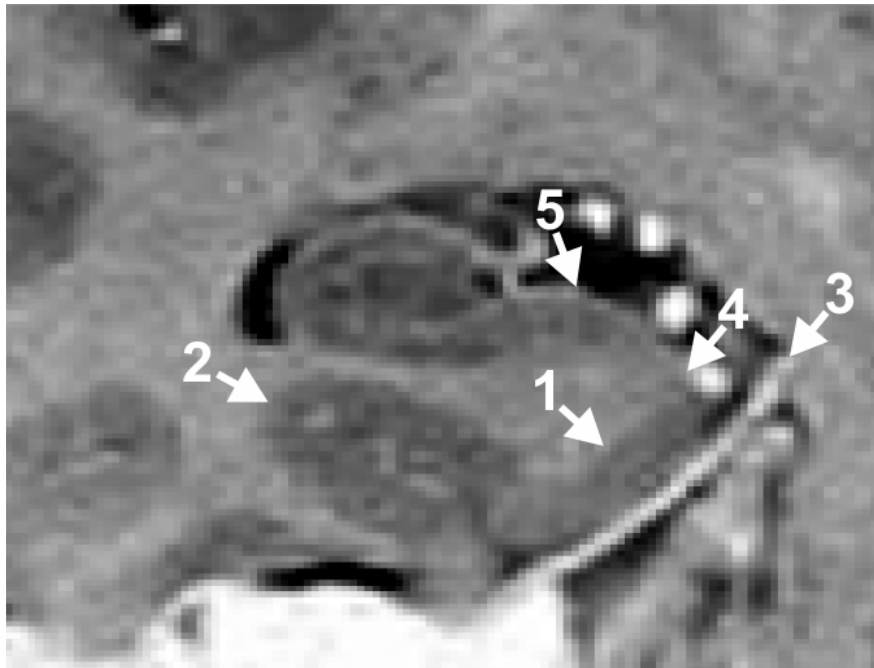


Figure 2.2 - The parahippocampal gyrus

The parahippocampal gyrus (1) is bounded laterally by the collateral sulcus (2). The cortical mantle runs along the surface of the tentorium cerebelli (3) to occupy the mesial aspect of the ambient cistern (4). The parahippocampal gyrus then turns laterally (5) and becomes contiguous with the hippocampus.

The hippocampus (from the greek "hippos" = horse; "kampos" = sea monster) occupies the floor of the inferior (temporal) horn of the lateral ventricle and demonstrates remarkable anatomical variability along its

longitudinal axis (11). The hippocampal head is the most anterior portion of the hippocampus. In the hippocampal head, the cortical mantle demonstrates remarkable complexity with the presence of internal digitations between regions of hippocampal neurons.

In comparison with the hippocampal head, the anatomical organization of the hippocampal body is more uniform. The hippocampal body consists of one cortical layer (the cornu ammonis/ammon's horn) "rolled up" on another (the dentate gyrus [DG]), to form a "swiss roll" shape (Figure 2.3) (13). As a result, most of the dentate gyrus is not visible when the hippocampus is viewed externally. However, small indentations created by the dentate gyrus (the margo denticularis) are visible on the mesial surface of the hippocampus. The margo denticularis is bounded superiorly by a conspicuous white matter structure on the external surface of the hippocampal body, which is called the fimbria. In the hippocampal tail, the fimbria becomes larger and detaches from the hippocampus to become the fornix (13).

2.2 Hippocampal cytoarchitecture

As described above, hippocampal cytoarchitecture is more uniform in the hippocampal body in comparison to the head and tail. Therefore, the description of hippocampal layers which follows reflects the organization of the structure in the hippocampal body. Several distinct layers can be identified upon histological examination of coronal sections at this level. The alveus is the outermost layer and is composed of efferent axons from hippocampal and subicular neurons. The next layer encountered, deep to the alveus, is stratum oriens which contains gamma amino butyric acid (GABA)-ergic inhibitory interneurons, called basket cells (13).

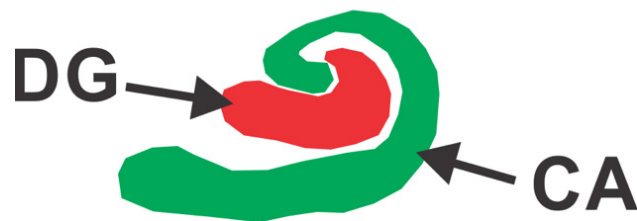
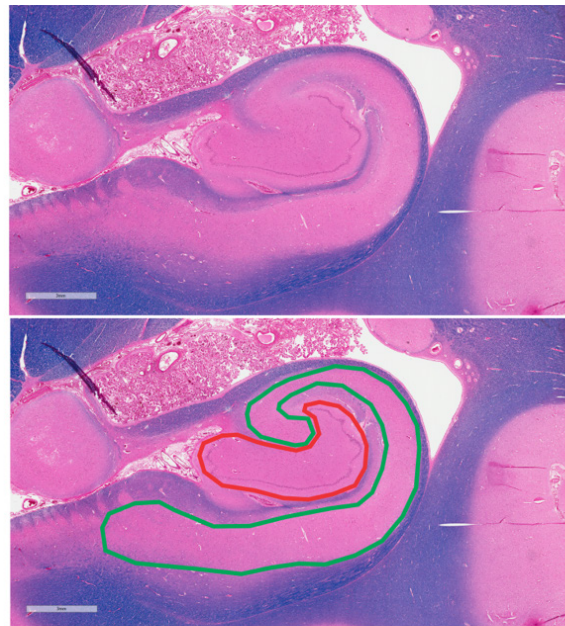


Figure 2.3 - Anatomy of the hippocampal body

A histological section is stained with hematoxylin and eosin (H&E) and luxol fast blue (LFB) to demonstrate the two subdivisions of the hippocampal body:
1) the cornu ammonis (CA, green); and 2) the dentate gyrus (DG, red)

Stratum pyramidale, located deep to stratum oriens, is composed of pyramidal neurons and the cytoarchitectural characteristics of this layer are used to delineate hippocampal subfields (14). The subiculum and CA1 fields are distinguished from each other by two criteria. First, the subiculum demonstrates a broad molecular layer, which thins significantly in CA1. Secondly, the subiculum is marked by myelinated fibers of the perforant path

(described below), which traverse the subiculum on the way to the DG. The absence of myelinated fibers in CA1 therefore provides a second mechanism to distinguish this field from the subiculum (Figure 2.4).

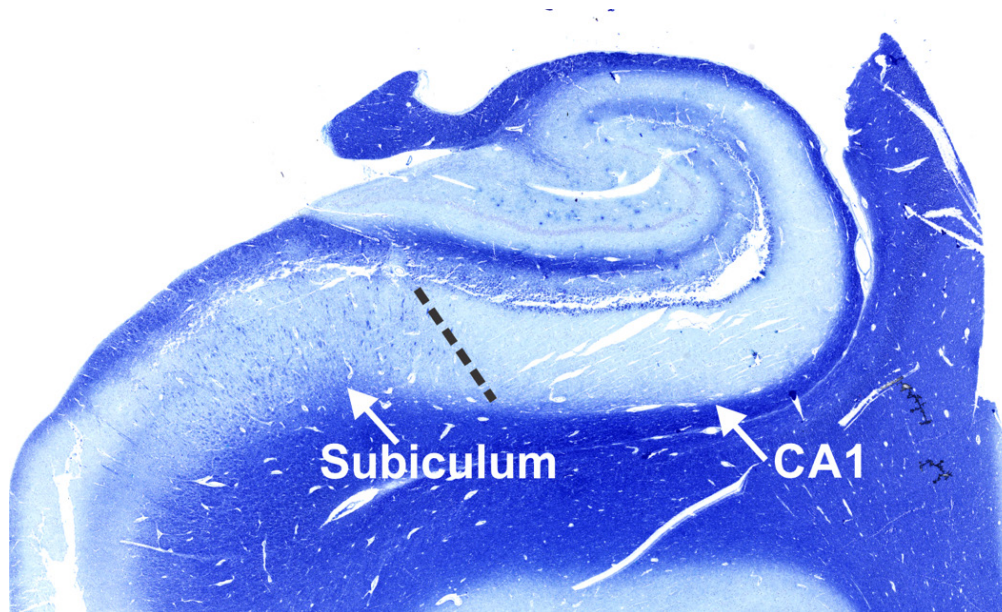


Figure 2.4 - Delineation of the subiculum/CA1 boundary

Cresyl violet / luxol fast blue staining enables clear differentiation of the subiculum from CA1. The subiculum demonstrates dense staining with luxol fast blue due to the presence of myelinated perforant pathway fibers. In contrast, CA1 does not contain these myelinated fibers of the perforant path and thus does not stain with luxol fast blue. This enables the boundary between these subfields (black line) to be readily identified.

CA1 can be distinguished from CA2 according to characteristics of the pyramidal cell layer (Figure 2.5). In comparison to CA1, CA2 neurons are: a) larger, b) more ovoid, and c) arranged in a more organized fashion (12) (Figure 2.5).

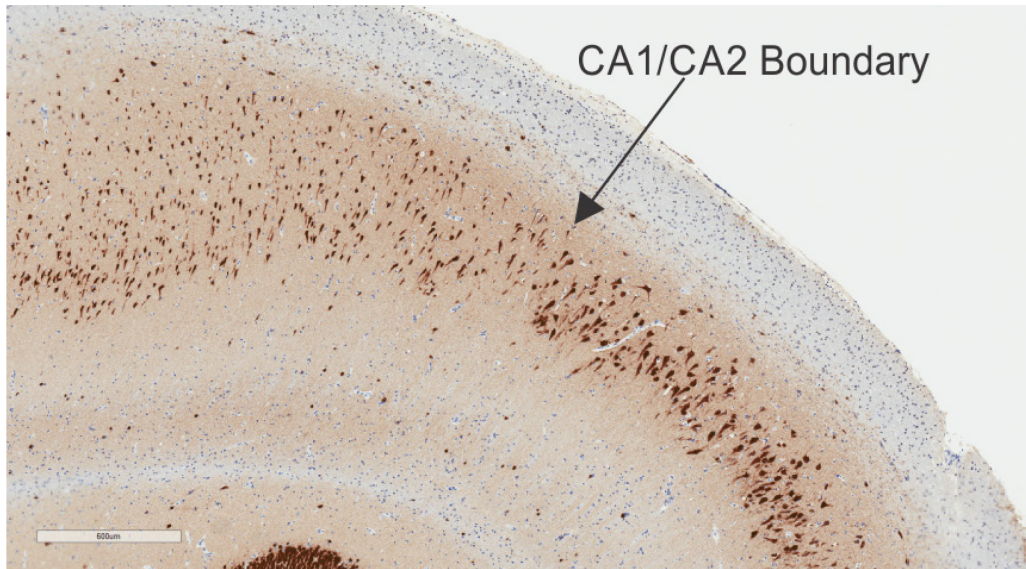


Figure 2.5 - Cytoarchitectonic definition of the CA1/CA2 boundary

The CA1/CA2 boundary is made clear with neuronal nuclear antigen (NeuN) staining. This stain highlights the dramatic increase in the packing density of neurons in CA2 in comparison to the CA1 subregion.

The CA3 subfield is contiguous with CA2, and curves inferiorly to enter the dentate gyrus. However, the cell layer of CA3 is broader in comparison with that of CA2. This feature is highlighted by NeuN staining, which demonstrates that the pyramidal cell layer broadens significantly in area CA3 in comparison to CA2 (Figure 2.6).

The CA3 and CA4 fields are both located within the concavity of the DG, which is also known as the "end folium" (15). However, CA3 neurons demonstrate an identifiable lamination pattern as cells in this field are arranged in a well-defined pyramidal cell layer. In contrast, no lamination is present in CA4 as neurons in this field are dispersed randomly throughout the end folium (Figure 2.7) (12).

Finally, the CA4 region is separated from the granule cell layer (GCL) by a hypocellular region termed the polymorphic layer (PM, Figure 2.7) (13). The GCL (Figure 2.7) is marked by numerous small granule cells and is therefore clearly distinguished from the other cellular layers of the DG (Figure 2.7) (13).

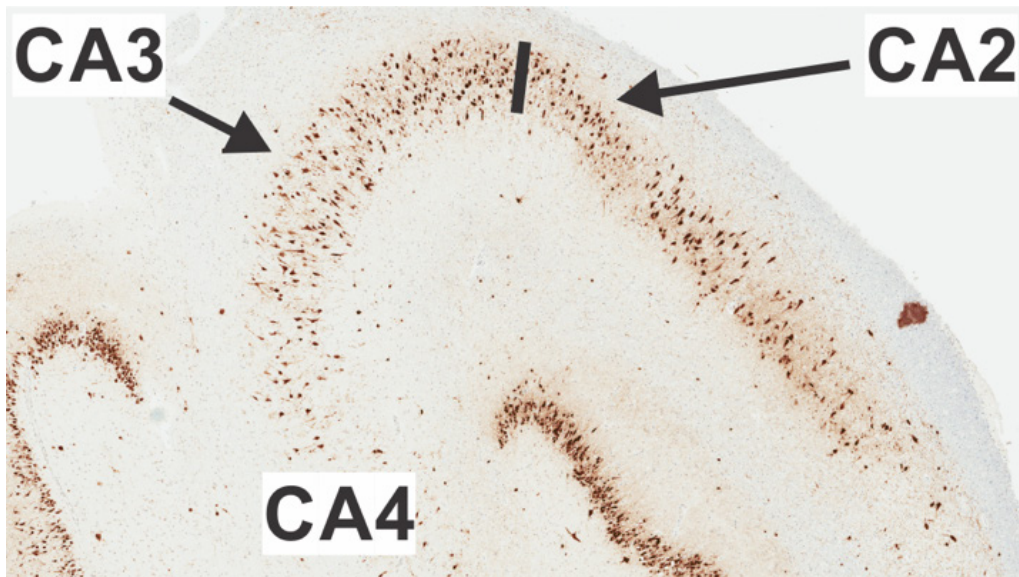


Figure 2.6 - Distinguishing between areas CA2 and CA3

NeuN staining of a hippocampal biopsy specimen resected from a patient with epilepsy. Area CA3 demonstrates a broader cell layer and reduced packing density in comparison to CA2.

Stratum radiatum is located deep to stratum pyramidale and is marked by the apical dendrites of pyramidal neurons (13). In stratum radiatum, these apical dendrites receive input from other brain regions - including the septal nuclei (13). In particular, Schaffer collaterals (described below) make connections with the apical dendrites of CA1 neurons in the stratum radiatum (13). The axons of Schaffer collaterals, however, are located deep to stratum

radiatum - in stratum lacunosum. In addition to Schaffer collaterals, stratum lacunosum also contains the fibers of the perforant path (described below) connecting the entorhinal cortex to the DG. Stratum lucidum is contiguous with stratum radiatum and consists of mossy fiber axons (described below) connecting the DG and CA3. Finally, the deepest layer of the cornu ammonis, stratum moleculare, is contiguous with the DG at the vestigial hippocampal sulcus (13).

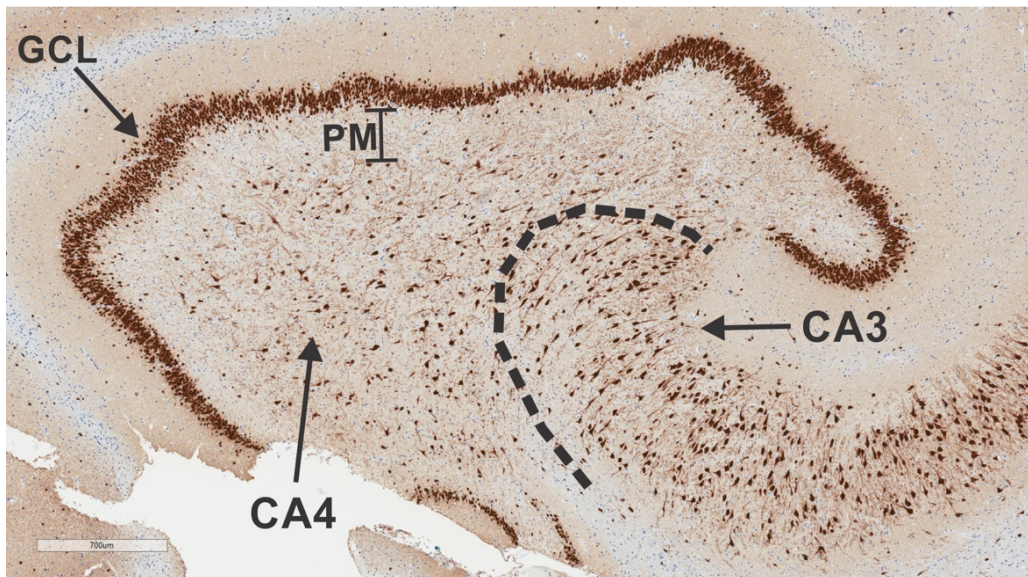


Figure 2.7 - Hippocampal subfields of the end folium

NeuN staining reveals several distinct histological subregions in the end folium.

The CA3/CA4 boundary (dashed line) represents a transition from the clear lamination identified in CA3 to the absence of any lamination in CA4. CA4 is separated from the granule cell layer (GCL) by a hypocellular region known as the polymorphic layer (PM). Finally, the GCL is readily identified by the presence of numerous granule cells organized in a narrow cellular layer with high packing density.

2.3 Hippocampal connectivity

The connectivity of the hippocampus is characterized by multiple excitatory loops. Firstly, the intra-hippocampal pathways described below provide amplification of synaptic inputs arising from the entorhinal cortex. Secondly, dense excitatory connections between hippocampal segments allow for summation of information along the longitudinal axis of the hippocampus (16). Finally, the hippocampus is extensively connected with other brain regions. These features allow the hippocampus to play a critical role in learning and memory (17). However, as described below, they also likely explain the frequent involvement of the hippocampus in drug resistant epilepsy (18).

The *perforant pathway* originates from pyramidal neurons in layer II of the entorhinal cortex (13). Axons from these neurons then traverse (perforate) the subiculum, but do not synapse here. Instead, these axons continue to the DG - where they make excitatory connections with the granule cells of the DG. Axons from the DG granule cells, termed mossy fibers, then run in stratum lucidum to make excitatory synapses on CA3 neurons. In addition, some axons of the perforant path bypass the DG and synapse directly in CA3 (13). The primary output of CA3 neurons are recurrent collateral fibers, called Schaffer collaterals, which run in stratum lacunosum and terminate in the stratum radiatum layer of area CA1. The *temporo-ammonic pathway* represents a second mechanism for information to enter the hippocampus. This pathway originates from cells in layer III of the entorhinal cortex (13). These neurons send axons directly to CA1, bypassing the multiple connections described above. Information from both the *perforant and temporo-ammonic pathways* thus reaches CA1, which then innervates the subiculum (13). Area CA1 and

the subiculum both send axons back to the entorhinal cortex, thus creating a closed loop system of neuronal connectivity within the hippocampus (13).

The connections between the hippocampus and brain structures outside of the MTL were initially described by Papez (13). The parahippocampal gyrus provides excitatory input to the entorhinal cortex, and information then passes through the hippocampus, as described above, terminating in the subiculum. The subiculum is the primary output region of the hippocampal formation. Axons from the subiculum enter the alveus and later become the fimbria-fornix. The fornix then ascends superiorly from the hippocampus and runs anteriorly below the corpus callosum, eventually reaching the mammillary bodies. Information then flows from the mammillary bodies to the thalamus (via the mammillo-thalamic tract), from the thalamus to the cingulate gyrus (via the internal capsule), and from the cingulate gyrus back to the parahippocampal gyrus (via the cingulum). Thus, the hippocampus communicates with diverse brain regions via well-characterized reciprocal connections (13). These pathways demonstrate bilateral abnormalities in patients with epilepsy (19) and may contribute to disruption of brain networks in such patients (20).

2.4 Epileptic activity

The propensity of the MTL to generate epileptic activity has been extensively studied in animal models. In this section, we first describe the unique physiological characteristics which have been documented for specific neuronal cell types in the MTL, and their potential relevance to epilepsy. Secondly, we introduce two established animal models of epilepsy and highlight key findings of these models in relation to the MTL. Third, we discuss anatomical changes of the MTL which have been demonstrated in experimental epilepsy models

and review their hypothetical relationship to human epilepsy. Finally, we consider how dysfunction of the MTL neuronal circuitry may contribute to the development of epilepsy.

Physiological properties of MTL neurons

The intrinsic properties of neurons in area CA3 and CA1 have been implicated in the generation of epileptic activity from the MTL (21). In contrast, granule cells of the DG are thought to inhibit propagation of excitatory activity in the healthy human hippocampus (22). In this subsection, we review the experimental evidence suggesting different physiological characteristics of neurons in specific hippocampal subfields.

Area CA3 CA3 neurons are intrinsically capable of generating bursts of electrical activity (23), which is generated at the proximal dendrites of these cells (24). As described above, CA3 makes extensive connections with CA1 via Schaffer collaterals. In addition, both CA3 and CA1 neurons make excitatory synapses with adjacent hippocampal neurons along the long axis of the hippocampal formation (16). A given CA3 neuron is therefore capable of exciting a large number of inter-connected cells throughout the hippocampus. It has been shown that burst firing in CA3 neurons causes similar activity in adjacent pyramidal cells (25). These characteristics likely allow the CA3 region to participate in memory retrieval based on partial cues (26-29). This function is termed "pattern completion" and is critical to normal human memory and learning (30). However, the physiology of CA3 neurons also imply that this region is capable of acting as a "pacemaker" for the potential generation of seizure activity (21).

Area CA1 CA1 pyramidal cells have also been shown to exhibit spontaneous burst firing in hippocampal slice preparations (21). However, in contrast to CA3 where burst firing is a ubiquitous finding (23), only a small subset of CA1 neurons demonstrate the potential for intrinsic burst firing (21). In addition, the burst firing of CA1 neurons is strongly dependent on extracellular calcium concentrations (31). Reduction of extracellular calcium is associated with induction of bursting activity, while increased extracellular calcium suppresses burst activity (31). Furthermore, bursting activity can be induced by pharmacological blockade of GABA-mediated inhibition (32). These findings suggest that physiological changes in the hippocampus (e.g. reduction of extracellular calcium or loss of GABA-mediated inhibition) could potentially result in excessive neuronal activity characteristic of epilepsy.

Granule cells of DG In contrast to CA3 and CA1 neurons, DG granule cells appear to act as a "brake" on excitatory activity in the hippocampus (21). DG granule cells are tonically inhibited by multiple GABA-ergic interneurons (22). These inhibitory interneurons receive strong input from the perforant pathway (33). As a result, perforant pathway stimulation activates only a very small percentage (< 5%) of DG granule cells (34). In addition, the DG granule cells transmit only a very small proportion of afferent information to area CA3 under control conditions. These characteristics are consistent with the potential role of the DG in pattern separation suggested by computational models (30) and animal studies (26). In addition, the term "dentate gate" has been used to denote a putative protective effect of the DG against excessive hippocampal excitation (33). As described below, loss of this "dentate gate" represents a potential explanation for the generation of spontaneous seizures in the hippocampus under pathological conditions.

Animal models of epilepsy

Animal models have demonstrated that seizures can result in morphological changes in the MTL. These anatomical changes are postulated to alter the neurophysiological characteristics of the MTL described above, potentially resulting in the neuronal circuit dysfunction described in subsequent sections. In this subsection, we review the documented changes in MTL microstructure observed in animal models of epilepsy.

Kindling Repetitive (tetanic), low intensity, electrical stimulation of the hippocampus results in after-discharges but not seizures (35). Repetition of tetanic stimulation, however, results in progressively longer after-discharges. Eventually, spontaneous seizures are seen in the absence of electrical stimulation (35). This phenomenon is known as kindling, and the kindling model is one of the most widely studied experimental models of epilepsy (21). In rats, kindling has been shown to result in anatomical changes in the hippocampus. In one study, application of perforant pathway stimulation resulted in subfield-specific neuronal loss in the hippocampus (36). Interestingly, the extent and degree of hippocampal damage varied according to the number of seizures induced. Neuronal loss was demonstrated in CA1 and CA4 after only 3 seizures, but the magnitude of neuronal loss in these regions increased with a greater number of seizures. Furthermore, neuronal loss in CA3 and the entorhinal cortex could be identified after 30 seizures. However, 150 seizures were required to cause neuronal loss in the granule cell layer of DG and CA2 (36). These findings suggest that distinct hippocampal subpopulations have different susceptibilities to the excitotoxic effects of seizures.

In addition to neuronal necrosis mediated by excitotoxicity, kindling results in several other morphological alterations in the rat hippocampus. Dentate gyrus granule cells demonstrate both apoptotic cell death and neurogenesis in response to kindling (37). These findings support the hypothesis that repetitive seizures result in changes to hippocampal microstructure, which might contribute to further epileptic seizures.

Kainic acid model Kainic acid, a glutamate agonist, produces repetitive limbic seizures when administered parenterally to rats (38). The hippocampus is prominently affected in kainic acid-induced limbic status epilepticus, demonstrating early electrographic evidence of epileptiform activity. This activity results in neuronal damage in area CA3, which is strongly correlated with the severity of electrographic abnormalities in the hippocampus. This neuronal loss occurs in the absence of hemodynamic compromise or generalized convulsions, suggesting that recurrent limbic seizures may cause excitotoxic cell death (38).

Anatomical changes in the MTL in experimental epilepsy

In animal models, recurrent seizures result in a number of microstructural alterations in addition to the neuronal loss described above. Several of these MTL anatomical changes have also been documented in human subjects with chronic epilepsy. Collectively, these changes could theoretically result in excessive excitability of the MTL in human epilepsy. In addition to being susceptible to seizure-induced damage, these findings provide physiological support for a role of the MTL as a potential source of ongoing seizure activity (39).

Granule cell dispersion In rats, experimental seizures result in several changes in the granule cell layer of the DG (21). The subgranular zone of the DG is a known site of neurogenesis under normal conditions (40). In response to seizures, however, there is a dramatic increase in the number of new neurons generated in the rat DG (41). As discussed above, the DG granule cells are typically considered as a "brake" to excessive excitatory activity in the hippocampus (33). Therefore, the increased proliferation of granule cells could be considered a compensatory response to recurrent seizures. However, animal models suggest that new granule cells generated following seizures are structurally and functionally abnormal. Two important abnormalities identified in DG granule cells induced by seizures include the formation of aberrant connections (see mossy fiber sprouting discussed below) and migration to ectopic locations (41). This latter phenomenon, characterized by disorganized ectopic neurons in the molecular layer of the DG and broadening of the granule cell layer of the DG, is termed granule cell dispersion (21).

Granule cell dispersion has also been identified in human subjects with chronic epilepsy (Figure 2.8) (42). This finding consists of a pathologically widened granule cell layer (2, Figure 2.8) and is often accompanied by the presence of ectopic granule cell neurons (3, Figure 2.8). In patients with epilepsy, a subset of these granule cells have been shown to remain electrophysiologically normal (43). However, the majority of granule cells from subjects with epilepsy are hyperexcitable (43) which could contribute to epileptic seizures in these patients. As discussed above, the DG receives strong tonic inhibition from multiple GABA-ergic inhibitory interneurons (22). In human subjects with epilepsy, however, these inhibitory interneurons demonstrate abnormal morphology, distribution, and synaptic connections (44). These findings could, again, be considered a compensatory response to

excessive hippocampal excitation. Loss of the normal inhibition of DG granule cells, however, could also result in loss of the normal "dentate gate" to hippocampal excitation (discussed further below).

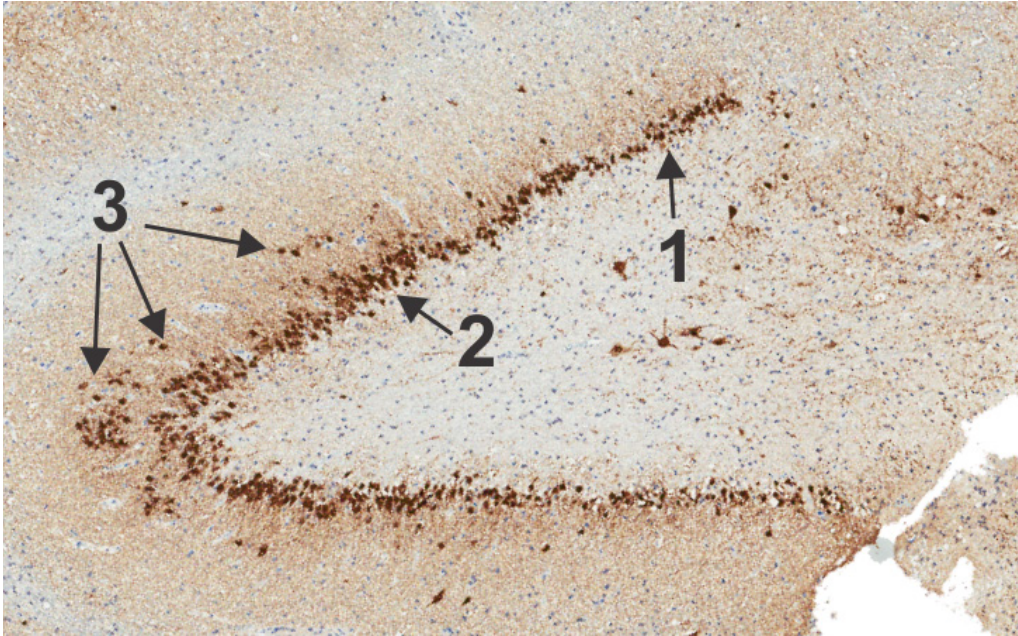


Figure 2.8 - Granule cell dispersion

A surgical specimen is shown from a patient with hippocampal sclerosis. Neuronal nuclear antigen (NeuN) staining of the granule cell layer of the dentate gyrus demonstrates granule cell dispersion. While some segments of the granule cell layer demonstrate normal thickness (1) other segments are pathologically widened (2). Furthermore, ectopic granule cell neurons can be identified (3) which are not seen in control specimens.

Mossy fiber sprouting As discussed above, new DG granule cells formed following experimental seizures form aberrant connections in the rat hippocampus (41). Synaptic reorganization is particularly well-documented for the mossy fiber pathway - which normally conveys information from DG

granule cells to area CA3. In rats treated with kainic acid or exposed to kindling, DG granule cells generate new mossy fiber axons which form excitatory synapses with other granule cells as well as CA3 neurons (45, 46). This phenomenon is known as mossy fiber sprouting and has also been documented in human subjects with chronic epilepsy (47, 48). Mossy fiber sprouting could potentially cause further seizures in patients with epilepsy by enabling recurrent excitation of DG granule cells and feed-forward excitation of CA3 neurons. This hypothesis is supported by animal studies demonstrating hyper-excitability of DG granule cells following kainate-induced mossy fiber sprouting (49).

Neuronal circuit dysfunction

As discussed above, multiple components of the normal MTL neuronal pathways are pathologically altered by induced seizures in animal models. Furthermore, similar abnormalities are seen in human subjects with chronic epilepsy. These observations have led to the hypothesis that neuronal circuit dysfunction both occurs as a result of seizures and also contributes to ongoing epileptic activity. In this way, MTL neuronal circuit dysfunction could be considered both the cause and consequence of recurrent seizures (21). In this subsection, we review the hypothetical mechanisms by which dysfunction of MTL circuits could contribute to ongoing seizures in patients with epilepsy.

Perforant pathway dysfunction The perforant pathway originates in the entorhinal cortex (13). Multiple lines of evidence suggest that the entorhinal cortex itself may contribute to ongoing seizures in patients with epilepsy. In tissue slice preparations, the medial entorhinal cortex has been shown to

generate epileptic activity in response to low magnesium concentrations (50). Furthermore, several neuropathological studies have documented abnormal tissue architecture of the entorhinal cortex in patients with chronic epilepsy (51-53). Activity generated in the entorhinal cortex is then transmitted via the perforant path to the granule cell layer of the DG.

Several factors could potentially contribute to the further development of putative epileptic activity in the granule cell layer of the DG. First, granule cell dispersion results in a loss of the normal "dentate gate" inhibition of hippocampal inputs (33). Secondly, mossy fiber sprouting results in recurrent excitation of DG granule cells and feed-forward excitation transmitted to area CA3. Finally, loss of inhibitory interneurons in the DG could result in a net excitation of DG granule cells.

Hippocampal neurons in area CA3 are intrinsically predisposed to generate epileptic activity due to their electrophysiological characteristics described above. Furthermore, CA3 neurons readily propagate epileptic activity via dense recurrent collaterals to area CA1 (Schaffer collaterals) and extensive excitatory connections along the hippocampal long axis (16). The summation of these multiple excitatory loops is postulated to overwhelm GABA-mediated inhibition in CA1 - resulting in transmission of epileptic activity from CA1 to the subiculum.

Finally, multiple lines of evidence suggest that the subiculum plays an active role in the generation of epileptic activity (54). The subiculum contains neurons capable of burst-firing (55), and these neurons increase in number following experimentally-induced seizures (56). These subicular burst neurons, like those in the entorhinal cortex, are capable of initiating epileptiform activity in slice preparations exposed to low magnesium concentration (57).

Interestingly, the subiculum does not display significant neuronal loss in human subjects with chronic epilepsy (54). This finding raises the possibility that burst-firing subicular neurons may remain intact and capable of generating epileptic activity in the presence of the otherwise severe hippocampal neuronal loss demonstrated in subjects with chronic epilepsy.

Temporo-ammonic pathway dysfunction Experimental evidence from animal models suggests an additional role of the temporo-ammonic (direct) pathway in the pathogenesis of epilepsy. In comparison with the perforant path, the direct temporo-ammonic pathway provides relatively weak input to area CA1 in control animals (58). In control animals, the excitatory input from entorhinal cortex to CA1 via the temporo-ammonic pathway is tightly regulated by feed-forward inhibition (59). Following status epilepticus, however, the direct temporo-ammonic pathway demonstrates a 10-fold increase in effectiveness (59). This finding suggests that the entorhinal cortex may directly stimulate CA1 neurons in subjects with chronic epilepsy. In combination with the perforant path, the temporo-ammonic pathway thus provides an additional mechanism by which the hippocampus may amplify epileptic activity.

Chapter 3 Epilepsy and mesial temporal lobe epilepsy

Epilepsy is a heterogeneous condition characterized by recurrent unprovoked seizures. Mesial temporal lobe epilepsy (MTLE) is a common form of epilepsy, which is nearly always refractory to medical treatment. In this chapter, we define several terms including: seizures, epilepsy, and drug resistant epilepsy. We then introduce MTLE as a clinical syndrome characterized by specific seizure types. Next, we describe the pathological hallmark of MTLE and consider potential etiologies for this condition. Finally, we review the aspects of the clinical epilepsy literature relevant to a comprehensive understanding of MTLE.

3.1 Definitions

Seizures

A seizure is defined as “a transient occurrence of signs and/or symptoms due to abnormally excessive or synchronous neuronal activity in the brain” (60). Prior to an observed seizure, many patients with epilepsy describe a predictable warning that a seizure will occur. These initial symptoms occurring before an overt seizure (*pre-ictally*) are termed an *aura* (latin for 'breeze') and are recognized only by the patient. In reality, however, an aura represents the onset of a seizure in brain regions which cause only subjective phenomena (symptoms). When electrical activity spreads to brain regions associated with

observable clinical features (termed 'eloquent cortex'), overt signs are noticed by external observers and this is termed the *ictal* phase of a seizure. Following a seizure (*postictally*), many patients describe residual symptoms such as unilateral weakness (Todd's paralysis) or somnolence. The constellation of symptoms and signs experienced by a patient during a seizure is termed the 'seizure semiology'.

A large number of seizure types exist, and a wide range of clinical symptoms and signs may occur during a seizure (61). Seizures can be divided broadly into two categories: 1) partial, also called focal, seizures - which arise from a discrete region of the brain; and 2) generalized seizures, which arise from bilaterally symmetrical brain networks (62). However, as discussed in the previous chapter, excessively synchronous neuronal activity is a common feature of all seizures (63).

An acute symptomatic (provoked) seizure is defined as "a clinical seizure occurring at the time of a systemic insult or in close temporal association with a documented brain insult" (64). Seizures can be provoked by a number of acquired conditions in otherwise healthy individuals, with the most common etiologies being traumatic brain injury, stroke, drug withdrawal, and central nervous system (CNS) infection (65). Acute symptomatic seizures occur in approximately 3.6% of the north american population (65). Provoked seizures are treated primarily by correction of the underlying cause, and the risk of future seizures (provided the underlying cause can be corrected) is much lower than for unprovoked seizures (66).

In patients with unprovoked seizures, a direct antecedent cause cannot be identified. Approximately 4.1% of the north american population will experience an unprovoked seizure at some point in their lives (67). In patients

presenting with a single unprovoked seizure, the risk of future seizures is approximately 33% (68). As the majority of such patients will never experience a recurrence, treatment with anticonvulsants is not usually initiated following a single seizure (69).

Epilepsy

Epilepsy is defined as “a disease of the brain characterized by an enduring predisposition to generate epileptic seizures and by the neurobiologic, cognitive, psychological, and social consequences of this condition” (70). The world health organization estimates that approximately 50 million people worldwide have epilepsy (1). The prevalence of epilepsy in Canada is approximately 0.4% (71), making epilepsy one of the most common neurological disorders in this country. People with epilepsy experience significant morbidity due to the social and occupational consequences of recurrent seizures. Furthermore, epilepsy is associated with comorbid mental health problems and premature mortality (72).

The diagnosis of epilepsy does not indicate the underlying cause, and use of the term 'the epilepsies' emphasizes the large number of potential etiologies for this condition (73). Depending on the etiology, epilepsy can begin at any age ranging from the neonatal period [where common causes include perinatal anoxia and cerebral malformations (74)] to late adulthood [where common causes are stroke and trauma (75)]. Epidemiological studies have demonstrated that patients who have had at least two unprovoked seizures, separated by more than 24 hours, have a high risk (approximately 73%) of having further seizures over time (68). In such patients, the diagnosis of epilepsy is made based on the high recurrence risk [of greater than 60% (70)],

and anticonvulsant treatment is usually recommended (69). However, the clinical diagnosis of epilepsy can also be supported by the results of diagnostic tests.

The electroencephalogram (EEG) can provide biological evidence to support a clinical diagnosis of epilepsy. The surface EEG is obtained by recording voltages from scalp electrodes and plotting the difference in voltage between electrode positions over time (Figure 3.1) (76-78). The scalp EEG is primarily generated by post-synaptic potentials in pyramidal neuron dendrites (79) occurring synchronously in sufficiently large regions of the cerebral cortex and oriented perpendicular to the recording electrodes (80). Epileptiform discharges, which reflect excessive cortical excitation (81), are identified in the interictal (between-seizures) EEG of some patients with epilepsy (Figure 3.1).



Figure 3.1 - The surface electroencephalogram (EEG)

The electrical voltage differences between several pairs of scalp electrodes (indicated on the left) are displayed over time. The surface EEG in this patient with temporal lobe epilepsy demonstrates interictal epileptiform activity originating from the left temporal lobe

In patients who have experienced at least one epileptic seizure, epileptiform activity on the EEG can increase the risk of recurrence (to greater than 60%) and thus indicate a diagnosis of epilepsy (70). Furthermore, EEG can be helpful in classifying a seizure disorder as generalized (82) versus focal (83), and can suggest a specific epilepsy syndrome (84). However, a negative (normal) EEG does not rule out a diagnosis of epilepsy in patients with clear unprovoked seizures (85).

Structural neuroimaging also plays an important role in the evaluation of patients with seizures and epilepsy (Figure 3.2). Approximately 12% of patients presenting with a single unprovoked seizure have a structural intracranial lesion (e.g. tumour or cortical malformation) (86). Computed tomography (CT) scanning is less sensitive than magnetic resonance imaging (MRI) for detecting these lesions (86). In patients with a single seizure, detection of a structural brain lesion is consistent with a diagnosis of epilepsy due to the high (greater than 60%) recurrence risk (70), and anticonvulsant treatment is generally recommended for these patients as well (69). However, the presence of a structural brain lesion does not indicate a diagnosis of epilepsy in the absence of clinical seizures.

Drug resistant epilepsy

Anti-epileptic drugs (AEDs, also known as anticonvulsants) are the primary treatment modality for patients with epilepsy. As discussed in chapter 2, the predisposition to unprovoked seizures in patients with epilepsy is mediated by: 1) excessive glutamatergic excitation of sodium channels; and 2) inadequate gamma-amino butyric acid (GABA)-mediated neuronal inhibition (63, 81, 87). Traditional anticonvulsant medications thus act primarily via two mechanisms

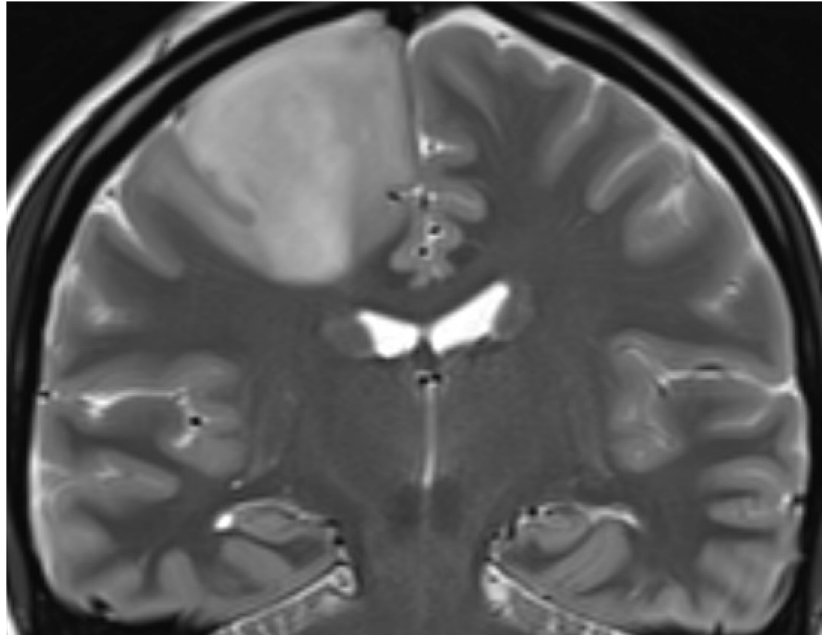


Figure 3.2 - MRI in the evaluation of a single seizure

Coronal T2-weighted MR Imaging is shown from a 32 year-old patient who presented with a single unprovoked seizure. The patient had not had any previous neuroimaging (e.g. CT scan). A large T2 hyperintense lesion is identified in the superior frontal lobe with local mass effect on the right lateral ventricle. Surgical resection revealed an anaplastic oligodendroglioma.

of action: 1) antagonism of voltage-gated sodium channels (e.g. carbamazepine, valproic acid, and phenytoin); and/or 2) enhancement of GABA-mediated neuronal inhibition (e.g. clobazam) (88). Newer anticonvulsant medications have also been developed with novel [e.g. levetiracetam, SV2A inhibition (89)] or multiple mechanisms of action [e.g. lamotrigine and topiramate (90, 91)].

Anticonvulsant medications are effective in controlling seizures for the majority (approximately 65-70%) of patients with epilepsy (2). In clinical practice, approximately 50% of patients with epilepsy will achieve seizure freedom with the first trial of anticonvulsant medication (92). An additional

13% of patients will respond to a second medication, but less than 5% will benefit from the third or subsequent anticonvulsant trials (2). As a result, drug resistant epilepsy is defined as: "failure of adequate trials of two tolerated, appropriately chosen and used antiepileptic drugs to achieve sustained seizure freedom" (93). Patients with drug resistant epilepsy suffer from the consequences of uncontrolled seizures, which are associated with reduced employment opportunities, social isolation, psychiatric comorbidities, and reduced quality of life (94). Furthermore, uncontrolled seizures are associated with increased mortality in patients with drug resistant epilepsy (95).

3.2 Mesial temporal lobe epilepsy

Mesial temporal lobe epilepsy (MTLE) is a clinical syndrome with several potential underlying causes. MTLE is characterized by a specific seizure semiology, which was initially described by John Hughlings Jackson in 1888. Since this time, these seizures have been given many names including psychomotor seizures, uncinate seizures, complex partial seizures, and dyscognitive seizures. In this section, we review the seizure semiology experienced by Jackson's patient as an example of the habitual seizures seen in patients with MTLE. Secondly, we review our current knowledge of the clinical characteristics and natural history of MTLE.

Seizure semiology in patient Z

MTLE is the most common clinical syndrome associated with drug resistant epilepsy (3). Jackson associated the clinical symptoms and autopsy findings of a patient with this condition, whom he called patient Z (96). Patient Z was a

physician who developed epilepsy in adulthood, characterized initially by small seizures now known to be characteristic of MTLE. In 1888, Jackson had described the classical symptoms and signs of focal temporal lobe seizures experienced by *other patients with MTLE*, including: abdominal discomfort "epigastric sensation", olfactory hallucinations "horrid smell", and impaired awareness "dreamy state" (97). In addition to these partial seizures, like most patients with MTLE, Z also later experienced infrequent generalized convulsive seizures which led him to begin seeing Jackson in 1877.

Following Z's death by chloral hydrate overdose in 1894, Jackson described his particular clinical course in exquisite detail (96), which is now known to be a classical description of MTLE (97). Patient Z did not initially seek medical attention for his small seizures, which began at age 20. During these small seizures, Z experienced "a recollection" and reported having "a sentence in his mind which was as if well remembered" (96). He described that, prior to his events he would be "attending to what was going on in my mind because it was interesting, and dim to what was going on outside. He could not, on recovery, remember what the interesting matter was." (96). Interestingly, Z did not experience the epigastric sensations or olfactory hallucinations described by other patients in Jackson's initial cohort (97). Patient Z's aura consisted solely of the symptoms described above (which Jackson called an "intellectual aura") combined with "a slight feeling of dread" (96). Patient Z described that he was partially able to control these small seizures by performing motor activities or speaking.

Z had been told that during these small events, there was "an indistinct smacking of the tongue like a tasting movement, generally accompanied by a motion of the lower jaw and sometimes by some twitching of the muscles round

one or both corners of the mouth or of the cheeks" (96). He was not aware of these movements, which are now known as 'oral automatisms' and are considered a classical feature of focal seizures in patients with MTLE. Jackson witnessed two of Z's seizures and provided further details of his behaviour during these events. Jackson described that: "in one he stopped talking to me and remained standing" (96). This is known as a 'speech arrest' and is also typical of seizures in MTLE, particularly those originating in the dominant hemisphere. Furthermore, typical of patients with MTLE, Z was noted to exhibit semi-purposeful but inappropriate behaviour during his seizures. Finally, Jackson described a clear alteration of awareness during Z's seizures, as he was unable to recall what had transpired during some of his episodes (96). In contrast, Z reported being able to partially function during some of his events and provided examples of seizures occurring during his work as a physician which were not noticed by patients or colleagues. During some of his seizures, however, he produced disorganized and incomprehensible clinic notes which clearly document the disruption of normal cognitive function during seizures in MTLE (96). The case of patient Z thus provided a seminal description of the habitual seizures experienced by patients with MTLE.

Clinical features of MTLE

Natural history The natural history of MTLE has been ascertained primarily from retrospective series (98). The mean age of onset for the habitual seizures described above is age 9, and approximately 50% of patients also experience generalized convulsions (99). The habitual seizures initially respond to medications and approximately 25% of patients report at least 1 year of seizure freedom during the early years of the disease (100). As a result, it takes an

average of nine years (100) for a patient with MTLE to fail two medications and be diagnosed with drug resistant epilepsy (93). However, long-term seizure freedom with medication alone is rare in MTLE and approximately 90% of patients will eventually become medically intractable (3). The protracted course of MTLE results in an average delay of 20 years from habitual seizure onset to referral for surgical treatment (98).

Risk factors A number of risk factors have been identified for the subsequent development of MTLE. In particular, many patients have a history of seizures in early childhood (99) - several years prior to the development of MTLE. These early seizures are often associated with an acquired cerebral insult [e.g. perinatal asphyxia, central nervous system (CNS) infection, or traumatic brain injury] (101). Based on the hypothesis that such cerebral insults represent a cause for seizures (discussed further below), they are known as an initial precipitating injury (IPI). In the vast majority of patients, the IPI occurs prior to age 5 (most commonly between 6 and 12 months) (102). Thus, the period of time between the IPI and the onset of habitual seizures (mean age 9) is typically several years (99). This has been termed the 'latent period' of MTLE (98).

3.3 Pathology of MTLE

The MTLE syndrome can be associated with several different forms of brain pathology (18). In this section we first review the pathology identified in Jackson's patient Z. We then introduce the most common pathological substrate of MTLE, which is known as hippocampal sclerosis. Finally, we review other cerebral lesions which can be associated with MTLE.

Pathology in patient Z

The circumstances surrounding Z's premature death due to chloral hydrate overdose at age 43, specifically whether he committed suicide, remain unknown (97). Ferrier had previously demonstrated that "certain movements of the lips, tongue and cheek-pouches follow on artificial excitation of a certain region of a monkey's cortex" corresponding to the uncinate gyrus (96). Jackson therefore postulated that Z's seizures originated in the same region. Indeed, an autopsy performed on patient Z revealed "a very small patch of *softening* in the left uncinate gyrus" confirming Jackson's hypothesis as correct (96).

The exact nature of this lesion, however, remains unclear. Dr. Walter Colman performed the autopsy and noted that "the consistence of the brain was natural except in the left uncinate gyrus, where it could be felt that there was a patch of softening beneath the surface" (96). He also noted that "on a section being made through the patch it was found to be a small cavity, collapsed and almost empty, with indefinite walls, situated in the uncinate gyrus, 5/8 inch below the surface just in front of the recurved tip of the uncus" (96). However, Colman described that "the uncinate region became so soft and friable during the hardening process that it was impossible to make satisfactory sections, and the microscope did not throw any further light on the cause of the lesion" (96).

Hippocampal sclerosis

Interestingly, Jackson was *not* the first to suggest a connection between epilepsy and the temporal lobes. In 1826, Bouchet and Cazavieles had described a *hardening* of the temporal lobes found at autopsy in patients with chronic epilepsy (97). However, Sommer was likely the first to propose (in

1880) that pathological changes in the hippocampus were the cause of epilepsy (103). In this seminal work, Sommer described neuronal loss predominantly in area CA1 (now known as the 'Sommer sector') but also affecting other hippocampal subfields (103). Sommer initially termed this "disease of the ammons horn" and since 1880 it has been given several names including 'ammon's horn sclerosis' and 'mesial temporal sclerosis'. The current classification system for this entity, however, uses the term hippocampal sclerosis (HS) which we will therefore use in the remainder of this thesis.

HS is now known to be the most common pathological finding in patients with MTLE (Figure 3.3) (18). As shown in Figure 3.3, HS consists microscopically of neuronal loss and astrocytic gliosis in the hippocampal pyramidal cell layers. Interestingly, individual hippocampal subfields demonstrate a differing degree of neuronal loss in HS. CA1 is referred to as the 'vulnerable sector' and demonstrates the greatest degree of neuronal loss (1, Figure 3.3) (103). This may reflect the convergence of multiple excitatory hippocampal pathways on CA1, as described in chapter 2. In contrast, CA2 is termed the 'resistant sector' as this region is often relatively preserved in patients with HS (2, Figure 3.3) (104). This finding may relate to a relative paucity of recurrent excitation entering CA2 from other hippocampal regions (105). Classical HS is also typically accompanied by severe neuronal loss in the CA4 region (3, Figure 3.3). As discussed in chapter 2, HS is often accompanied by dispersion of the granule cell layer of the dentate gyrus (DG) which may reflect aberrant neurogenesis following seizures.

The early literature concerning HS was based on autopsy studies of patients with chronic epilepsy who subsequently passed away. The development of epilepsy surgery (described further below), subsequently

enabled pathological analysis of hippocampal biopsy specimens from living patients with MTLE. In such patients, the hippocampus which appeared to be generating seizures (based initially on seizure semiology and EEG) was termed the 'ipsilateral' hippocampus, while the 'contralateral' hippocampus was assumed to be relatively normal. The catastrophic case of patient H.M., who developed severe anterograde memory loss following bilateral hippocampal resections, confirmed that only one hippocampus can be removed surgically (17). Pathological analysis in patients with MTLE is thus typically restricted to a small portion of the 'ipsilateral' hippocampus.

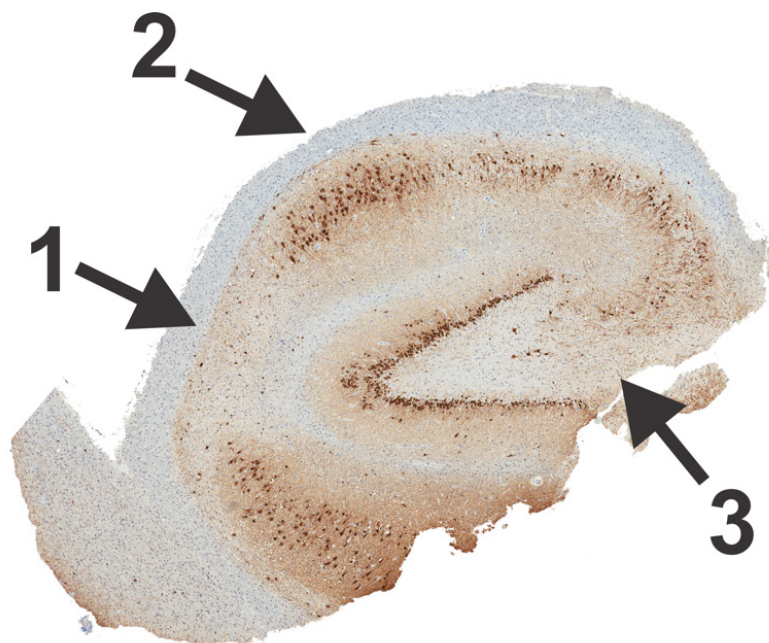


Figure 3.3 - Pathology of hippocampal sclerosis

A hippocampal specimen is shown from a patient with MTLE who underwent temporal lobectomy for treatment of drug resistant epilepsy. Neuronal nuclear antigen (NeuN) staining demonstrates severe neuronal loss in the distal segment of CA1 (1), sparing of the CA2 sector (2) and severe neuronal loss in CA4 (3).

Early surgical series demonstrated that HS is commonly identified in hippocampal biopsy specimens from patients with MTLE (106). Subsequent autopsy studies, however, have demonstrated that patients with chronic epilepsy often have bilaterally asymmetric HS (15). In addition, sclerosis of the temporal neocortex (including the entorhinal cortex and parahippocampal gyri) is often seen in subjects with MTLE (107). Furthermore, the amygdala often demonstrates pathological involvement in patients with MTLE (52). These studies demonstrate that HS is a bilaterally asymmetric process which affects the hippocampus but also multiple other structures of the mesial temporal lobes.

MTLE due to structural lesions

MTLE is a clinical syndrome and only 50% of patients with MTLE demonstrate HS upon pathological analysis (18). In this section, we first consider other cerebral lesions which are associated with MTLE. We then discuss the concept of dual pathology, which refers to the coexistence of such structural lesions with HS. Finally, we introduce the concept of MTLE without identifiable pathology - which is currently known as *No HS*.

Tumors Following HS, tumors represent the second-most common cause of MTLE (Figure 3.4) (18). While several rare tumors may cause MTLE, the most common tumors encountered in MTLE are gangliogliomas and dysembryoplastic neuroepithelial tumors (DNETs) (18). Both of these entities are low-grade and slow-growing tumors which present clinically with recurrent seizures (108). As described below, these tumors are differentiated from each other primarily by histological analysis.

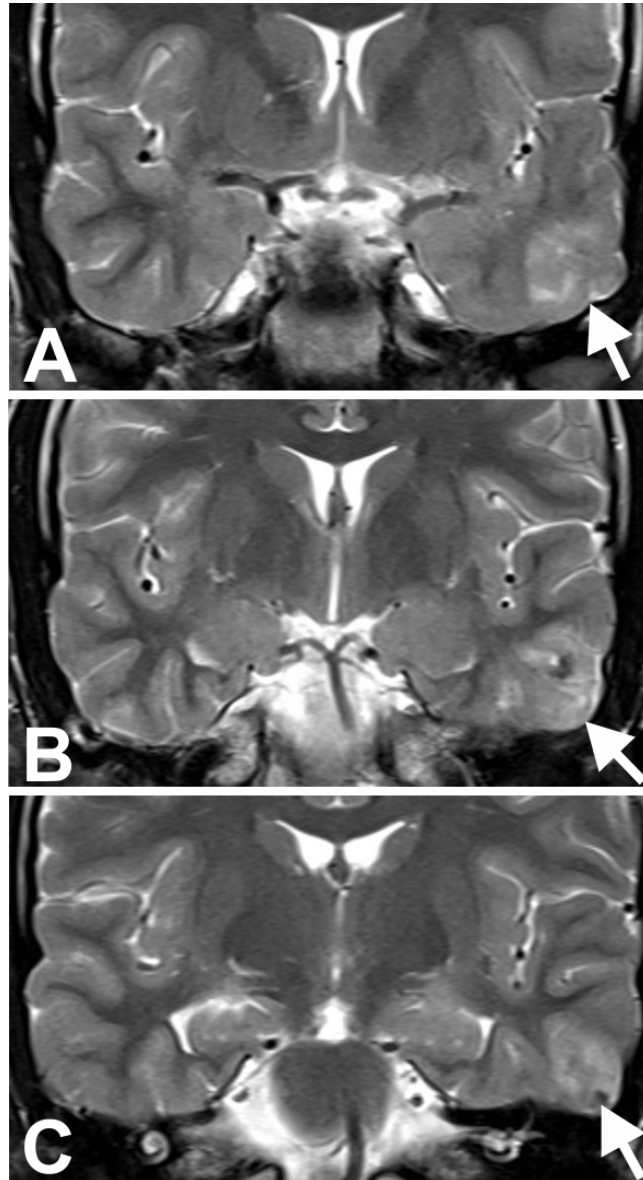


Figure 3.4 - Temporal neocortical low-grade tumor causing epilepsy

Coronal T2-weighted MR Images are shown from a patient who presented with recurrent generalized convulsions. Panels A-C represent sequential slices moving in the rostral to caudal direction. A T2-hyperintense lesion is identified in the left middle and inferior temporal gyri (arrows). The lesion demonstrates heterogeneous enhancement and has remained stable on repeated imaging. It is believed to represent a low-grade neoplasm and has not yet been resected.

Gangliogliomas are characterized by "nodular or compact aggregates of dysplastic neurones" (108) while DNETs demonstrate a pathognomonic feature known as the 'glioneuronal element'. The glioneuronal element consists of "microcolumns of oligodendrocyte-like cells with an intervening myxoid matrix surrounding floating neurones" (108). In comparison with HS, tumor-related MTLE is associated with a similar age of seizure onset but a shorter duration of epilepsy prior to surgical treatment (18). This observation may reflect the fact that these lesions are readily identified with neuroimaging and represent an obvious indication for surgical removal.

Focal cortical dysplasia The cerebral cortex normally demonstrates a characteristic lamination pattern which varies according to brain region (12). In focal cortical dysplasia (FCD), this normal lamination pattern is disrupted and histological analysis reveals dyslamination of the cerebral cortex (109). FCD is the third most common lesion identified in patients with MTLE, following HS and tumors (18). Two histological subtypes of FCD are commonly identified in surgical series. Type II FCD is more common and is characterized by cortical dyslamination accompanied by dysmorphic neurons (109). The less common variant, termed Type I FCD, consists of isolated abnormal lamination without dysplastic neurons (109). FCD is associated with the earliest age of seizure onset (mean age 6 years), which likely reflects the congenital nature of this pathology (18).

The neuroimaging features of FCD are demonstrated in Figure 3.5. Coronal T1-weighted imaging reveals marked thickening of the cortical mantle in the mesial occipital lobe. This is associated with markedly hypointense signal from the cerebral white matter in this region. Neuropathological evaluation following surgical resection revealed type I FCD.

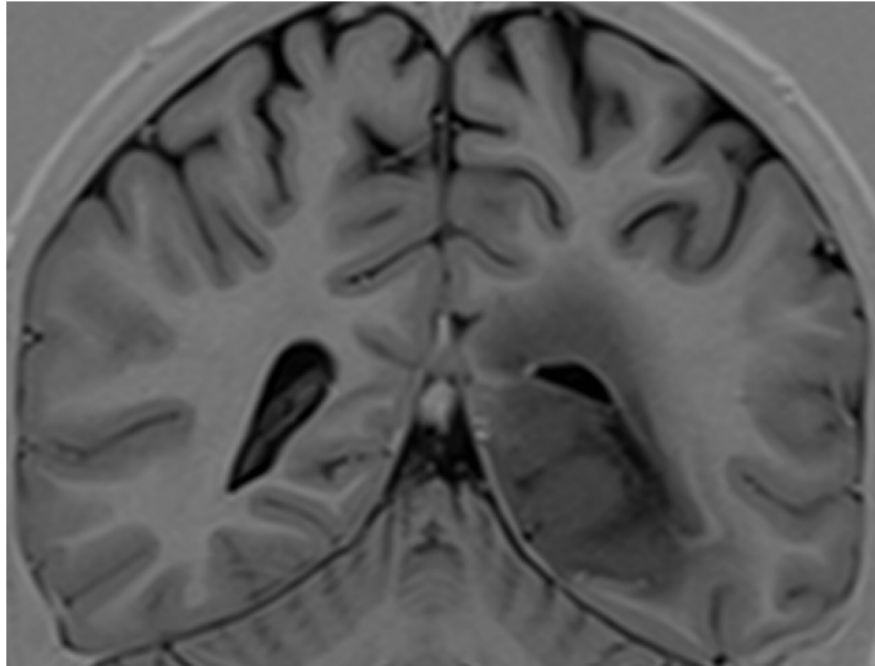


Figure 3.5 - MRI of focal cortical dysplasia (FCD)

Coronal T1-weighted MR Imaging is shown from a patient with long-standing drug resistant epilepsy. There is thickening of multiple gyri in the left mesial occipital lobe which is accompanied by markedly hypointense signal from the cerebral white matter in this region. Following surgical resection, neuropathological examination revealed Type I FCD.

Cavernous angioma Cavernous angiomas (Figure 3.6, also known as cerebral cavernous malformations or cavernomas) are an uncommon cause of MTLE, representing approximately 5% of cases in large surgical series (18). These lesions are characterized histologically by "closely apposed dilated vascular channels without intervening brain parenchyma" (110). Interestingly, cavernous angiomas are associated with the oldest (mean 25.4 years) age of seizure onset (18). These lesions are known to change with time, often demonstrating "repeated intralesional hemorrhages" (Figure 3.6) (111), which may partially explain the later age of onset in these patients.

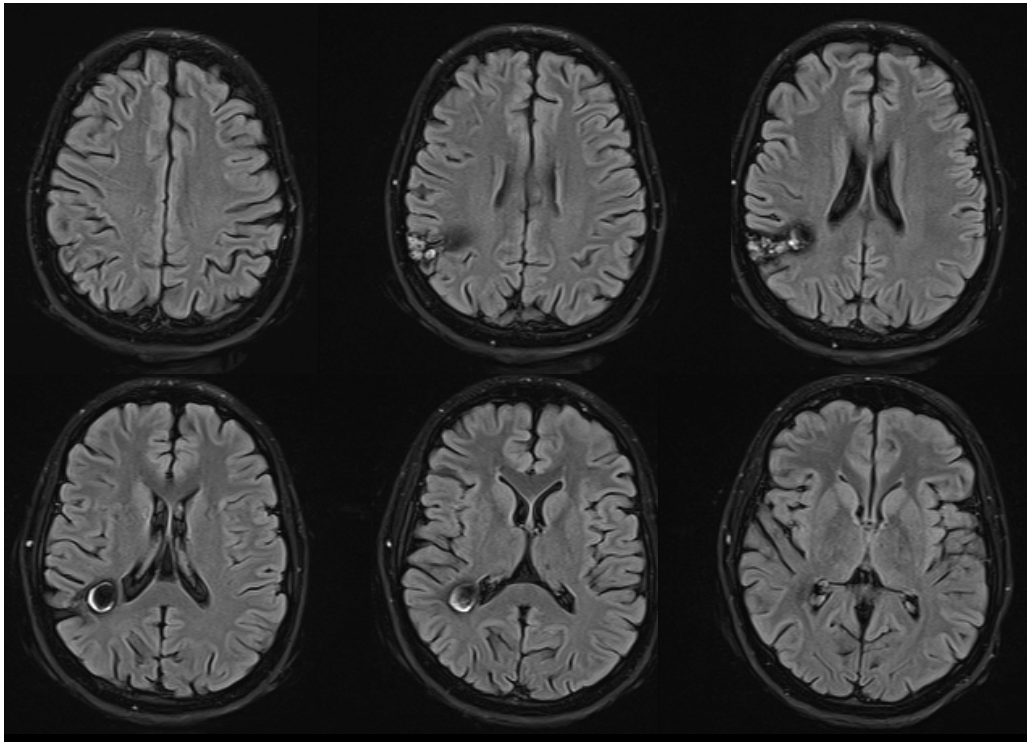


Figure 3.6 - Cavernous angioma

FLuid-Attenuated Inversion Recovery (FLAIR) images are shown from a patient with drug resistant epilepsy, demonstrating a cavernous angioma in the right parietal region. The lesion demonstrates a heterogeneous appearance due to the presence of blood products of different ages, suggesting multiple previous intralesional hemorrhages.

Dual pathology The term dual pathology is used to denote the coexistence of HS and another epileptogenic lesion such as those listed above (tumor, FCD, cavernous angioma) (112). The frequency of dual pathology has varied across surgical series. In initial reports, 30% of patients with HS were found to have a coexistent structural lesion (112). Subsequent quantitative MRI studies reported a lower frequency with approximately 15% of patients having dual pathology (113). In patients with dual pathology, removal of both the structural

lesion and the sclerotic hippocampus results in the highest likelihood of seizure freedom (114). This finding provides further evidence that, even in the presence of a structural lesion, the hippocampus plays a causative role in recurrent seizures in patients with MTLE.

No HS As emphasized above, MTLE is a clinical syndrome characterized by specific seizure types and is not synonymous with HS. In some patients with MTLE, the hippocampus responsible for seizures is identified solely on the basis of clinical semiology and EEG findings (115). Indeed, multiple series have demonstrated that a normal hippocampus (termed "No HS") is found in 25-50% of patients with MTLE who undergo surgical resection (4). This observation has important implications for currently accepted theories regarding the etiology of MTLE, as discussed in the next section.

3.4 Etiology of MTLE

Multiple lines of evidence suggest that MTLE has several possible etiologies. In this section, we discuss current concepts regarding the etiology of MTLE due to structural lesions and MTLE associated with HS. Finally, we consider current knowledge gaps related to the etiology of MTLE with No HS.

Structural lesions

As discussed above, the case of patient Z provided early evidence that structural lesions of the temporal lobe are causally related to seizures. The finding of temporal lobe epileptiform activity on surface EEG in patients with MTLE (116, 117) provided further insights into this relationship. In 1930, Dr. Wilder

Penfield reported that removal of structural brain lesions was sufficient to eliminate seizures in some patients with epilepsy (118). Over the ensuing decades, Penfield provided further evidence demonstrating a cause-effect relationship between structural brain lesions and MTLE (119).

In October 1950, Penfield reported the results of temporal lobe excisions performed in 51 patients with epilepsy from 1939-1949 (120). The majority of patients in this series had structural lesions of the temporal lobe, identified intra-operatively, which Penfield termed "atrophic lesions" (120). The resections in these cases included the "atrophic lesion" as well as adjacent tissue identified as epileptogenic using electrocorticography (EEG measured directly from the brain surface). Interestingly, however, the mesial temporal structures (amygdala, hippocampus, and uncus) *were not* removed in these initial cases. Penfield found that 53% of patients (27/51) treated with this approach had remained seizure-free for one year following surgery (120). This finding, combined with the previous literature described above, provided strong evidence that structural lesions are sufficient to cause seizures in some patients.

In contemporary epilepsy surgery practice, structural brain lesions associated with epilepsy are termed "epileptogenic lesions" (115). However, removal of the 'epileptogenic lesion' is not always sufficient to prevent further seizures. This fact is exemplified by the situation of dual pathology, described above, in which resection of both the lesion and the sclerotic hippocampus results in the highest likelihood of seizure freedom (114).

Hippocampal sclerosis

HS causes the MTLE syndrome Although HS had previously been documented in autopsy studies of patients with chronic epilepsy, many

investigators believed that HS was *only* the result (rather than the cause) of recurrent seizures (104). Definitive proof that HS causes seizures was eventually provided by the observation that surgical removal of the sclerotic hippocampus could prevent further seizures in patients with MTLE.

In February 1951, Bailey and Gibbs reported their results from twenty-five patients with epilepsy treated surgically between 1947 and 1950 (121). The surface EEG was used to lateralize the epileptic focus prior to operation. Surgical exploration also revealed anatomical abnormalities (which Bailey called "atrophy of the convolutions") in many of these patients (121). However, the surgical resections in this series were based primarily on the results of invasive EEG recordings. The operations were performed under general anesthesia and the anesthetic was titrated to maximize the amount of epileptiform activity. The temporal lobe was then sampled with both electrocorticography and depth electrode recordings (discussed further below), and the cortical regions demonstrating epileptiform activity were resected (121). The mesial temporal structures, including the hippocampus, were *always spared*. Bailey and Gibbs found that 60% of patients (15/25) treated with this procedure remained seizure-free at least 6 months following the operation.

In 1955, Falconer was the first to demonstrate that the removal of a sclerotic hippocampus was sufficient to eliminate seizures in patients with HS (122). This seminal finding was enabled by Falconer's 'en bloc' surgical resection technique, which allowed neuropathological demonstration of HS in hippocampal biopsy specimens resected from patients with MTLE (106). The high rate of surgical cure in MTLE subjects, whom Falconer treated with temporal lobectomy, provided strong evidence that HS was causing seizures in these patients (106).

Falconer's observations were further supported by the development of stereotaxic depth electrodes, which allowed the direct measurement of epileptiform activity from the mesial temporal structures (123). In patients with MTLE and apparently *bitemporal* epileptiform discharges based on surface EEG, depth electrode studies demonstrated *unilateral* mesial temporal onset of all seizures in the majority of patients (124). Collectively, these results are consistent with the basic science literature discussed in chapter 2 which suggest that the mesial temporal structures are highly epileptogenic.

Etiology of HS While in many cases HS has been shown to be *the cause of* seizures (125), several lines of evidence also suggest that HS can be *caused by* seizures and other brain injuries (39). In 1880, the same year that Sommer proposed HS as a potential etiology for epilepsy, Pflieger reported a case of HS in a patient who died of status epilepticus (21). Pflieger suggested, based on the tenuous blood supply to the hippocampus, that HS could be induced by recurrent seizures (21). As discussed in chapter 2, this hypothesis is strongly supported by animal models which have demonstrated that neuronal loss and other anatomical changes do occur in the hippocampus following seizures. Indeed, early surgical series demonstrated that the presence of HS was strongly correlated with an early history of childhood seizures several years prior to the development of chronic epilepsy (106).

Approximately 2-5% of otherwise healthy children will experience at least one seizure associated with a high fever (termed a 'febrile seizure') between the ages of 6 months and 6 years (126). The high prevalence of febrile seizures (up to 75%) *ascertained retrospectively* in patients with HS led to the initial suggestion that febrile seizures caused HS (125). However, only approximately 2% of children who experience a febrile seizure, *followed*

prospectively, will eventually develop epilepsy (126). Furthermore, the risk of subsequent epilepsy is much higher in children who were developmentally abnormal prior to the febrile seizure (126).

In addition, certain clinical features of febrile seizures are strongly linked to the future development of epilepsy (127). Annegers et al. identified three "complex features" which, if present, increased the likelihood of subsequent epilepsy: focality, duration greater than 15 minutes, and multiple seizures within the same febrile illness (127). Children whose seizures had none of these complex features were found to have a 2.4% risk of subsequent epilepsy, which is only slightly higher than that seen in the general population (127). In contrast, the risk of subsequent epilepsy was found to be different for children with one (6-8%), two (17-22%), and three (49%) complex features (127). This finding provides compelling epidemiological evidence that complex febrile seizures are associated with an increased risk of epilepsy. Therefore, complex febrile seizures (including febrile status epilepticus) are considered a form of initial precipitating injury (IPI) as discussed above.

Indeed, it was shown in a subsequent retrospective study that approximately 81% of patients with MTLE have a history of convulsions in childhood or infancy (99). In this study, a complex febrile seizure had occurred in childhood in 67% of patients who eventually developed MTLE (99), while an additional 14% had another form of IPI. Furthermore, subsequent studies demonstrated that a history of an IPI was much more common in patients with HS (87%) in comparison to those with No HS (23%) (102).

A *prospective* study has also suggested that prolonged febrile seizures can *cause HS* in some patients (128). In this study, children with prolonged febrile seizures underwent MRI immediately after the seizure and one year

later. Approximately 10% of children demonstrated acute swelling of one hippocampus, and the majority of these children were found to have MRI evidence of HS one year later (128). While this study strongly suggests a causative role of IPIs for patients with HS, it also confirms that the vast majority of children who experience an IPI *do not appear* at risk to develop MTLE (128). This observation has led several authors to investigate potential factors that might explain why only some children develop MTLE following an IPI.

It is possible that children who develop MTLE following an IPI have pre-existing anatomical abnormalities of the mesial temporal lobe (129). Microdysgenesis refers to a subtle form of cortical dyslamination that could serve as a nidus for seizures (129). Neuropathological studies have demonstrated that cytological features of microdysgenesis are encountered in some patients with HS (130). Furthermore, immature Cajal-Retzius cells (which normally disappear during development) are identified in both microdysgenesis (131) and HS specimens (132). Collectively, these studies support the hypothesis that some patients with HS have subtle cortical malformations that predispose them to seizures following an IPI (127).

Genetic factors may also play a role in the development of HS following an IPI (21). This hypothesis is supported by the discovery of several families with MTLE (133). Furthermore, some patients with familial MTLE have been shown to have histological features of HS which are indistinguishable from those with the sporadic form of the disease (134). In addition, genetic polymorphisms of a gene commonly implicated in epilepsy (SCN1A) have been recently discovered in patients with HS (135). These observations support

the notion that genetic factors may contribute to the eventual development of HS and MTLE (39).

No HS

As discussed above, multiple series have consistently documented that between 25-50% of patients who undergo surgery for MTLE have no identifiable pathology in the resected hippocampal specimen (4). Several potential explanations exist for this interesting finding. Firstly, as discussed above, the entire hippocampus is rarely examined in surgical neuropathology series. Recent autopsy studies have demonstrated that HS varies along the hippocampal long axis, with some patients demonstrating 'no HS' in some portions of an otherwise sclerotic hippocampus (136). Likewise, it is not possible to pathologically evaluate the entire temporal lobe in patients who undergo epilepsy surgery. It is known that anatomical abnormalities in the temporal neocortex (107) and amygdala (137) are relatively common features in patients with MTLE (138). In addition, focal cortical dysplasias are frequently identified in patients with HS (139). These findings raise the intriguing possibility that occult anatomical abnormalities exist in patients who receive a diagnosis of 'No HS', but these abnormalities cannot be captured by currently available neuropathological techniques.

3.5 Clinical aspects

MTLE is the most common form of drug resistant epilepsy encountered in clinical practice (21). In this section, we review the clinical approach to

diagnosis and treatment of MTLE. Finally, we review the effectiveness of epilepsy surgery as a treatment for MTLE.

As discussed above, EEG was the first modality to detect abnormalities in patients with MTLE (118). Indeed, surface EEG remains a critical tool in the contemporary evaluation of epilepsy surgery candidates (115). In nearly all patients with MTLE (96%), the surface EEG demonstrates interictal (between-seizures) epileptiform activity from the anterior temporal lobes (140). This activity is often (60%) lateralized to the side responsible for the patient's habitual seizures (140). As discussed above, the surface interictal EEG (in combination with intra-operative EEG recording) was used to determine the location of cerebral resection in the earliest epilepsy surgeries (121, 122). This was further augmented by the development of stereotaxic depth electrode implantations which allowed the direct monitoring of epileptiform activity from the mesial temporal regions (Figure 3.7) (124).

Long-term video EEG (telemetry) monitoring, however, revolutionized the approach to epilepsy surgery by allowing physicians to determine the location of seizure onset (141). This procedure involves the continuous acquisition of scalp EEG data over the course of approximately two weeks, during which time the patient is admitted to hospital. A patient's medication is usually reduced or discontinued completely in an attempt to record seizures. This allows the seizure semiology and region of scalp EEG onset to be examined. Consistently lateralized (occurring on the same side in each seizure) build-up of ictal EEG activity has been shown to occur in approximately 80% of MTLE patients, and this provides strong evidence that seizures originate from this hemisphere (99).

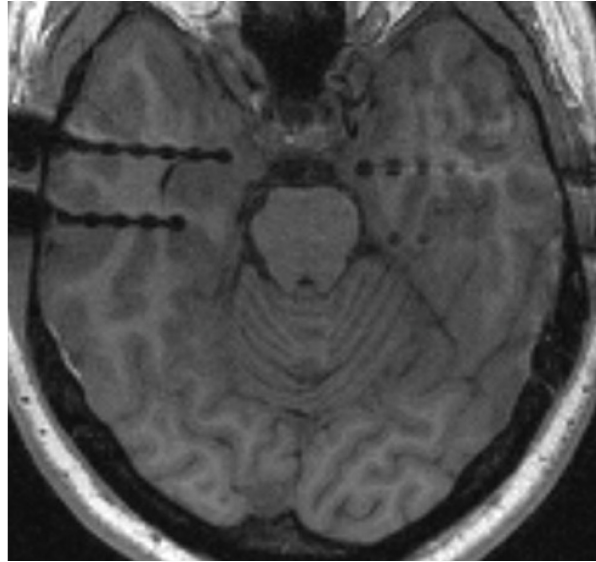


Figure 3.7 - Depth electrode implantation

An axial T1-weighted MR Image is shown from a patient with drug resistant epilepsy who underwent depth electrode recording. Two depth electrodes are shown in the right hippocampus. Separate electrode contacts are visible as discrete regions of low T1 signal along the length of each depth electrode. Depth electrodes were also inserted in the left hippocampus but are not well-visualized on this slice.

The discovery of MRI as a non-invasive method to detect HS has also revolutionized the care of patients with MTLE (142). The classical qualitative MRI characteristics of HS (Figure 3.8) include: a) reduced hippocampal volume (atrophy) (143), b) increased T2 signal (hyperintensity) (144), and c) loss of the normal hippocampal internal architecture (143).

The detection of these qualitative features is enhanced by acquisition of high resolution coronal imaging through the temporal lobes and interpretation by experienced neuroradiologists in the context of seizure semiology and EEG results (145). These MRI features are strongly correlated with the presence of HS detected pathologically following temporal lobectomy (specificity of 86%)

(144). Furthermore, patients with qualitatively evident HS are much more likely to achieve seizure freedom (62%) following temporal lobectomy than those without these changes (36%).

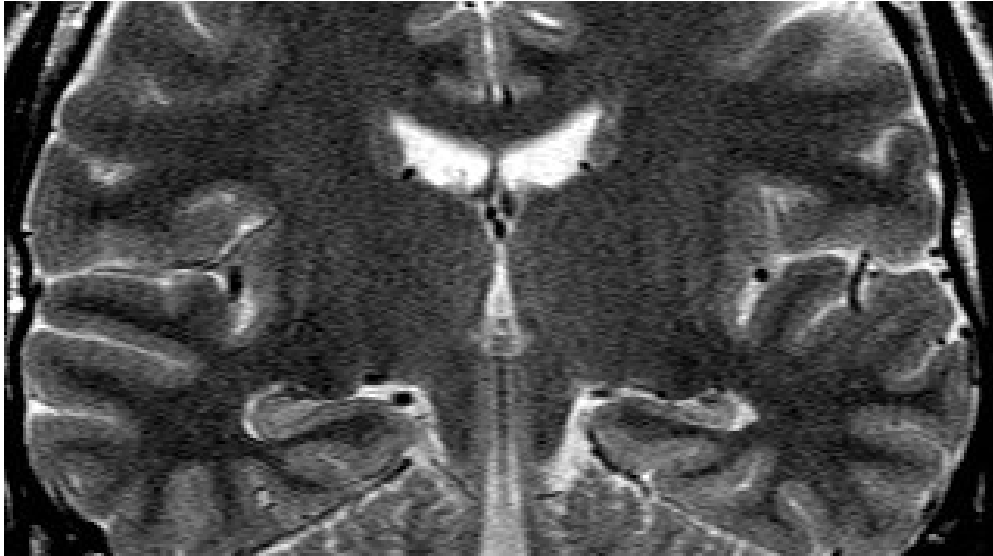


Figure 3.8 - Hippocampal sclerosis on MRI

A T2-weighted coronal MR Image is shown from a patient with drug-resistant mesial temporal lobe epilepsy. The left hippocampus demonstrates the three classical features of hippocampal sclerosis: a) atrophy, b) hyperintensity, and c) loss of the normal internal architecture. The patient's habitual seizures were found to arise from the left mesial temporal lobe. Neuropathological evaluation following surgical resection revealed hippocampal sclerosis.

The sensitivity of MRI for HS can be increased by the use of quantitative MRI techniques. Hippocampal atrophy can be quantified by measurement of whole hippocampal volumes and the degree of hippocampal volume loss is correlated with the extent of neuronal loss in the hippocampus (146). Furthermore, T2 hyperintensity may be quantified by measurement of

T2 relaxometry (147), which correlates with the extent of astrocytic gliosis in resected hippocampal specimens (148). Interestingly, while early studies reported a very high (97%) sensitivity of MRI for HS (149), more recent studies suggest this is not the case (150). Bell et al. reported 40 patients with MTLE, all of whom had normal qualitative high resolution MRI and whole hippocampal volumetry (150). They found HS upon pathological analysis in 7/40 patients, suggesting that state-of-the art MRI with quantification misses this diagnosis in approximately 17% of cases (150). This finding supports the future development of advanced MRI techniques to improve the non-invasive diagnosis of HS.

Multiple studies have subsequently confirmed Penfield's original finding that surgical treatment is beneficial for patients with drug resistant epilepsy (151). In 2001, over 60 years following Penfield's initial series, the first randomized controlled trial (RCT) of temporal lobectomy for MTLE was published (152). In this study, patients who underwent surgery were far more likely to achieve seizure freedom (58%) than those treated medically (8%) (152). Subsequent studies have demonstrated that surgical treatment reduces mortality in patients with drug resistant epilepsy (153). Furthermore, the effect of surgery is durable over time, with approximately 50% of patients remaining seizure-free 10 years following temporal lobectomy (154). However, these data also emphasize the remarkably consistent finding across previous series that only approximately 50-60% of patients with MTLE achieve seizure freedom from surgery. This finding has prompted previous authors to investigate whether more rigorous patient selection may enable surgical outcomes to be improved (6). Furthermore, as discussed in the next section, neuropathological data suggest that different MTLE subtypes have distinct prognoses for surgical cure (8).

Chapter 4 Mesial temporal lobe epilepsy subtypes

Recent studies suggest that mesial temporal lobe epilepsy (MTLE) consists of distinct disease subtypes which have different pathological characteristics and clinical features. In this chapter, we review the evidence for MTLE subtypes and what is currently known about each form of the disease. We highlight the current knowledge gaps in our understanding of MTLE subtypes and emphasize the findings which have been discordant between studies. We then discuss several limitations of surgical neuropathology studies in the evaluation of MTLE subtypes. Finally, we explain why in vivo diagnosis holds potential to improve our current understanding of these conditions.

4.1 Pathological characteristics

MTLE subtypes are defined by the presence or absence of hippocampal sclerosis (HS) in specific hippocampal subfields. The histological features of HS include neuronal cell loss [identified by staining with neuronal nuclear antigen (NeuN) (155)] and astrocytic gliosis [identified by immunohistochemistry for glial fibrillary acid protein, GFAP (5)].

ILAE Type 1 HS The neuropathological findings of classical HS were first described by Sommer (103). Classical HS is characterized by neuronal loss which is most prominent in CA1 but also evident in CA3 and CA4 (103). In contrast, there is relative sparing of the CA2 subfield in classical HS (156).

Classical HS is now known as International League Against Epilepsy (ILAE) Type 1 HS (5) and we therefore use this terminology throughout the remainder of this thesis

ILAE Type 2 HS This subtype is defined pathologically by neuronal loss and gliosis restricted to the CA1 subfield with sparing of CA4, and was therefore initially termed "CA1 Predominant HS" (157). As this entity is now known as Type 2 HS (5), this term is used for "CA1 Predominant HS" in the remainder of this thesis.

ILAE Type 3 HS Margerison and Corsellis were the first to describe the pathological findings of a distinct MTLE subtype, which they called 'end folium sclerosis', in patients with chronic epilepsy (15). They identified neuronal loss and gliosis restricted to the CA4 region (also known as the end folium) in a subset of patients with MTLE who underwent autopsy (15). This entity is now known as ILAE Type 3 HS (5), and we will therefore use this term to denote 'end folium sclerosis' throughout the remainder of this thesis.

No HS As discussed in chapter 3, early neuropathology studies documented that some patients with MTLE were found to have a normal hippocampus following surgical resection (106). This entity is termed no hippocampal sclerosis with gliosis only (No HS) in the current ILAE classification system (5).

Reliability One previous study has examined the inter-rater reliability of HS subtype classification according to the ILAE system (5). Several iterations of neuropathological assessments were performed in order to develop a consensus

classification system (5). The final iteration involved classification of 30 HS specimens by 10 independent neuropathologists. Reliability data [kappa statistics (158)] were reported for Type 1 HS (0.71), Type 2 HS (0.63), Type 3 HS (0.78), and No-HS (0.91) (5). These data demonstrate that HS subtype classification according to the ILAE scheme is reproducible between neuropathologists and support the use of this system to explore clinico-pathological correlations in patients with MTLE (5).

4.2 Prevalence

As discussed above, Margerison and Corsellis were the first to describe clinico-pathologic subtypes of MTLE (15). These authors studied 55 patients with chronic epilepsy who subsequently underwent autopsy (15). They identified 26 patients with clinically definite MTLE and found 18/26 cases (70%) of Type 1 HS, 4/26 cases (15%) of Type 3 HS, and 4/26 cases (15%) of No HS. The patients included in this study were from a long-stay hospital for patients with intellectual disability and thus were different from patients with MTLE typically evaluated for epilepsy surgery (15).

The study by Margerison and Corsellis provided initial evidence suggesting that Type 1 HS is the most common subtype of MTLE (15). Further studies have shown that this is also the case in patients with MTLE who undergo epilepsy surgery. Several surgical series have demonstrated that Type 1 HS is the most common MTLE subtype. Type 1 HS is identified in 60-80% of surgical specimens from patients with MTLE who are treated with epilepsy surgery (4, 8, 157, 159-164). As discussed in chapter 3, No HS is also a common histological finding in surgical specimens from subjects with MTLE. Indeed, No HS is the final diagnosis in 10-20% of patients with MTLE who

undergo temporal lobectomy (4, 8, 157, 162, 163, 165) making this the second most common histological finding in subjects with MTLE. The prevalence of Type 2 HS has varied significantly across surgical series. However, many studies have found this to be the third most common pathological subtype - representing approximately 5-15% of HS specimens (4, 8, 157, 163, 166, 167). Finally, Type 3 HS represents the rarest HS subtype and is found in 1-5% of surgical specimens from subjects with MTLE (4, 8, 159, 163, 168).

The data summarized above represent the prevalence of HS subtypes in patients with MTLE who undergo temporal lobectomy. As HS subtypes can only be diagnosed following surgical resection, the true prevalence of the various MTLE subtypes remains unknown. There is increasing recognition that not all patients with MTLE develop drug resistant epilepsy (169). It is possible that patients with Type 2 HS and Type 3 HS have a more benign disease course than those with Type 1 HS (169), which would potentially explain the lower prevalence of these subtypes in surgical series.

4.3 Clinical features

Several lines of clinical evidence also support the hypothesis that MTLE consists of multiple disease subtypes. Firstly, the pathogenesis of MTLE appears to differ between patients. An initial precipitating injury (IPI) is believed to play a causative role in many patients with this condition (39). However, the cause remains unknown in the significant proportion (approximately 30%) of MTLE patients with no history of IPI. Secondly, only 50% of patients with MTLE achieve seizure freedom following temporal lobectomy (154) suggesting that many patients have epileptic networks extending beyond the anterior temporal lobe. These findings support the

hypothesis that MTLE is a heterogeneous syndrome with significant variability between patients. In this section, we summarize the evidence that suggests MTLE subtypes are distinct clinico-pathological entities.

Initial Precipitating Injury

Previous IPI Several studies have suggested that the likelihood of a prior IPI varies according to MTLE subtype. A history of an IPI can be obtained from 50-80% of patients with Type 1 HS (4, 8, 163, 165, 167, 170). The incidence of an IPI was initially believed to be lower in patients with No HS (8), but subsequent reports have found a similar likelihood of prior IPI in patients with No HS and Type 1 HS (4, 163). Likewise, Type 2 HS appears to be associated with a high probability of prior IPI. The percentage of Type 2 HS patients with a prior IPI has varied between 40-90% in reported series (4, 8, 163, 165). In contrast, most reported surgical series have found a low incidence of IPI (0-20%) in patients with Type 3 HS (8, 163, 170). However, not all reports have demonstrated a lower rate of IPI in patients with Type 3 HS. One study found that 100% of 53 patients with Type 3 HS had a prior history of IPI (4). Therefore, the relationship between MTLE subtype and prior IPI remains unclear from the current literature.

Febrile seizure IPI Several types of IPIs (e.g. perinatal anoxia, traumatic brain injury, and central nervous system infection) have been associated with MTLE. However, febrile seizures are the most common type of IPI (102). Approximately 50-60% of patients with Types 1-3 HS have a history of a complex febrile seizure (4, 161, 163, 165). In contrast, febrile seizures are documented in only 0-5% of patients with a histological finding of No HS (8,

163, 167). This is consistent with earlier studies which also demonstrated a lower rate of febrile seizures in subjects with No HS (102).

As discussed in chapter 3, prolonged febrile seizures are thought to be causally related to HS (39). Indeed, patients with HS demonstrate morphological changes of the hippocampus (e.g. mossy fiber sprouting and granule cell dispersion) similar to those documented in animal models of status epilepticus (36, 45, 47). However, the data summarized above reveal several gaps in our current understanding of the causes of MTLE. Firstly, only approximately 50-60% of patients with HS have a previous history of complex febrile seizures. The etiology of HS in patients with no history of complex febrile seizures or other IPIs remains unknown. Furthermore, the lower incidence of febrile seizures in patients with No HS suggests that different etiologies are involved in patients with this entity. Further clinico-pathological studies of MTLE subtypes are thus essential to improve our understanding of the relationship between complex febrile seizures and MTLE.

Age at IPI Significant anatomical and physiological changes occur in the human brain throughout the first two decades of life. Therefore, it is possible that an IPI at a young age could result in different morphological changes in the hippocampus compared with an IPI at a later age. This could be reflected by distinct MTLE subtypes according to the age at which an IPI occurs. Only two studies have reported age at IPI in MTLE subtypes (4, 8). Both studies demonstrated a young age (1.8-2.5 years) at IPI in patients with Type 1 HS.

However, the two studies produced discordant results for the remaining MTLE subtypes (4, 8). Blumcke et al. described an older age at IPI for patients with Type 2 HS (6 years) and No HS (16 years), and also found that none of

their seven patients with Type 3 HS had any history of IPI (8). In contrast, Thom et al. found a similar age at IPI for patients with Type 1 HS (1.8 years), Type 2 HS (1.8 years), Type 3 HS (2.4 years), and No HS (1.2 years) (4). However, as only two studies have reported age at IPI across subtypes this characteristic remains incompletely explored in patients with MTLE.

Duration of latent period The latent period refers to the period of time between the IPI and the onset of habitual seizures. During this time it is believed that morphological changes, which promote further seizures, occur in the hippocampus (39). It is therefore possible that patients with a longer latent period develop a distinct pattern of morphological changes (reflected by different MTLE subtype patterns) in comparison to patients with shorter latent periods. Indeed, two studies have suggested that the duration of the latent period may differ between MTLE subtypes (4, 163). These studies both found that Type 1 HS was associated with a latent period of approximately 6 years. In contrast, patients with Type 3 HS were shown to have a longer latent period between 15-17 years (4, 163). The latent period was also found to be longer (11-17 years) in patients with a histological diagnosis of No HS (4, 163).

These observations support the hypothesis that specific MTLE subtypes are associated with different durations of the latent period, which may have relevance to the underlying pathogenesis of these conditions. In particular, these findings suggest that patients with Type 1 HS develop clinical seizures more rapidly following an IPI than those with Type 3 HS and No HS. This raises the possibility that Type 1 HS is capable of producing spontaneous epileptiform activity more readily (i.e. is more 'epileptogenic') in comparison with Type 3 HS and No HS.

However, the duration of the latent period associated with Type 2 HS remains unclear from previous studies (4, 163). Thom et al. found a similar duration for the latent period in subjects with Type 2 HS (4.1 years) compared with those with Type 1 HS (6.1 years) (4). In contrast, Coras et al. found that patients with Type 2 HS (13.5 years) had a longer latent period than those with Type 1 HS (6 years). Therefore, the relationship between MTLE subtype and latent period duration also requires further investigation with future studies.

Clinical course

Age of habitual seizure onset As discussed in chapter 3, most patients with congenital brain lesions *do not* develop seizures at birth. For example, patients with focal cortical dysplasia develop seizures at a mean age of 6 years (18). This observation is consistent with the idea that epileptic networks take time to develop (or 'mature') in patients with structural brain lesions. Therefore, the age of habitual seizure onset is considered an important characteristic of MTLE subtypes. Indeed, several studies have demonstrated that patients with No HS have the latest age of onset (15-20 years) amongst the various MTLE subtypes (8, 163, 164, 167). Furthermore, Type 1 HS is consistently associated with the earliest (4-9 years) age of habitual seizure onset (4, 8, 157, 161, 163, 164, 168, 171). This finding suggests a difference in the 'maturation' of epileptic networks between MTLE patients with Type 1 HS and No HS. As discussed above, these data are consistent with the hypothesis that Type 1 HS is a more 'epileptogenic' MTLE subtype than No HS.

In the original paper by Margerison and Corsellis, patients with Type 3 HS were found to have a later age of seizure onset (mean = 16 years) compared to patients with classical HS (mean = 6 years). Indeed, multiple subsequent

studies have confirmed that Type 3 HS is associated with a later age of onset in comparison with other MTLE subtypes. The age of habitual seizure onset for patients with Type 3 HS has consistently been in the 14-19 year age range across studies (4, 8, 163, 168). These findings are consistent with Margerison and Corsellis' observations that "whereas an early onset of fits is likely to be associated with the presence of a classical Ammon's horn sclerosis (Type 1 HS)...those patients with a later onset tend to show...damage restricted to a single area...the lesion itself consisting of an end folium sclerosis (Type 3 HS)" (15). The similar age of onset for patients with Type 3 HS and No HS suggests that these entities might share similar underlying etiologies and pathogenesises.

However, whether patients with Type 2 HS have a different age of onset in comparison to those with other MTLE subtypes remains unclear. The age of habitual seizure onset reported for Type 2 HS (5-17 years) has varied significantly across studies (4, 8, 157, 161, 163, 165, 167). Therefore, further studies are required to improve our understanding of the age of onset in patients with Type 2 HS.

Duration of epilepsy prior to surgery Previous reports have suggested that progression of anatomical changes occurs over time in patients with MTLE (172). It is therefore possible that patients with a longer disease duration prior to surgery may manifest a more severe, or more extensive, pattern of hippocampal abnormalities. In contrast, those patients with a shorter disease duration might be expected to show milder, or more restricted, hippocampal neuronal loss. Indeed, several studies have suggested that Type 1 HS, in which the histological changes are the most extensive, is associated with the longest duration of intractable epilepsy (24-28 years) (4, 8, 157, 161, 163, 165, 167). In contrast, a histological finding of No HS appears to be associated with the

shortest duration (9-18 years) of epilepsy prior to surgical resection (8, 163, 164, 167, 171).

These findings raise the interesting possibility that Type 1 HS might represent the final common pattern of pathology associated with a prolonged duration of recurrent seizures prior to surgery. In contrast, No HS could be considered the earliest and mildest form of MTLE in which neurophysiological changes are present but neuronal loss is not yet appreciable with histological analysis.

Interestingly, Type 3 HS is consistently associated with an intermediate duration of epilepsy prior to surgery of 14-17 years (4, 8, 163, 170). This is a longer disease duration than is typically seen in patients with No HS (mean = 12 years). In contrast, this is shorter than the duration of epilepsy prior to surgery identified in most subjects with Type 1 HS (mean = 26 years). These data suggest that Type 3 HS might represent an intermediate form of pathology on a continuum between No HS and Type 1 HS. As discussed below, this hypothesis cannot presently be tested as the hippocampus can only be evaluated at one time point (the time of temporal lobectomy) in surgical neuropathology series.

However, whether Type 2 HS also represents a milder form of pathology between No HS and Type 1 HS remains unclear. Type 2 HS has been identified in patients with a broad range of disease durations (6-30 years) prior to surgery (4, 8, 157, 161, 163, 165, 167, 170). Therefore, the hypothesis of atypical HS subtypes as intermediate phenotypes between No HS and Type 1 HS requires further study.

Surgical outcome The likelihood of surgical cure following temporal lobectomy provides critical information regarding the anatomical substrates of epilepsy in patients with MTLE. Sustained seizure freedom suggests that the structures removed were "necessary and sufficient" for the generation of recurrent seizures (115). In contrast, lower rates of seizure freedom following temporal lobectomy imply an epileptic network which includes additional structures beyond the anterior temporal lobe. Previous studies have consistently demonstrated that patients with Type 1 HS have a higher likelihood of surgical cure than those with no HS. The percentage of patients with Type 1 HS who achieve seizure freedom is approximately 70-90% (4, 8, 157, 161, 163-168). In contrast, only 40-60% of patients with No HS are rendered seizure-free following surgery (4, 8, 157, 163, 164). These findings are consistent with previous studies demonstrating that MRI evidence of HS is predictive of a higher likelihood of seizure freedom following epilepsy surgery (149, 173). However, they also strongly support the notion that many patients with MTLE but No HS can achieve seizure freedom with epilepsy surgery (150). Preoperative methods that detect those subjects with No HS who will achieve seizure freedom with temporal lobectomy are therefore urgently needed.

In their seminal paper, Margerison and Corsellis were the first to suggest that atypical pathological findings might have an impact on the likelihood of surgical cure: "In the present study, end folium sclerosis (Type 3 HS) could be seen as an isolated lesion when the prognosis following lobectomy might be expected to be particularly *favourable*" (15). However, whether patients with atypical forms of MTLE (Type 2 and Type 3 HS) have a different prognosis from those with Type 1 HS remains unclear from the current pathological literature. The prognosis for these forms of HS has varied dramatically across previous studies. Patients with Type 2 HS have been

reported to have a 30-90% likelihood of being seizure-free following surgery (4, 8, 157, 161, 163, 165-167, 170), while those with Type 3 HS have been shown to have a 25-100% chance of achieving seizure freedom (4, 8, 163, 168, 170). Therefore, the prognostic significance of a Type 2 HS or Type 3 HS diagnosis remains unclear from the surgical neuropathology literature.

4.4 Limitations of surgical series

Surgical neuropathology studies have provided initial evidence that MTLE consists of distinct disease subtypes (5). However, these studies have also produced discordant findings for a number of clinical variables (discussed above). Indeed, assessment of surgical specimens obtained during epilepsy surgery only enables evaluation of *a portion* of the *ipsilateral* hippocampus at a *single point in time*. In this section we consider the limitations of this approach and suggest that these limitations may explain the discordant results reported in the current literature.

Long axis variability of HS As discussed in chapter 2, the hippocampus demonstrates significant anatomical variation along its longitudinal axis (13). In surgical pathology series, only *a portion* of the hippocampal body is available for HS subtype classification (5). However, an autopsy study has shown that HS subtype patterns demonstrate significant variability along the hippocampal long axis (136). In this study of patients with chronic epilepsy, Thom et al. found that the pattern of HS was consistent along the longitudinal axis in only 30% of hippocampi (136). It is important to recognize that, as with the Margerison and Corsellis study (15), Thom et al. examined a cohort of patients with chronic epilepsy which may differ from those with MTLE who present for epilepsy surgery. However, Thom et al. did include one patient with

MTLE who could be considered representative of those patients included in surgical pathology series (136). Interestingly, this patient demonstrated bilateral HS with significant variability along the longitudinal axis on both sides (136). These results collectively suggest that variability of HS along the hippocampal long axis may represent a potential explanation for the discordant results obtained from prior surgical neuropathology studies.

Bilateral HS Margerison and Corsellis also recognized that HS is frequently present bilaterally in patients with chronic epilepsy (15). In their autopsy cohort of 36 patients with HS, 17 (47%) demonstrated bilateral hippocampal abnormalities (15). Subsequent quantitative neuropathology studies have confirmed that bilateral HS can also be identified in patients with MTLE (Figure 4.1) (174).

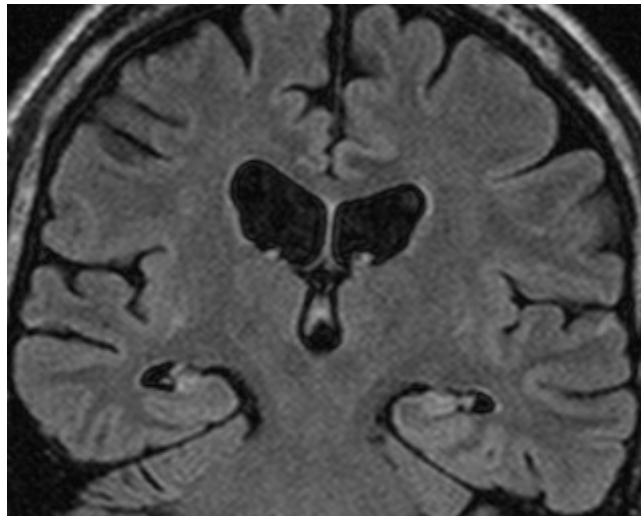


Figure 4.1 - Bilateral hippocampal sclerosis

A coronal T2-weighted FLuid-Attenuated Inversion Recovery (FLAIR) Image is shown from a patient with drug resistant epilepsy. The hippocampi are severely atrophic and demonstrate increased T2 signal bilaterally, consistent with a diagnosis of bilateral hippocampal sclerosis.

Indeed, patients with MTLE and 'unilateral' HS typically demonstrate bilateral white matter abnormalities (19). Furthermore, the presence of bilateral hippocampal atrophy (detected with quantitative MRI) is predictive of a poor outcome following temporal lobectomy (175). Therefore, a comprehensive evaluation of MTLE subtypes would ideally also include assessment of the 'contralateral' hippocampus. However, the hippocampus can only be resected unilaterally as bilateral resection results in catastrophic memory loss (17). As a result, evaluation of MTLE subtype in the contralateral hippocampus is currently only possible post-mortem (136). These factors emphasize the need for neuroimaging techniques which would enable MTLE subtype classification of the 'contralateral' hippocampus and may provide useful information regarding surgical prognosis.

Progression over time As discussed above, surgical series cannot evaluate whether MTLE subtypes demonstrate progression over time. However, the results of several MRI studies suggest that MTLE is a progressive disease. Whole hippocampal volumetry demonstrates an increase in hippocampal atrophy over time in patients with MTLE (176). Furthermore, atrophy appears to worsen over time in other mesial temporal structures, including the entorhinal cortex and amygdala (177). In addition, progressive gray matter loss outside of the mesial temporal lobe has been demonstrated in patients with MTLE (172, 178). These findings raise the intriguing possibility that MTLE subtypes may evolve in a given patient over time. Indeed, a recent study has demonstrated progressive changes in hippocampal subregions over time using surface-based analysis (179). These findings encourage the future development of MRI methods which enable in vivo diagnosis of MTLE subtypes.

4.5 Rationale for in vivo diagnosis

In vivo MRI holds potential to transform our current understanding of MTLE subtypes by enabling preoperative diagnosis of these conditions. Furthermore, preoperative MRI could potentially enable the use of MTLE subtype diagnosis to guide surgical decision-making. In this section, we outline the potential research and clinical applications of preoperative MTLE diagnosis.

Prospective evaluation As discussed above, our current understanding of MTLE subtypes is based primarily on surgical series. However, there is increasing recognition that not all patients with MTLE develop drug resistant epilepsy requiring surgical treatment. In the absence of methods for preoperative diagnosis, whether some MTLE subtypes have a relatively benign disease course will therefore remain unclear. Furthermore, MTLE subtypes cannot currently be studied at multiple time points. As a result, whether these conditions exist on a continuum of severity, with worsening over time, remains unknown. In vivo MRI-based analysis of MTLE subtypes holds promise to address these questions by allowing preoperative diagnosis.

Bilateral MTLE subtype diagnosis Several studies have demonstrated that HS is a bilaterally asymmetric process. Since hippocampal resection can only be performed unilaterally, the hippocampus 'contralateral' to the resection (which is left intact) is highly likely to contribute to surgical failures following temporal lobectomy. In vivo MRI could enable diagnosis of MTLE subtypes in the 'contralateral' hippocampus, which is currently impossible, and therefore improve our ability to predict surgical outcomes in patients with MTLE.

Evaluation of hippocampal long axis Autopsy studies strongly suggest that HS demonstrates variability along the hippocampal long axis. However, surgical series enable assessment of only a small portion of the hippocampal body. In contrast, in vivo MRI would allow evaluation of MTLE subtypes along the entire longitudinal axis of the hippocampus and could potentially resolve current controversies regarding the clinical implications of MTLE subtype diagnoses.

Patient management The development of MRI methods to characterize MTLE subtypes holds promise to inform the clinical management of patients with this condition. At present, unselected patients with MTLE have a 50-60% likelihood of becoming seizure-free following temporal lobectomy. However, surgical series consistently demonstrate that patients with Type 1 HS have a 70-90% chance of achieving seizure freedom. Unfortunately, this information cannot currently be used to guide surgical decision-making. Preoperative diagnosis of MTLE subtypes with in vivo MRI, however, could potentially allow these data to be used to counsel patients contemplating surgery for drug resistant epilepsy.

Chapter 5 In vivo MRI of MTLE

In vivo MRI holds tremendous potential to allow non-invasive preoperative diagnosis of mesial temporal lobe epilepsy (MTLE) subtypes. High resolution MRI of the hippocampus allows visualization of the hippocampal internal architecture in controls and subjects with MTLE. This allows segmentation and volumetric measurement of the specific hippocampal subfields which define MTLE subtypes. These methods have been used to characterize specific subfield involvement in subjects with HS. Furthermore, some studies suggest that subregional volumetry detects specific subfield involvement in patients thought to have No HS based on conventional imaging. Recent studies have defined the histological correlates of these MRI findings suggesting that in vivo measurements provide useful information regarding tissue microstructure. In this chapter, we review the previous studies that support the hypothesis that MTLE subtypes can be diagnosed preoperatively with in vivo MRI.

5.1 Hippocampal subfield imaging

The hippocampal internal architecture is partially visible on high resolution MR Images acquired at 1.5 tesla (standard magnetic field strength for clinical MRI) (145). However, acquisition of MRI at ultra-high field ($> 3T$) results in dramatically improved spatial resolution and better contrast between grey and white matter (180). This enables clear visualization of several anatomical landmarks of the hippocampus (alveus, stratum lacunosum moleculare [SLM], and dentate gyrus [DG]) in control subjects (180).

Disruption of the normal hippocampal internal architecture is a cardinal sign of hippocampal sclerosis (HS) which is detected in many patients with MTLE upon qualitative analysis of 1.5 T MRI (144). However, recent 3 T MRI studies have clearly demonstrated that the internal landmarks of the hippocampus remain visible in subjects with radiologically apparent HS (7). Eriksson et al. evaluated high resolution (0.53 X 0.53 X 2 mm) T2 images in 4 patients with radiographically apparent HS (7). Furthermore, they correlated the MRI findings with histopathological evaluation (which revealed Type 1 HS in each case) (7). The MR Images revealed an internal lamina of low signal (in many studies known as the "dark band"). Histopathological examination with luxol fast blue (LFB) staining confirmed that this region of hypointense signal corresponds to the myelinated fibers of SLM (7). Eriksson et al. demonstrated that the SLM remains visible in subjects with HS and delineates the DG (located mesial to the SLM) from the cornu ammonis (located lateral to the SLM) (7). They also provided a qualitative description of subfield abnormalities in patients with HS. Atrophy and T2 hyperintensities were identified in the cornu ammonis and DG subregions in each subject (7). Furthermore, the regions of T2 hyperintensity were shown to represent areas of gliosis (identified by histological analysis of GFAP staining) (7). These results demonstrated, for the first time, that subfield abnormalities could be detected in subjects with MTLE using in vivo MRI.

5.2 Manual hippocampal subfield volumetry

Mueller et al. were the first to quantify subfield pathology in subjects with MTLE using in vivo MRI (10). They used 4 T MRI to acquire high resolution (0.4 X 0.4 X 2 mm) MR Images of the hippocampus in 34 controls, 15 MTLE

patients with HS, and 18 MTLE patients with No HS (10). Hippocampal subfields (entorhinal cortex [ERC], subiculum [SUB], CA1, CA2, CA3, and CA3&DG) were measured on 5 slices (10 mm) of the anterior hippocampal body (10).

Mueller et al. demonstrated subfield-specific atrophy patterns in subjects with HS. In comparison to controls and MTLE patients with No HS, patients with HS had lower volumes for ERC, SUB, CA1, CA2, and CA3&DG subfields (10). Furthermore, atrophy was found to be more severe (signified by lower Z scores) at the CA1 and CA3&DG regions in comparison to ERC, SUB, and CA2 (10). This pattern was consistent with the pathological pattern of HS, which demonstrates greatest severity of neuronal loss in CA1 (103) but relative sparing of the CA2 subfield (156) and SUB (54). Interestingly, Mueller et al. found that individual patients with HS demonstrated distinct patterns of subfield involvement (10). Four patterns of HS were identified: global atrophy of all hippocampal subfields (in 6 patients), CA1 and CA3&DG volume loss (in 5 patients), selective involvement of CA1 (in 2 patients), and isolated atrophy of CA3&DG (in 1 patient) (10). Correlation with histopathological MTLE subtypes was not possible in this study as only a subset of patients subsequently had surgery. However, this seminal paper provided initial evidence that in vivo MRI detects subfield-specific volume loss in patients with MTLE.

Furthermore, Mueller et al. identified subtle subfield abnormalities in a subset of their 18 patients deemed to have No HS based on normal qualitative analyses and whole hippocampal volumetry. Three (17%) of these patients were found to have subtle changes (one in the contralateral SUB, one in CA3&DG bilaterally, and one in the ipsilateral ERC and SUB) in various subfields. These findings suggest that subfield volumetry may provide

additional information to conventional imaging regarding the anatomical changes present in patients with MTLE.

Subsequent studies have confirmed these findings using both 3T and 7T MRI. Na et al. correlated 3T MRI-based volumetry of the CA4/DG region with histopathology in 39 MTLE patients with HS (181). They identified 21 patients with DG pathology and 18 subjects with a normal DG based on pathological evaluation of resected hippocampal specimens (181). The patients with DG pathology were found to have lower CA4/DG volumes on MRI, suggesting a relationship between MR-defined subfield atrophy and subregional pathological changes (181).

Henry et al. confirmed Mueller's observation that individual patients demonstrate different patterns of subfield-specific atrophy (182). In this study, 7T MRI (resolution 0.25 X 0.25 X 1.2 mm) was performed in 11 controls and 8 MTLE patients with HS based on clinical MRI scans (182). Measurements were obtained for CA1-CA3 and CA4&DG regions throughout the entire hippocampal body (182). Three patterns of subfield-specific volume loss were identified: atrophy of both CA1-CA3 and CA4/DG (in 1 patient), atrophy of CA1-CA3 only (in 6 patients), and volume loss restricted to the CA4&DG region (in 1 patient) (182). However, these MRI findings were not correlated with pathological analysis of resected hippocampal specimens (182).

Evaluation of reliability is an important aspect of the manual hippocampal segmentation literature. *A single investigator* performs segmentations of the same hippocampi on two separate occasions in order to determine *intra-rater* reliability. *A second investigator* then segments the same subjects to enable evaluation of *inter-rater* reliability. The level of agreement between

segmentations can be assessed using two measures: the intra-class correlation coefficient (ICC) and the dice similarity coefficient (DSC).

The ICC (183) is used to determine the level of agreement between *volume measurements* obtained from repeated segmentations of the same subfield across trials. It is calculated using the formula: $ICC = \frac{Sb^2}{Sb^2 + Sw^2}$, where Sb : between-subjects variance and Sw : within-subject variance. The value for ICC ranges from 0 (no agreement) to 1 (perfect agreement).

In contrast, the DSC determines the *degree of spatial overlap* between segmentations at the voxel level (184), calculated as: $DSC = \frac{2 TP}{2 TP + FP + FN}$, where TP : True Positives (voxels labelled in both segmentation trials), FP : False Positives (voxels not labelled in trial 1, but 'falsely' labelled in trial 2), and FN : False Negatives (voxels labelled in trial 1, but 'falsely' not included in trial 2). The value for DSC ranges from 0 (no overlap) to 1 (perfect overlap).

5.3 Automated hippocampal subfield volumetry

Manual hippocampal subfield volumetry is time-consuming (requiring several hours for a single hippocampal segmentation by an experienced investigator), requires advanced knowledge of hippocampal neuroanatomy, and is associated with a steep learning curve (requiring approximately 3-6 months of dedicated training). As a result, several studies have investigated the ability of automated subfield segmentation protocols to detect subregional changes in patients with MTLE. In this subsection, we review the findings of automated hippocampal subfield volumetry studies performed to date in subjects with MTLE.

Freesurfer (185), an open source software for MRI analysis, has been used by several investigators to segment hippocampal subfields in subjects with MTLE (186-188). Schoene-Bake et al. performed automated subfield segmentation (189) of volumetric T1 MR Images (resolution 1 X 1 X 1 mm) acquired on a 3 tesla MRI system (188). They found that patients with MTLE (n=82) had lower mean volumes of several subfields (CA1, CA2-CA3, CA4-DG, and SUB) in comparison to healthy controls (n=81) (188). These results were replicated by Bin Kim et al., who applied an identical methodology in a cohort of 47 subjects with MTLE and 41 controls (187). Jardim et al. applied the same segmentation protocol (189) to 1.5 T volumetric T1 MR Images (resolution 1 X 1 X 1 mm) from 62 subjects with MTLE and demonstrated a significant correlation between subregion volumes and neuronal densities in the CA1, CA3, and CA4 subfields (186). Sone et al. applied two automated methods (190, 191) to measure hippocampal subfields on high resolution (voxel size 0.43 X 0.43 X 2 mm) T2 MR Images acquired at 3 tesla (192). They identified maximal atrophy at the CA1 and CA4/DG subfields in 25 MTLE patients with HS in comparison to 25 subjects with No HS and 45 healthy controls (192). Collectively, these studies suggest that automated segmentation methods detect subfield atrophy in patients with HS. However, these studies did not detect significant volume loss in patients with No HS. In contrast, some manual volumetry studies have detected abnormalities in patients with No HS in comparison to healthy controls.

5.4 Findings in MTLE patients with No HS

Mueller et al. provided preliminary evidence that some patients with No HS (based on whole hippocampal volumetry) demonstrate subregional atrophy

when analyzed with hippocampal subfield volumetry (10). Two studies have subsequently replicated these findings with independent patient cohorts across a range of magnetic field strengths (193, 194). Staba et al. studied 10 patients with high resolution (voxel size 0.4 x 0.4 x 3 mm) T2-weighted MR Imaging performed at 3 tesla (194). Separate measurements were made for several hippocampal subfields (ERC, SUB, CA1, and CA2/CA3/DG) and compared to volumes obtained from 13 healthy controls (194). They found that patients with MTLE demonstrated reduced volumes of the ERC, SUB, and CA2/CA3/DG subfields (194). The authors postulated that their patients demonstrated a different pattern of atrophy (with sparing of CA1) than expected because their cohort included only 2 patients with histologically confirmed HS (194).

Santyr et al. performed high resolution (voxel size 0.5 x 0.5 x 1.5 mm) imaging at 7T in a cohort of 9 patients with MTLE and No HS (193). Subfield measurements (SUB, CA1, CA2/CA3, and CA4/DG) were performed manually and compared to the same measures obtained from 20 healthy controls (193). They found that 3 (33%) of their patients with No HS manifested subregional atrophy that was not detected with whole hippocampal volumetry (193). Interestingly, one patient demonstrated a classical pattern of subfield atrophy (volume loss in CA1 and CA4/DG) which was identical to that seen in their cohort of 4 MTLE patients with HS (193). In contrast, two patients showed atrophy of CA2/CA3 contralateral to the seizure focus (193). These results suggest that subfield-specific atrophy in MTLE differs between patients, emphasizing the importance of individualized assessment of hippocampal subfield measurements in patients with this condition.

5.5 Relationship to memory dysfunction

As discussed in chapter 2, the hippocampus plays a critical role in learning and memory (17). Furthermore, the hippocampus demonstrates pathological changes in the majority of patients with MTLE (4, 8, 163). As a result, memory dysfunction is common finding in patients with MTLE (195). In addition, computational models (30) and animal experiments (26) suggest that hippocampal subfields perform specific roles in normal memory function. Therefore, recent studies have investigated whether distinct hippocampal subregions are involved in memory dysfunction in patients with MTLE (196, 197).

Mueller et al. measured subfield volumes (ERC, SUB, CA1, CA1-CA2, and CA3&DG) in 22 controls, 18 MTLE patients with HS, and 25 MTLE patients with No HS (196). In patients with HS, atrophy of CA3/DG was associated with neuropsychological deficits in memory encoding (196). In contrast, volume loss in CA1 was correlated with deficiencies in memory retrieval and recognition memory (196). These findings suggest that dysfunction of the CA3/DG region may be responsible for memory encoding deficits in patients with MTLE.

This hypothesis was evaluated in an fMRI study of memory encoding performed by Das et al. (197). In this study, fMRI activation of specific hippocampal subfields was compared between 18 patients with MTLE and 19 healthy controls (197). MTLE patients demonstrated reduced activation of the CA3/DG subfield during memory encoding in comparison with healthy controls (197). These findings suggest that specific hippocampal subfields mediate different aspects of memory dysfunction in patients with MTLE. This provides further support for the importance of characterizing subfield pathology in

patients with MTLE. However, as pathological data were not available in these patients the histological correlates of the specific subfield involvement demonstrated in these studies has remained unclear.

5.6 Histological correlates of MRI findings

Recent studies have examined the correlation between in vivo MRI findings and histopathological data (9, 198). Kwan et al. found that qualitative 7T MRI interpretations and pathological diagnoses were concordant in 7/10 patients with MTLE who underwent surgery (198). Goubran et al. performed a detailed analysis of the histopathological and MRI correlates of MTLE which included 3T in vivo MRI, 7T in vivo MRI, and 9.4T ex vivo MRI (9). In vivo MRI, ex vivo MRI, and postoperative histology were coregistered using a recently described methodology (199). MRI metrics included subfield volumes, quantitative T1, quantitative T2, and diffusion tensor imaging. Furthermore, quantitative histological methods were used (quantitative field fraction of NeuN and GFAP; neuron size) to determine the pathological correlates of MRI measurements (9). Subfield volumes (CA1, CA2/CA3, and CA4/DG) were correlated with neuronal densities in the same regions, as previously shown using stereological methods (168). In addition, quantitative T2 was correlated with quantitative field fraction of GFAP in CA1, providing further support for the hypothesis that T2 hyperintensity reflects astrocytic gliosis (148). Interestingly, mean diffusivity was negatively correlated with neuronal density in CA4/DG, suggesting that neuronal loss in HS is accompanied by less sequestration of water within neurons resulting in an overall increase in water diffusion (9). Furthermore, quantitative T1 was found to negatively correlate with neuronal density and neuronal size in the CA4/DG region. The authors

postulate that this may relate to reduced intracellular water as a consequence of cell loss in HS (9). These findings suggest that quantitative MRI holds significant potential to further clarify the microstructural characteristics of subfield involvement in subjects with MTLE.

5.7 Preoperative diagnosis of MTLE subtypes

The findings of previous studies (summarized above) support the hypothesis that MTLE subtypes can be diagnosed noninvasively with in vivo MRI. Indeed, a recent qualitative 7T MRI study has provided initial evidence that this is the case (200). Stefanits et al. studied 13 patients with MTLE who eventually underwent surgical resection of the hippocampus for treatment of epilepsy (200). MTLE subtypes were determined pathologically according to the ILAE classification criteria (5). They identified 6 patients with Type 1 HS, 2 with Type 2 HS, and 5 with No HS. Preoperative 7T MRI (resolution 0.33 x 0.33 x 1.5) was performed in each subject and images were evaluated by four independent neuroradiologists (200). Each radiologist designated a predicted MTLE subtype based on qualitative evaluation of the preoperative MRI scan (200). These authors found that all four radiologists predicted the correct pathological subtype in 8/13 (62%) subjects (200). In combination with multiple previous reports, this study provides further support for our hypothesis that MTLE subtypes can be accurately diagnosed with in vivo MRI (200).

Chapter 6 Ex vivo MRI

The human hippocampus consists of multiple distinct layers, has several discrete histological subregions, and demonstrates remarkable anatomical variability along its longitudinal axis (11, 13). While improvements in spatial resolution have enabled the visualization of some internal landmarks in patients with MTLE (7), histological features cannot be identified with in vivo MRI. However, ex vivo scanning enables acquisition of MR Images with much higher spatial resolution and thus permits direct visualization of hippocampal cytoarchitecture (201). Furthermore, coregistration of ex vivo MRI and histology has been described (199), which enables the direct mapping of histological subfield definitions onto MR Images (202). In addition, ex vivo MRI of hippocampi resected from patients with MTLE has revealed the microstructural correlates of MRI changes in patients with this condition (9, 203). In this chapter, we review the previous literature describing ex vivo MR Imaging of the human hippocampus, which serves as an introduction to the methodology we use in chapter 9 of this thesis.

6.1 Microscopic anatomy

As discussed above, ex vivo MRI provides dramatically improved spatial resolution in comparison to in vivo MRI. Several studies have described visualization of distinct hippocampal lamina using ex vivo MRI. Furthermore, ex vivo MRI enables quantitative evaluation of hippocampal white matter using DTI.

Hippocampal layers

As discussed in chapter 2, the human hippocampus demonstrates a laminar organization. Several studies have demonstrated that the various hippocampal layers are characterized by distinct T2 signal characteristics on ex vivo MRI (201, 204). Wieshmann et al. found that the white matter and molecular layers (e.g. alveus and stratum radiatum) of the human hippocampus were associated with low T2 signal whereas the pyramidal cell layer was associated with high T2 signal (201). However, a subsequent study suggested a more complicated relationship between hippocampal cytoarchitecture and signal characteristics (205). Interestingly, Fatterpekar et al. found that very low signal could be seen in two tissue types: heavily myelinated tissue (as expected) and densely cellular tissue with no myelin (which was unexpected) (205). The alveus, stratum radiatum and stratum lacunosum demonstrated low signal as expected for white matter or hypocellular regions (205). In addition, the pyramidal cell layer (CA1-CA4) was shown to demonstrate expected high signal in comparison to adjacent layers (205). These findings suggest that myelin content and neuronal density are important contributors to the MRI signal identified in ex vivo hippocampal specimens.

However, the seminal study by Fatterpekar et al. also generated a number of unexpected findings (205). Neuronal packing density is known to be highest in the CA2 subfield (14) and Fatterpekar et al. confirmed this upon histological examination of their samples (205). Interestingly, however, this increase in neuronal density was accompanied by an unexpected decrease in signal intensity from the CA2 subfield (205). Furthermore, the hippocampal region with the highest packing density (the granule cell layer of the DG) was associated with a discrete region of low signal (205). In addition, several

hypocellular molecular layers (particularly the polymorphic layer of the DG) were found to have high signal intensity (205). These findings raise the intriguing hypothesis that the differences in T2 signal between hippocampal subregions may also reflect additional microstructural tissue characteristics other than neuronal density and myelin content. Further studies are required to explore this hypothesis in healthy controls and patients with MTLE. However, recent studies have also used ex vivo MRI to characterize the diffusion characteristics of specific hippocampal lamina.

Hippocampal white matter

As discussed in chapter 2, the hippocampus contains multiple white matter pathways. Recent ex vivo studies have investigated the diffusion characteristics of intra-hippocampal white matter using diffusion tensor imaging (DTI) (9, 206, 207). Shepherd et al. examined mean diffusivity (MD) and fractional anisotropy (FA) in several internal lamina of the human hippocampus (207). These authors found that stratum pyramidale (CA1-CA4) was characterized by high MD and low FA, suggesting that there is high overall diffusion with low directionality in these neuron-containing regions (207). In contrast, the fimbria and SLM were associated with low MD and high FA (207). This finding suggests a relatively low amount of diffusion which is highly direction-dependent (207) in these white matter regions. However, it is important to recognize that these parameters were measured from cadaveric brain specimens obtained post-mortem. The diffusion characteristics of these regions in vivo, which is likely dependent on normal cerebral perfusion and neurophysiology, may differ in comparison to ex vivo measurements (207).

Recent work has addressed this hypothesis by measuring MD and FA values with in vivo and ex vivo MRI of hippocampi resected during epilepsy surgery (9). Goubran et al. found a significant correlation (across subjects) between the ex vivo and in vivo diffusion parameters (9). However, the relationship between neuronal densities and MD values (measured in vivo) observed by Goubran et al. was different from that suggested by the ex vivo data of Shepherd et al. (9, 207). Goubran et al. found a negative correlation between neuronal densities and MD values, suggesting that the presence of neurons is associated with lower MD values (9). In contrast, Shepherd et al. found higher MD values in cell-rich areas such as the stratum pyramidale (CA1-CA4) in comparison to white matter (SLM and fimbria) (207). These discordant results support the interesting hypothesis that in vivo diffusion parameters of the hippocampus may differ from those seen in ex vivo specimens, which warrants further examination in future studies.

DTI has also been used to map the location of intra-hippocampal white matter pathways (206). Augustinack et al. performed high resolution (0.2 x 0.2 x 0.2 mm) DTI of six post-mortem cerebral hemispheres and coregistered the diffusion images to high resolution (0.1 x 0.1 x 0.1 mm) structural images (206). As discussed in chapter 2, the axons of the perforant pathway originate from pyramidal neurons in layer II of the entorhinal cortex and traverse the subiculum to reach the granule cell layer of the dentate gyrus (13). Furthermore, perforant pathway dysfunction has been hypothesized to play a role in the pathogenesis of MTLE (33). Augustinack et al. utilized DTI tractography (208) to visualize the perforant pathway in their six autopsy brain specimens (206). These findings confirm the ability of ex vivo MRI to visualize the hippocampal internal anatomy in unprecedented detail.

6.2 Methodology

As discussed in chapter 2, the mesial temporal lobe is an anatomically complex region with several discrete histological subregions. Therefore, several studies have described approaches to predict histological features with ex vivo MRI. In this subsection, we summarize this prior literature which forms this basis for our experimental approach in chapter 9 of this thesis.

Mapping the cytoarchitecture of the mesial temporal lobe

The mesial temporal lobe (MTL) contains several cortical regions which are defined by transitions in cytoarchitecture. Recent studies have demonstrated the feasibility of mapping these cytoarchitectural features of the MTL using ex vivo MRI (206, 209-211). These studies leverage the increased spatial resolution of ex vivo MRI to enable direct correlation with histological measures.

As discussed in chapter 2, the entorhinal cortex is characterized by "cell islands" (12) which create grossly visible "verrucae" (11). In 2005, Augustinack et al. found that high resolution (0.1 mm isotropic) ex vivo MRI allowed direct visualization of verrucae in the entorhinal cortices of autopsy-derived cerebral hemispheres (211). These verrucae were shown to correspond to cell islands of the entorhinal cortex with subsequent histological analysis (211). This study thus provided initial evidence that some histological features of the MTL can be directly visualized with ex vivo MRI.

In 2009, the same group used these results to predict the location of the entorhinal cortex on in vivo MR Images (210). Fischl et al. studied 17 cerebral

hemispheres with both high resolution ex vivo MRI (to enable detection of entorhinal cell islands) and in vivo MRI (to allow potential translation to in vivo MR Images) (210). They found that ex vivo MRI (0.1 mm isotropic voxels) measurements of the entorhinal cortex were strongly predictive of histology-defined measures of this region (210). Fischl et al. then coregistered the high resolution ex vivo MR Images to low resolution (1 mm isotropic voxels) images of the same samples (210). Finally, low resolution images were spatially averaged to create a probability map of the entorhinal cortex for potential application to in vivo segmentation (210). This seminal work thus described a novel approach to the development of histologically validated segmentation protocols for potential application to in vivo MRI. This paradigm is based on histological "ground-truth" measures which are then directly mapped onto ex vivo MRI. This approach has subsequently been used by others to map the human hippocampus (202) which formed the basis for our experimental work described in chapter 9.

Hippocampal subfields

Adler et al. were the first to map histologically defined hippocampal subfield labels onto ex vivo MR Images (202). In this study, high resolution (0.16 mm isotropic voxels) T2-weighted MRI was performed on a single cadaveric hippocampus (202). The hippocampus was then divided into six equal blocks, which were each imaged a second time individually at high resolution (0.2 mm isotropic voxels) (202). The blocks were then serially sectioned at 0.2 mm (to match the slice thickness of the MRI) and a single 5 cm slide was stained with cresyl violet and luxol fast blue (202). This methodology allowed for direct coregistration of histological subfield labels (SUB, CA1, CA2, CA3 & DG)

onto ex vivo MR Images (202). Adler et al. were thus able to produce a histology-derived segmentation of the human hippocampus using ex vivo MRI (202). While this was performed in a single cadaveric specimen, subsequent work from this group supports the feasibility of combining multiple histologically segmented MR Images to create a probabilistic atlas (212).

In earlier work, Yushkevich et al. acquired high resolution (0.2 mm isotropic voxels) ex vivo MR Images from three autopsy-derived hippocampi (213). Manual segmentation of ex vivo MRI was performed based on a standard anatomical reference (13) and histological measurements were not performed in this study (213). Yushkevich et al. then used advanced computational methods to generate a probabilistic atlas of several hippocampal subfields from these three subjects (213). This work demonstrates the feasibility of modelling the complex anatomy of the human hippocampus using computational techniques. Indeed, this same group subsequently utilized a similar approach to develop a histologically-derived subfield ex vivo MRI atlas from multiple histological specimens (212). This approach holds potential to enable translation of histology-derived segmentation protocols to in vivo MRI (214).

Wisse et al. studied a cohort of ten subjects who had undergone recent high resolution (voxel size 0.4 x 0.4 x 2 mm) in vivo MRI and subsequently passed away (214). High-resolution (0.2 mm isotropic voxels) ex vivo MR Images were then obtained from hippocampi removed from these same subjects post-mortem (214). Wisse et al. demonstrated the feasibility of coregistering ex vivo MR Images of the whole hippocampus to in vivo MRI (214). This methodology could thus be used to translate hippocampal subfield transitions from histology (202), to intermediate ex vivo atlases (213) in order to generate

probabilistic maps of the hippocampus in vivo (214). This work holds significant potential to eventually allow histology-derived hippocampal segmentation in subjects with MTLE.

Hippocampal subfields in MTLE

Recent studies have described coregistration of in vivo MRI, ex vivo MRI, and neuropathology specimens in subjects with MTLE (199) and used this methodology to examine the histological correlates of in vivo MRI findings (9). Coregistration of surgical neuropathological data to ex vivo MRI poses specific problems as a consequence of the requirement in clinical practice to reserve some biopsy material for future clinical use (199). As a result serial sectioning of specimens, as performed by Adler et al. (202), is not possible in hippocampal biopsies obtained during epilepsy surgery (199).

Goubran et al. developed a novel methodology to coregister ex vivo MRI with such "sparsely sectioned" specimens resected from patients with MTLE (199). These authors have subsequently used ex vivo MRI to enable coregistration of neuropathological specimens and in vivo MR Images (9). As discussed above, this approach has enabled ex vivo / in vivo validation of quantitative MRI parameters (e.g. MD and FA) on a subfield-specific basis (9). Furthermore, as discussed in chapter 5, this method enables MRI parameters and quantitative histology to be correlated in specific hippocampal subfields (9). This methodology has enabled this group and others to examine the ex vivo MRI characteristics of hippocampal specimens resected from patients with MTLE, which is described in the next section.

6.3 Ex vivo MRI in MTLE

Coras et al. performed ex vivo T2-weighted and diffusion MR Imaging in 18 patients with HS and 15 autopsy controls (203). As described above, Fatterpekar et al. (205) had previously studied the T2 signal intensity profiles of individual hippocampal lamina with ex vivo MRI. Interestingly, Coras et al. showed that this normal seven-layer architecture was present in healthy controls, but absent in sclerotic hippocampi (which demonstrated an altered four-layer organization) (203). Coras et al. also performed DTI tractography, which revealed disruption of the normal intra-hippocampal white matter pathways in patients with HS in comparison to autopsy controls (203).

The above findings demonstrate the ability of ex vivo MRI to discern the intermediary anatomical changes which link microscopic abnormalities (e.g. mossy fiber sprouting) to macroscopic observations (e.g. grossly evident hippocampal sclerosis). This concept was further expanded by Modo et al., who studied a single surgical hippocampal specimen resected from a patient with MTLE (215). Ex vivo MRI was performed for a total of 124 hours to generate ultra-high resolution diffusion images (0.1 mm isotropic voxels) (215) which enabled precise delineation of several intra-hippocampal white matter pathways. Furthermore, Modo et al. identified an abnormal white matter pathway in the dentate gyrus which could represent mossy fiber sprouting as demonstrated in animal models (45) and surgical specimens from patients with MTLE (47). This interesting finding provides further evidence of the potential for ex vivo MRI to detect anatomical changes that contribute to the pathogenesis of MTLE.

Previous studies have demonstrated an increase in MD values measured from the sclerotic hippocampus in patients with MTLE (216). As discussed in chapter 5, Goubran et al. demonstrated that elevated MD values in the CA4/DG region were correlated with reduced neuronal densities in this area (9). Coras et al. also measured MD values from individual hippocampal subfields in patients with HS and autopsy controls (203). The MTLE cohort in this study included 13 subjects with Type 1 HS (in whom neuropathological evaluation revealed neuronal loss in CA1 and CA4) and 5 subjects with Type 2 HS (who demonstrated neuronal loss in CA1 but had normal CA4 neuronal densities) (5). They found that subjects with type 1 HS had elevated MD in both CA1 and CA4, while those with type 2 HS manifested elevated MD only in the CA1 subfield (203). This interesting finding provides further support for the potential role of quantitative MRI in the preoperative diagnosis of MTLE subtypes.

6.4 Summary

In conclusion, high resolution ex vivo MRI holds substantial potential to enable the future diagnosis of MTLE subtypes with in vivo MRI. Recent studies have demonstrated that histological subfield transitions can be directly mapped to ex vivo MR Images. Furthermore, ex vivo segmentations can be spatially averaged to generate probabilistic hippocampal maps for potential in vivo translation. Finally, quantitative MRI has been validated as a non-invasive measure of histological changes in patients with MTLE. These findings provide the essential background information for our experimental work, which is described in the following section of this thesis.

II Experiments

Chapter 7 Neuronal densities in MTLE

Abstract

Background The utility of MRI-based hippocampal subfield volumetry as a diagnostic test for hippocampal sclerosis (HS) is based on the hypothesis that specific hippocampal subfields are differentially affected in HS. While qualitative studies suggest selective involvement of certain hippocampal subfields in this condition, whether quantifiable differences exist remains unclear. Neuronal density measurement is the most widely used technique for measuring subfield pathological change in HS. Therefore, a systematic review and meta-analysis of studies reporting neuronal densities in temporal lobe epilepsy was performed in order to quantify subfield pathology in hippocampal sclerosis.

Methods Studies were identified by searching the Medline and Embase databases using the search terms: cell count, hippocampus, and epilepsy. Of the 192 studies identified by the literature search, seven met all inclusion and exclusion criteria. Random effects meta-analyses were performed, comparing: (i) neuronal densities in control (n = 121) versus HS (n = 371) groups for subfields CA1-4; and (ii) amount of neuronal loss in HS between subfields CA1-4.

Results Statistically significant neuronal loss was observed comparing HS to control groups in all subfields CA1-4 ($p < 0.001$ for all comparisons). Significantly greater neuronal loss was demonstrated in HS comparing CA1 versus CA2 ($p < 0.001$), CA3 ($p = 0.005$), and CA4 ($p = 0.003$). Greater

pyramidal cell loss was also demonstrated in CA3 relative to the CA2 subfield ($p = 0.003$). No significant differences were identified comparing CA2 and CA4 ($p = 0.39$); or comparing CA3 and CA4 ($p = 0.64$).

Conclusions HS is characterized by pathology in all hippocampal subfields. Quantifiable differences exist in the involvement of specific hippocampal subfields in HS. Neuronal loss is greatest in CA1, intermediate in CA3 and CA4, and least in CA2. Further studies are required to determine if this pattern can be detected using in vivo MRI.

A version of this Chapter was published in
Steve TA, Jirsch JD, Gross DW. Quantification of subfield pathology in
hippocampal sclerosis: A systematic review and meta-analysis. *Epilepsy
Research* 2014;108:1279-1285

7.1 Introduction

Hippocampal sclerosis (HS) is the most common pathological finding in drug resistant temporal lobe epilepsy (217). This entity is synonymous with mesial temporal sclerosis and Ammon's horn sclerosis, and consists of hippocampal neuronal loss and astrocytic gliosis. Identification of HS with preoperative MRI is predictive of favourable outcomes from temporal lobectomy (149). Reduction in MRI-measured hippocampal volume is strongly suggestive of HS as the underlying pathology (218). However, recent studies have suggested that a significant proportion of pathologically proven HS cases remain undetected, even when whole hippocampal volumetry is normal (150).

High-field MRI (>1.5T) yields images of sufficient resolution to delineate the internal architecture of the hippocampus in healthy individuals (180) and patients with HS (7). Preliminary studies have suggested that measurement of hippocampal subfields may detect atrophy in patients with normal whole hippocampal volumes (10). Subfield volumetry may also allow detection of HS subtypes preoperatively (182), which might provide useful prognostic information (8). However, the utility of hippocampal subfield volumetry as a diagnostic test for HS is based on the hypothesis that specific hippocampal subfields are differentially involved in HS.

While qualitative analysis suggests that selective involvement of certain hippocampal subfields occurs in HS, whether quantifiable differences exist remains unclear. Qualitatively, pathologic change is most pronounced in the CA1 subfield (103), while the CA2 subregion is relatively spared (104). Neuronal loss in hippocampal subfields can be quantified by measurement of pyramidal cell densities (219). However, such quantitative studies generally

demonstrate significant neuronal loss in all hippocampal subfields (168, 220, 221) and the quantitative degree to which various hippocampal subfields are involved in HS therefore remains unclear (222).

Due to limitations related to inadequate sample size, individual surgical series often lack statistical power to detect quantitative differences in involvement of hippocampal subfields (223). Therefore, a systematic review and meta-analysis of studies reporting neuronal densities in temporal lobe epilepsy was performed in order to quantify subfield pathology in hippocampal sclerosis.

7.2 Methods

This study was designed and conducted according to previously published guidelines for performing systematic reviews and meta-analyses (224). A structured screening form was used for selection of studies.

Literature Search

Studies were identified by searching the Medline (1948 to present) and Embase (1974 to present) databases. The search strategy was as follows: [(cell count*.mp.) OR (exp cell count/)] AND [(hippocamp*.mp.) OR (exp hippocampus/)] AND [(epilep*.mp.) OR (exp epilepsy/)]; limited to humans. The last search was run on April 29th, 2014.

Eligibility criteria and study selection

Studies were eligible for this review if they met the following inclusion criteria: a) both HS and control groups were studied; b) neuronal cells in CA1-4 were identified by conventional staining techniques (hematoxylin and eosin, luxol fast blue and cresyl violet, or NeuN); c) neuronal counts were reported as mean and standard deviation. Exclusion criteria were as follows: a) sample size < 4 in either group; b) review articles; c) animal studies; or d) repeated analysis of subjects. In order to exclude the possibility of repeated analysis of subjects, only one study from a given epilepsy centre was eligible for inclusion. In this case, the study with the largest sample size in the HS group was selected. One reviewer (TS) performed the literature search, screened all studies (titles, abstracts, and full text articles), and extracted relevant data. Where inadequate quantitative data were included in the original report, corresponding authors were contacted via e-mail in an effort to obtain the relevant data.

Data collection

Data collected from each selected study included first author last name, year of publication, sample sizes of HS and control groups, neuronal counting technique employed, anatomical location of sampling from the hippocampus, and neuronal densities (mean and standard deviation) in subfields CA1-4.

Meta-analyses

Neuronal cell counts in HS versus control groups A random effects meta-analysis comparing neuronal cell counts in HS versus control groups was conducted with Stata statistical software (225). Pooled standardized mean

differences (SMDs) and 95% confidence intervals (95% CIs) were calculated comparing HS and control neuronal densities at each of the subfields CA1-4. Differences between HS and control groups were deemed significant a priori if the pooled 95% CI did not include zero ($p < 0.05$). Heterogeneity was assessed by means of the I^2 statistic (226), which tests the hypothesis that differences in SMDs between studies occurred due to chance alone.

Subfield-specific neuronal loss A random effects meta-analysis comparing magnitude of neuronal cell loss between subfields CA1-4 was conducted with RevMan statistical software (227). The first step of this analysis involved calculation of mean neuronal density differences in each hippocampal subfield (CA1-4) between HS and control groups. In a second step, SMDs between each of the subfields CA1-4 were calculated, for a total of six comparisons: (a) CA1 vs. CA2, b) CA1 vs. CA3, c) CA1 vs. CA4, d) CA2 vs. CA3, e) CA2 vs. CA4, and f) CA3 vs. CA4). Lastly, pooled SMDs and 95% CIs were calculated for each subfield comparison. Differences between subfields were deemed significant a priori if the pooled 95% CI did not include zero ($p < 0.05$).

7.3 Results

Study selection

The literature search and study selection flow diagram is shown in Figure 7.1. In addition to the 234 studies identified through database searching, five were found by searching citation lists of reference articles. One hundred and ninety-two abstracts were screened and 67 studies were excluded according to the eligibility criteria. One hundred and twenty-five full text articles were

reviewed. The most common reasons for exclusion were that all hippocampal subfields were either not measured (57/118) or not reported separately (29/118). Additional reasons for exclusion were: inadequate quantitative data (14/118), repeated analysis of subjects (11/118), lack of a control group (5/118), and inadequate sample size (2/118). Therefore, the final analysis included seven studies (4, 134, 157, 223, 228-230).

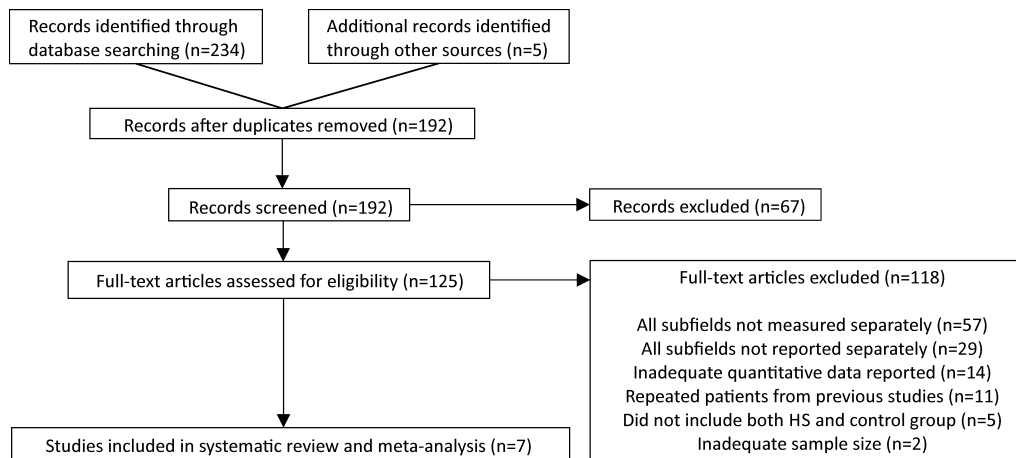


Figure 7.1 - Literature search and study selection flow diagram

Qualitative analysis of included studies

Studies meeting eligibility criteria for the systematic review and meta-analysis are displayed in Table 7.1. Only two of the seven included studies reported neuronal densities separately for HS subtypes: [type 1 (CA1 and CA4 affected), type 2 (CA1 predominantly affected), and type 3 (CA4 predominantly affected)] (5). One study reported cell counts separately for type 1 & 2 HS

(157), while another reported data separately for type 1-3 HS (4). Inadequate data were therefore available in the literature to allow separate analyses of quantitative neuronal loss in each of the HS subtypes. Data representing HS subtypes, from De Lanerolle et al. and Thom et al., were therefore pooled prior to statistical analysis. As a result, neuronal densities from all included studies represent data for “undifferentiated” HS (type 1-3 HS combined).

All of the studies included in the present review used a two-dimensional cell counting technique, which is widely used in the epilepsy neuropathology literature (219, 221). A detailed discussion of the various neuronal counting methods is beyond the scope of this paper. In brief, three dimensional cell counting has been proposed as the optimal method for quantification of hippocampal pyramidal neurons (168, 231), but is infrequently applied in epilepsy histopathology studies.

The anatomical location of sampling from the hippocampus in each study is shown in Table 7.1. All studies measured neuronal densities from the

Study	Control^a	HS^{a,b}	Section Location
Blumcke 1996	9	20	Body
Mathern 1997	34	31	Anterior-body
Foldvary 1999	7	43	Mid-body
De Lanerolle 2003	26	81	Mid-body
Andrioli 2007	4	9	Body
Andrade-Velanca 2008	20	39	Anterior-body
Thom 2010	21	148	Mid-body
Total	121	371	

Table 7.1 - Characteristics of included studies

^aFigures represent number of subjects ^bHippocampal sclerosis

hippocampal body. Two studies did not specify the anterior-posterior location of sectioning, two studies specified sampling from the anterior-body, and three studies used the mid-body for analysis. None of the included studies measured neuronal densities from the hippocampal head, posterior hippocampal body, or the hippocampal tail.

Meta-analyses

Neuronal cell counts in HS versus control groups Forest plots displaying differences in neuronal densities between HS and control groups in CA1-4 subfields are displayed in Figure 7.2. Statistically significant reduction in neuronal cell counts was demonstrated in CA1, CA2, CA3, and CA4 subfields ($p < 0.001$ for all comparisons). Statistically significant heterogeneity was identified comparing HS and control densities in all subfields ($p < 0.001$ for each subfield).

Subfield-specific neuronal loss Forest plots displaying differences in magnitude of neuronal cell loss in subfields CA1-4 are displayed in Figure 7.3. Significantly greater neuronal loss was demonstrated in CA1 versus CA2 ($p < 0.001$), CA1 versus CA3 ($p = 0.005$), CA1 versus CA4 ($p = 0.003$), and CA3 versus CA2 ($p = 0.003$). No significant differences were identified comparing CA2 and CA4 ($p = 0.39$); or comparing CA3 and CA4 ($p = 0.64$).

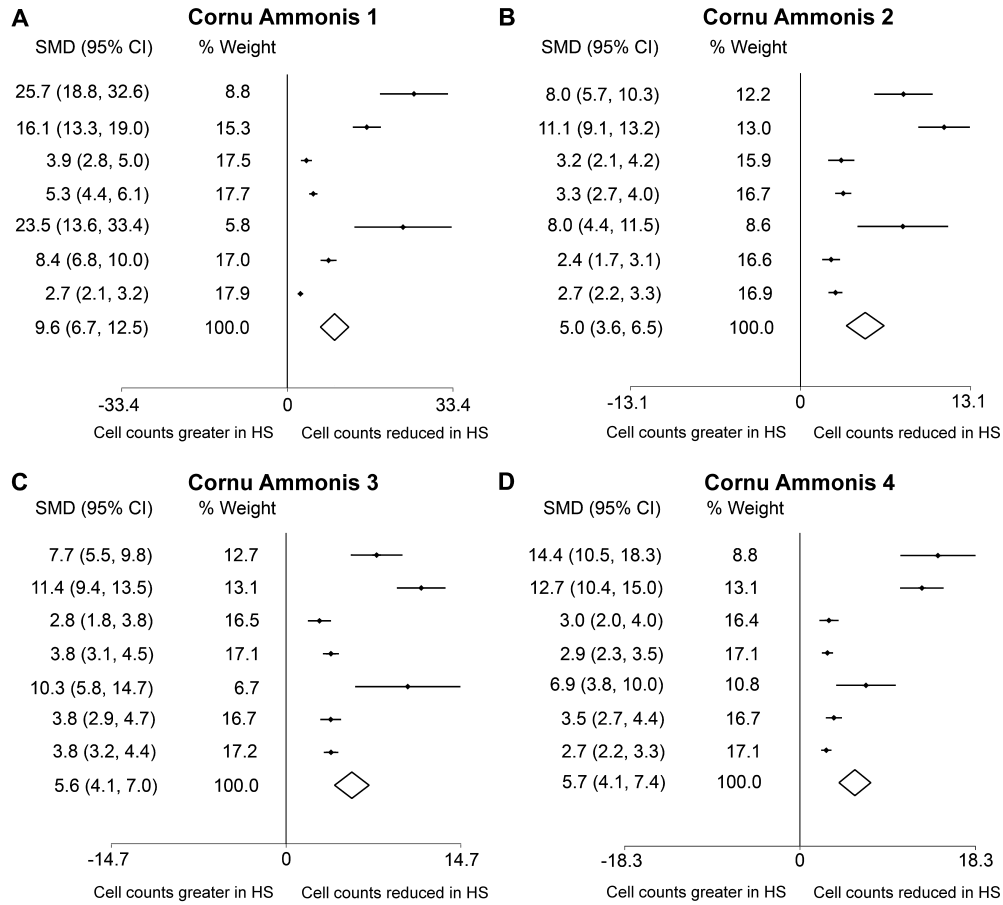


Figure 7.2 - Neuronal cell counts in hippocampal sclerosis versus control

Standardized mean differences (SMD) and 95% confidence intervals (95% CI) are displayed comparing neuronal cell counts at CA1 (A), CA2 (B), CA3 (C), and CA4 (D) subfields in hippocampal sclerosis (HS) versus control groups. Statistically significant reduction in neuronal densities were demonstrated in CA1 ($p < 0.0001$), CA2 ($p < 0.0001$), CA3 ($p < 0.0001$), and CA4 ($p < 0.0001$) subfields.

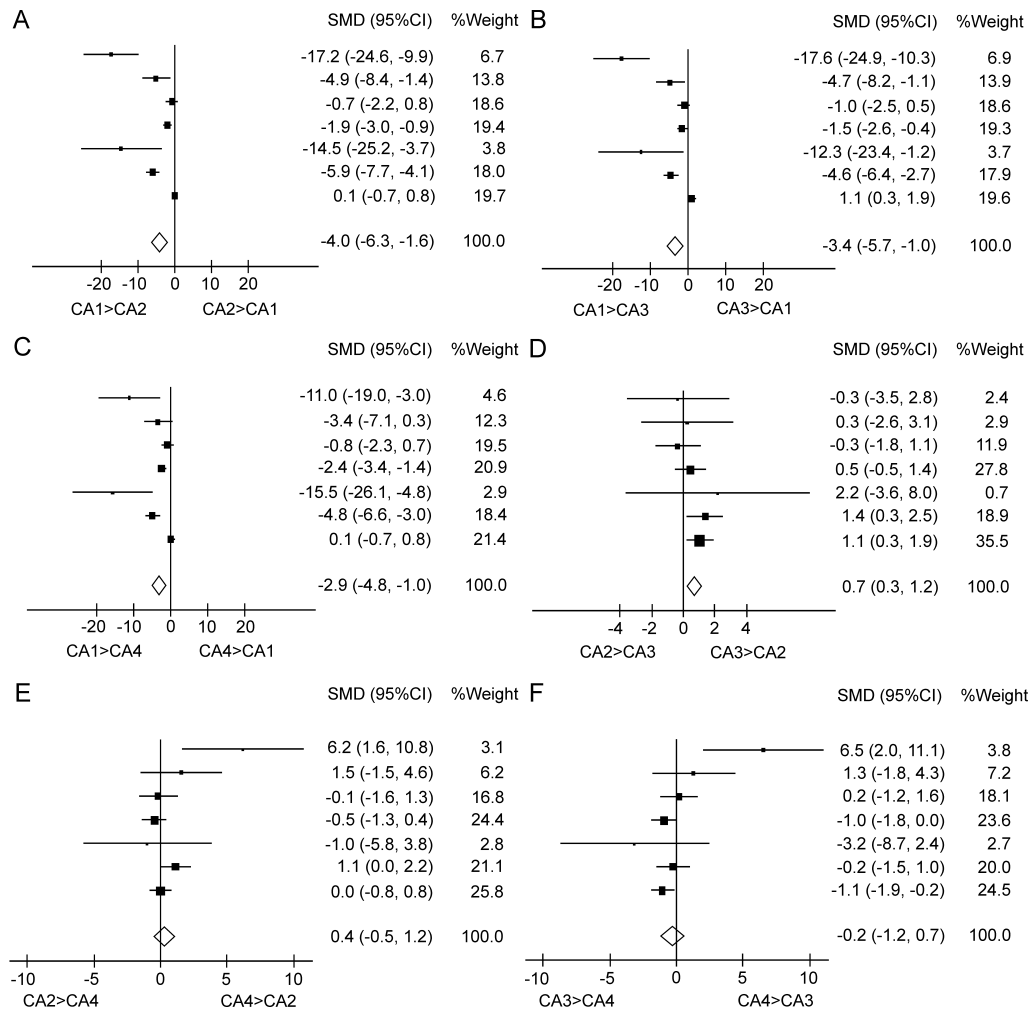


Figure 7.3 - Subfield-specific neuronal loss in hippocampal sclerosis

Standardized mean differences (SMD) and 95% confidence intervals (95% CI) are illustrated comparing magnitude of neuronal cell loss between subfields CA1-4 in hippocampal sclerosis. Significantly greater neuronal loss was demonstrated in CA1 versus CA2 (SMD -4.0; 95% CI -6.3, -1.6; $p=0.0009$), CA1 versus CA3 (SMD -3.4; 95% CI -5.7, -1.0; $p=0.005$), CA1 versus CA4 (SMD -2.9; 95% CI -4.8, -1.0; $p=0.003$), and CA3 versus CA2 (SMD 0.7; 95% CI 0.3, 1.2; $p=0.003$). No significant differences in neuronal loss were demonstrated comparing CA4 versus CA2 (SMD 0.4; 95% CI -0.5, 1.2; $p=0.39$) and CA3 versus CA4 (SMD -0.2; 95% CI -1.2, 0.7; $p=0.64$).

7.4 Discussion

Significance

The present study showed that in HS, quantifiable differences exist in the involvement of specific hippocampal subfields. Neuronal loss is greatest in CA1, intermediate in CA3 and CA4, and least in CA2. This pattern of neuronal loss is consistent with classical neuropathological observations in HS (104), and is often evident upon qualitative microscopic inspection of HS specimens (217).

Our results demonstrate that CA1 suffers the greatest magnitude of neuronal loss in HS. This finding is in agreement with qualitative neuropathological observations suggesting CA1 is most involved in HS (103). Predominant neuronal loss in the CA1 region was also demonstrated in a recently reported quantitative analysis (8). This suggests that histologically accurate measurement of the CA1 subfield will be critical to the development of MRI-based hippocampal subfield volumetry with high sensitivity and specificity in the diagnosis of HS (213, 232).

We also found greater neuronal loss at CA3 compared to the CA2 subfield. However, the magnitude of this difference (SMD 0.7) was approximately one third of that demonstrated for CA1 comparisons (SMD 2.9 or greater). The small size of this difference may explain why a previous quantitatively-analyzed surgical series (8) did not find a disparity in neuronal loss between CA3 and CA2.

In our study, neuronal loss in the CA4 subfield was statistically equivalent to that in both CA2 and CA3. Our data suggest that CA4

demonstrates slightly less neuronal loss than CA3, and slightly more neuronal loss than CA2; however, these differences were not statistically significant.

Future Directions

Future research is required to determine if this pattern can be detected using in vivo MRI. Subfield volumetry studies of HS published in the literature to date have combined multiple subfields into composite measurements [CA3 and CA4 (10); CA1 and CA2 and CA3 (182)]. In future studies, the use of histologically-based segmentation techniques may enable these subfields to be discerned individually (202), which might allow detection of subfield-specific atrophy patterns in vivo.

Limitations

Our analysis revealed a high degree of variability in magnitude of neuronal loss, between studies, in each hippocampal subfield. There are several possible reasons for this observation. Firstly, studies included in the present analysis varied with respect to anterior-posterior location of the hippocampal body studied, and neuronal densities have recently been shown to vary (in both HS and control) along the longitudinal axis of the hippocampus (136). Another possible explanation is that the present study used neuronal density data for “undifferentiated” HS (type 1-3 HS combined). This was necessary as inadequate data were available in the literature to allow separate analyses of quantitative neuronal loss in each of the HS subtypes (only 2/7 studies reported data separately for HS subtypes). An unequal distribution of subtypes in the various studies could therefore contribute to the variability in magnitude of

neuronal loss observed. However, it is unclear why the prevalence of HS subtypes would vary substantially across studies.

It is possible that the significant heterogeneity encountered may have hindered our ability to detect differences in subfield-specific neuronal loss. While the large differences demonstrated for CA1 argue against this as a major limitation, it is possible that small differences in neuronal loss for the CA2/CA4 and CA3/CA4 comparisons remained undetected. The small number of studies eligible for inclusion (n=7) represents another limitation. It is possible that the systematic search missed some studies, but this was felt to be unlikely as the authors also searched citation lists thoroughly for any unidentified studies. A final limitation relates to the two-dimensional counting technique used in the included studies. Some authors have questioned the reliability of such methods, due to possible effects of fixation-induced tissue shrinkage on density measurements (231). None of the identified studies used a three-dimensional counting technique, which has been proposed to be superior for quantification of neuronal cell number (231). This observation demonstrates that two-dimensional cell counting remains the most commonly used technique for neuronal quantification in the epilepsy neuropathology literature.

7.5 Conclusions

HS is characterized by pathology in all hippocampal subfields. Quantifiable differences exist in the involvement of specific hippocampal subfields in HS. Neuronal loss is greatest in CA1, intermediate in CA3 and CA4, and least in CA2. Further studies are required to determine if this pattern can be detected using *in vivo* MRI.

Chapter 8 Neuronal density and subfield areas

Abstract

Hippocampal sclerosis (HS) is the most common lesion identified in patients with medically intractable epilepsy. HS subtypes, defined by neuronal densities in CA1 and CA4, have been shown to have distinct outcomes from epilepsy surgery but at present cannot be diagnosed preoperatively. MRI-based measurement of hippocampal subfields could potentially allow diagnosis of HS subtypes in vivo, but neuronal density cannot be directly measured with in vivo MRI. In vivo studies therefore use subfield volumes or areas, as a surrogate of neuronal number, to define subfield involvement. The relationship between tissue area and neuronal densities in hippocampal subfields, however, has not been clearly defined. In the present study, we compared hippocampal subfield areas and neuronal densities in a cohort of six elderly controls. Subfield areas and densities did not demonstrate a significant correlation in any of the subfields (CA1, CA2, CA3, or CA4). Our results add to an existing body of literature in HS suggesting a complex relationship between tissue areas and neuronal number. However, our results also emphasize the limitations of two dimensional cell counting techniques which are essentially ubiquitous in the epilepsy neuropathology literature. In vivo diagnosis of HS subtypes will benefit from future studies combining quantitative MRI with stereological evaluation of the human hippocampus.

8.1 Introduction

Hippocampal sclerosis (HS) is the most common neuropathological finding in intractable epilepsy (18). While temporal lobectomy can potentially cure patients with HS, approximately 50% of patients continue to have disabling seizures following surgery (154). Surgical specimens from patients with HS can demonstrate classical involvement of both CA1 and CA4 (ILAE type 1 HS), CA1 predominant disease (ILAE type 2 HS), or end folium (CA4) sclerosis (ILAE type 3 HS) (5). Neuropathological classification of HS subtypes has been shown to predict surgical outcomes (4, 8). However, diagnosis of HS subtypes is currently not possible preoperatively, and this information can therefore not currently be used to guide surgical decision-making.

HS subtypes are defined pathologically based on neuronal density measurements in hippocampal subfields CA1 and CA4 (8). This method uses a two-dimensional cell counting technique (233) which is practical to apply in surgical specimens and thus is extensively used in the neuropathology literature (221, 234). Measurement of neuronal density in this manner, however, does not provide information regarding total neuron number or tissue volume (231). Stereological methods have been applied to determine neuronal numbers and subfield volumes in HS (168), but such studies are rare (235).

Measurement of hippocampal subfield volumes with in vivo MRI could potentially enable preoperative diagnosis of HS subtypes (7). High resolution acquisitions visualize the hippocampal internal architecture (180), allowing segmentation of hippocampal subfields on coronal MR Images (236). Using this methodology, CA1 and CA4 subfield volumes can be measured in patients with HS (10). Subfield *volumes*, as measured with in vivo MRI, represent the

product of the subfield *area* multiplied by the *slice thickness*. However, whether subfield area measurements are an accurate predictor of the neuronal densities used to characterize HS subtypes remains unknown. In the present study, we therefore aimed to examine the relationship between hippocampal subfield areas and neuronal densities in human subjects without any history of epilepsy or other neurological disease.

8.2 Materials and Methods

We studied cerebral hemispheres (3 Left / 3 Right) obtained post-mortem from six subjects (age 61-96) with no known history of neuropsychiatric disorders. We have previously reported histological and MRI data from these subjects in an earlier study (237). The cerebral hemispheres had been fixed in formaldehyde post-mortem for an average of six months. The hippocampi (n=6) were removed from each cerebral hemisphere and cut into four equal 5 mm blocks (n=4X6=24). These blocks were then embedded with paraffin and a single 5 μ m histological section was taken from each block. Six of the blocks contained only tissue from the hippocampal head and were therefore not analyzed. This yielded a final n=18 histological sections for our study, which were stained for nissl substance (with cresyl violet) and myelin (with luxol fast blue) as previously described (238).

The cytoarchitectural criteria used for hippocampal subfield delineation (12-14) are illustrated in Figure 8.1. Histological segmentation was performed by an experienced neuropathologist (Author RC), who has several years of experience measuring hippocampal subfields in surgical specimens. The Subiculum/CA1 boundary was identified according to two criteria. First, the transition from Subiculum to CA1 was marked by a significant narrowing of

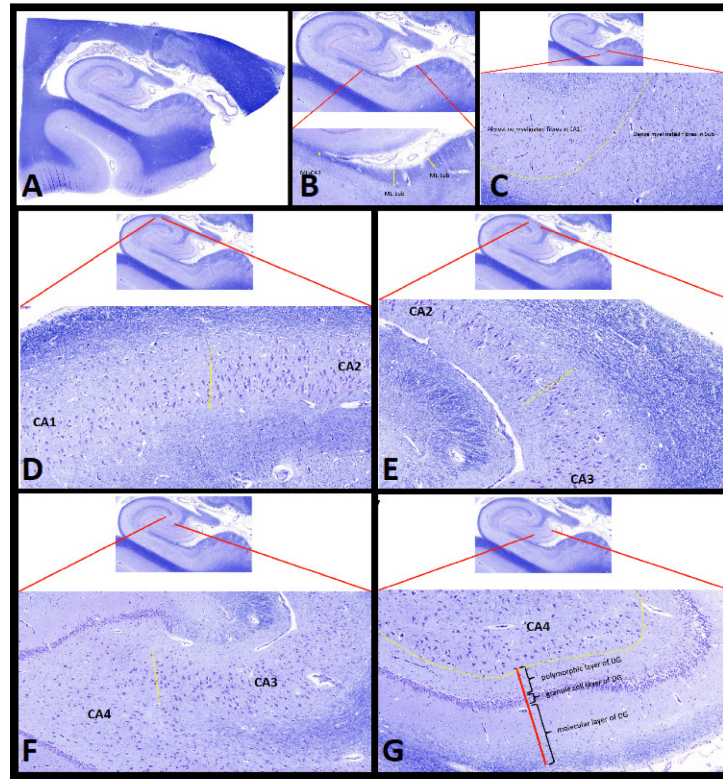


Figure 8.1 - Cytoarchitectural definitions of subfield boundaries

- A) Tissue sections stained for Nissl substance (with cresyl violet) and myelin (with luxol fast blue) were used to define hippocampal subfield boundaries. B) Subiculum/CA1 criterion 1: The broad molecular layer of the Subiculum (ML-Sub) was differentiated from the narrow molecular layer of CA1 (ML-CA1). C) Subiculum/CA1 criterion 2: The pyramidal cell layer of the Subiculum contained the dense myelinated fibers of the perforant path, while these were absent in CA1. D) CA1/CA2: Pyramidal cells in CA1 (triangular, smaller, and less organized) were differentiated from CA2 neurons (ovoid, larger, and more organized). E) CA2/CA3: CA3 was identified as an arcuate subfield entering the concavity of the dentate gyrus. The CA3 subfield consisted of a broader layer of cells which were less organized than in CA2. F) CA3/CA4: CA4 neurons were also located within the concavity of the dentate gyrus. In contrast to the lamination present in CA3, the CA4 subfield was composed of larger ovoid neurons with no lamination. G) The granule cell layer of the dentate gyrus was distinct from CA4. Between the granule cell layer of the dentate gyrus and CA4, there was a layer with low cellularity (the so-called polymorphic or plexiform layer)

the molecular layer (Figure 8.1B). Second, the pyramidal layer of the Subiculum contained dense myelinated fibers of the perforant path which were absent in CA1 (Figure 8.1C).

The transition from CA1 to CA2 was marked by a change in pyramidal neuron cytoarchitecture (Figure 8.1D). In comparison to CA1, neurons in the CA2 subfield were: i) more ovoid (versus triangular neurons in CA1), ii) larger, and iii) more organized (demonstrating greater lamination than in CA1). The transition from CA2 to CA3 was defined by an expansion of the pyramidal cells into a broader layer with less organized lamination than in CA2 (Figure 8.1E). Neurons from both the CA3 and CA4 subfields were located within the concavity of the dentate gyrus. In contrast to the lamination present in CA3, however, the CA4 subfield demonstrated no lamination (Figure 8.1F). Finally, CA4 neurons were separated from the dentate gyrus granule cell layer by a hypocellular region (the polymorphic or plexiform layer) (Figure 8.1G).

The methodology employed for measurement of hippocampal subfield areas is shown in Figure 8.2. First, subfield boundaries were defined according to the histological criteria listed above. Next, the pyramidal cell layers were delineated to define four hippocampal subfields: CA1, CA2, CA3, and CA4 (red, Figure 8.2). Subfield areas were directly measured from all 18 slices using Zen microscopy software (Carl Zeiss AG, Germany).

The technique used for estimation of neuronal densities is described in Figure 8.3. Neurons (identified as pyramidal cells demonstrating both a nucleus and nucleolus) were counted in four separate microscope fields for each subfield, each of which measured 250 μm x 250 μm (area 0.0625 mm^2). Neuronal counts from these four fields were added (cells/0.25 mm^2) and multiplied by a factor of 4 to yield the estimated neuronal density (cells/ mm^2).

This procedure was performed in each subfield (CA1-4), as shown in Figure 8.3.

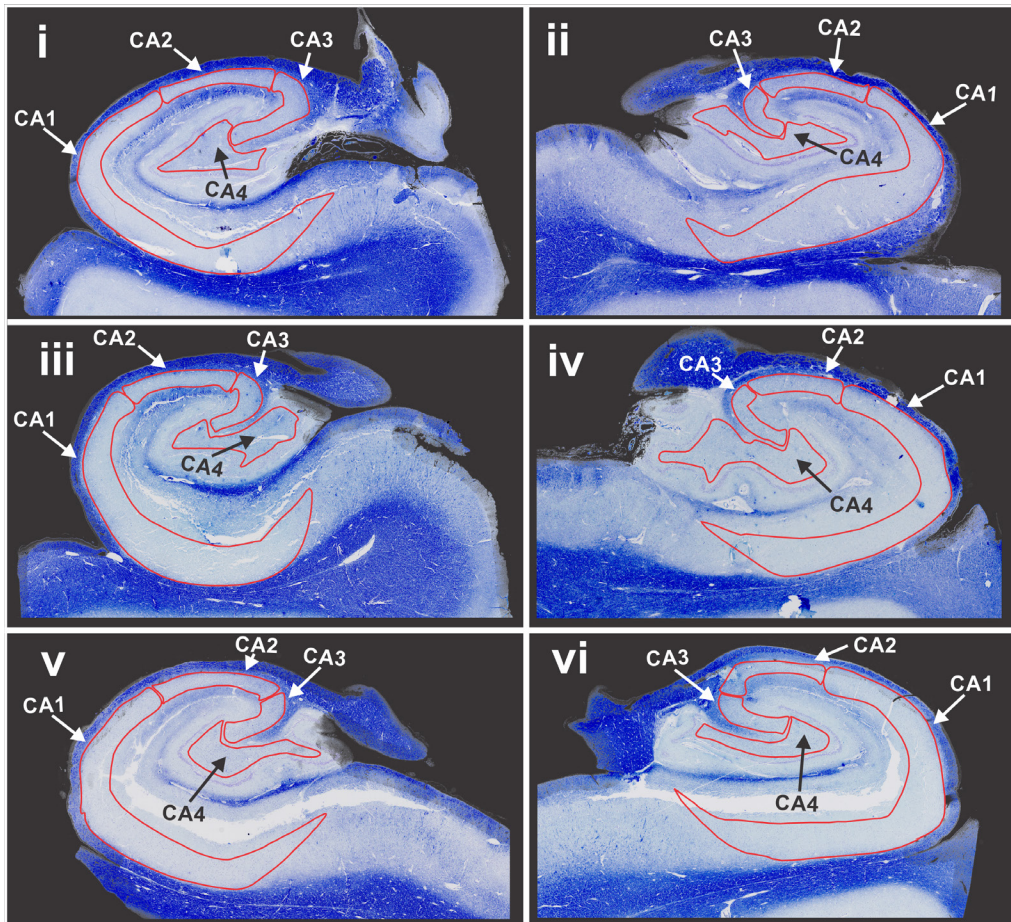


Figure 8.2 - Measurement of hippocampal subfield areas

Cytoarchitectural criteria were used to define the pyramidal cell layer of each hippocampal subfield (CA1, CA2, CA3, and CA4). Measurements of subfield areas (red) are shown for a single section from each hippocampus (i-vi).

8.3 Results

Mean hippocampal subfield areas were as follows: CA1 = 1.4×10^7 mcm² (95% confidence interval = 1.2×10^7 to 1.5×10^7 mcm²; range = 1.0×10^7 to 1.9×10^7 mcm²); CA2 = 1.9×10^6 mcm² (95% confidence interval = 1.6×10^6 to 2.3×10^6 mcm²; range = 1.0×10^6 to 2.9×10^6 mcm²); CA3 = 1.5×10^6 mcm² (95% confidence interval = 1.2×10^6 to 1.8×10^6 mcm²; range = 6.5×10^5 to 3.6×10^6 mcm²). CA4 = 3.5×10^6 mcm² (95% confidence interval = 2.9×10^6 to 4.2×10^6 mcm²; range = 2.1×10^6 to 5.9×10^6 mcm²).

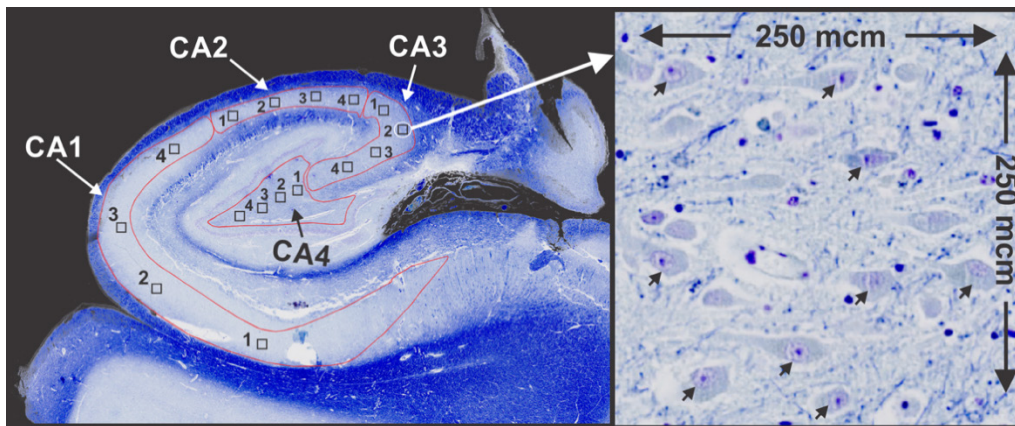


Figure 8.3 - Estimation of neuronal densities in hippocampal subfields

Neuronal densities were estimated in each hippocampal subfield (CA1, CA2, CA3, and CA4). Pyramidal neurons containing a nucleus and nucleolus were identified (arrows) on tissue sections stained with cresyl violet. In each subfield, neurons were counted in four (1-4) randomly placed microscope fields measuring 250 x 250 mcm (area 0.0625 mm²). Neuronal counts from these four fields were added (cells/0.25 mm²) and multiplied by a factor of 4 to yield the estimated neuronal density (cells/mm²).

Mean neuronal densities were as follows: CA1 = 126 cells/mm² (95% confidence interval = 112 to 141 cells/mm²; range = 84 to 180 cells/mm²); CA2

= 173 cells/mm² (95% confidence interval = 160 to 186 cells/mm²; range = 128 to 232 cells/mm²); CA3 = 146 cells/mm² (95% confidence interval = 129 to 163 cells/mm²; range = 84 to 200 cells/mm²); CA4 = 112 cells/mm² (95% confidence interval = 97 to 126 cells/mm²; range = 68 to 160 cells/mm²).

Scatter plots comparing neuronal densities and subfield areas in CA1-CA4 hippocampal subregions are shown in Figure 8.4. A statistically significant relationship between subfield areas and neuronal densities was not identified in any of the four subfields.

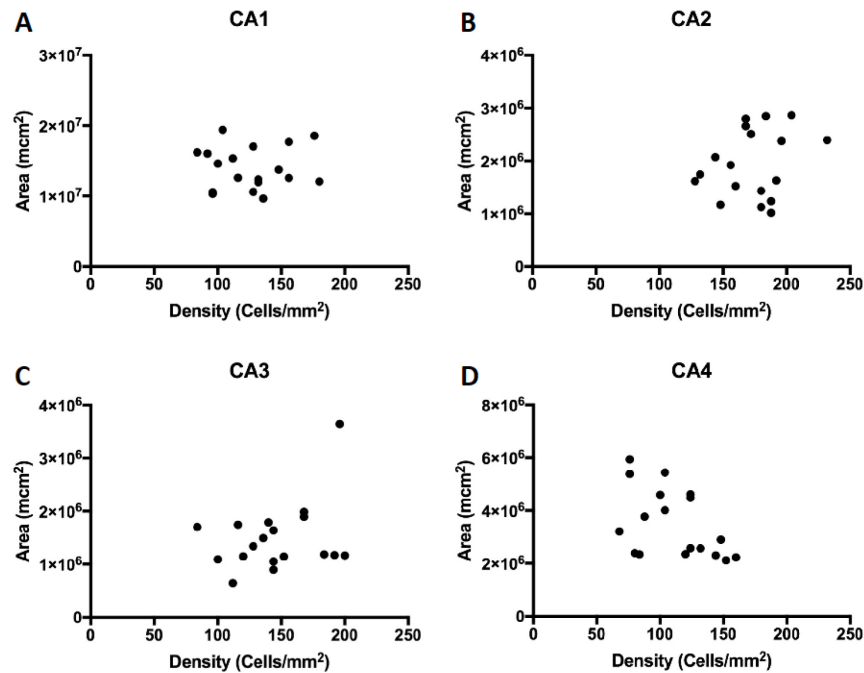


Figure 8.4 - Comparison of neuronal densities and subfield areas

Neuronal densities (cells/mm²) and subfield areas (mcm²) were compared in CA1 (A), CA2 (B), CA3 (C), and CA4 (D) hippocampal subregions. A statistically significant relationship between subfield areas and neuronal densities was not identified in any of the four subfields.

8.4 Discussion

In the present study of *neurologically healthy elderly subjects*, histological subfield area measurements were not predictive of neuronal density estimates in hippocampal subregions. The results of previous studies *in patients with HS* (displayed in Table 8.1) are conflicting regarding the correlation between subfield cell densities and hippocampal areas/volumes. While some studies have documented significant correlations between hippocampal volumes and neuronal densities, a number of studies have not found a relationship between these two variables.

Methodological considerations represent a potential explanation for the discordant results from MRI-histology correlation studies performed to date (Table 8.1). As in the present study, nearly all of the quantitative neuropathological studies performed in HS subjects have utilized two-dimensional cell counting to quantify neuronal numbers (219, 221, 233, 234). While this method has the advantage of being applicable in neuropathological specimens prepared for diagnostic (as opposed to research) purposes, it has a number of important limitations [reviewed in (231)]. Most importantly, the two-dimensional cell counting method does not allow measurements of tissue volumes or total neuronal numbers. This is particularly relevant in HS, a condition where hippocampal tissue volumes are known to be reduced (142). Neuronal densities measured with a two-dimensional cell counting method from atrophied tissue would be expected to underestimate actual neuronal loss, which may affect correlation with MRI measures of hippocampal volume.

To our knowledge, only one quantitative MRI study reported in the literature has utilized stereological methods to quantify neuronal loss in hippocampal subfields (168). In this study, neuronal numbers in each hippocampal subfield (CA1, CA2, CA3, CA4, and granule cell layer of the

Study	Hippocampal Area or Volume measurement modality	Neuronal quantification method	Hippocampal subfield correlations	
			Not significant	Significant
Bronen et al. 1991 (239)	In vivo MRI Hippocampal body area on a single slice at level of red nucleus	Two-dimensional cell counting	CA1 & CA2	CA3 & CA4 GCL
Cascino et al. 1991 (240)	In vivo MRI Hippocampal head and body back to posterior commissure	Qualitative grading of neuronal loss		Subiculum CA1, CA2, CA3 & CA4
Lenz et al. 1992 (241)	In vivo MRI Hippocampal body volumes from three anterior slices	Two-dimensional cell counting		CA1, CA2, CA3 & CA4 GCL
Lee et al. 1995 (242)	In vivo MRI Whole hippocampal volume	Two-dimensional cell counting	Subiculum CA4 GCL	CA1, CA2 & CA3
Van Paesschen et al. 1997 (168)	In vivo MRI Estimated whole hippocampal volume	Stereological quantification of neurons		CA1, CA2, CA3, & CA4 GCL
Briellmann et al. 2002 (148)	In vivo MRI Whole hippocampal volume	Two-dimensional cell counting	CA1	GCL
Coras et al. 2014 (203)	Ex vivo MRI Hippocampal subfield areas	Quantitative field fraction of NeuN immunostaining	Subiculum CA1, CA2, CA3 & CA4	
Goubran et al. 2016 (9)	In vivo MRI Hippocampal subfield volumes	Quantitative field fraction of NeuN immunostaining		CA1, CA2/3, CA4
Present study	Direct histological measurements of subfield areas	Two-dimensional cell counting	CA1, CA2, CA3 & CA4	

Table 8.1 - Previous studies

GCL - Granule cell layer of the dentate gyrus

dentate gyrus) were correlated with estimated hippocampal volume as measured with MRI.

Further studies are required to examine the relationship between quantitative MRI and histopathology in hippocampal subfields. While high resolution MRI allows quantitative measurement of hippocampal subfield volumes in subjects with HS (7, 10), correlation of MRI with quantitative neuropathology has yielded inconsistent results (Table 8.1). The results of the present study in *elderly controls*, in addition to some previous studies of *HS subjects*, suggest that a simple relationship between tissue area and neuronal density does not exist. There are several potential explanations for this finding. It is possible that loss of other cell types, such as glial cells, may contribute to hippocampal volume loss. In addition, axonal loss may contribute to reduced tissue volume in subjects with HS. Future studies incorporating both quantitative MRI and stereological measurements of hippocampal tissue would therefore be an important next step towards in vivo diagnosis of HS subtypes. However, whether stereological measurements could be routinely applied to clinical surgical specimens remains uncertain.

Finally, while the current ILAE HS subtype classification is based on subfield cell densities, area/volume changes are also recognized on histology which would be expected to demonstrate better correlations with in vivo MRI subfield measurements. If this is demonstrated as would be expected, it would be reasonable to explore whether histologically and MRI based subfield volume changes demonstrate similar ability to predict surgical outcome as compared to subfield cell densities.

8.5 Conclusions

In the present study, we analyzed hippocampal subfield areas and neuronal densities in healthy elderly subjects. In agreement with many previous studies in HS, we did not find a significant correlation between cell counts and subfield areas. Our results emphasize the limitations of two dimensional cell counting techniques which are widely used in the epilepsy neuropathology literature. The development of methods for in vivo diagnosis of HS subtypes will benefit from future studies combining quantitative MRI with stereological measurements of hippocampal tissue.

8.6 Supplementary Methods

In this section, we provide additional details regarding the methodology we employed to obtain neuronal density measurements from our cadaveric hippocampi.

Tissue Blocks We studied 6 cadaveric hippocampi which had been fixed in formalin for approximately six months. Our aim was to obtain neuronal density measurements at several locations along the anterior-posterior axis of the hippocampus. We therefore divided each hippocampus into four equal 5 mm blocks. These hippocampal blocks were then embedded in paraffin and a single 5 mcm section was obtained from each block with a microtome. These 5 mcm sections were then stained with cresyl violet and luxol fast blue in order to highlight neurons and myelin respectively.

Neuronal cell counting We used the method described by Blumcke et al. to measure neuronal densities in hippocampal subfields (5). I completed a research elective in Blumcke's lab in Erlangen, Germany in order to learn this

technique. During this elective, I was provided with an introduction to the histological criteria used to segment hippocampal subfields by an experienced neuropathologist (Dr. Roland Coras, University of Erlangen). This was followed by training in the two-dimensional neuronal density measurement techniques used in the surgical neuropathology literature. Following this training, Dr. Coras and I performed an inter-rater reliability experiment in order to ensure I was obtaining accurate measurements. This research elective therefore provided the author with essential experience in the histological definition of hippocampal subfield boundaries. Furthermore, this training was critical to the development of our histology-derived segmentation protocol, which is described in the next chapter.

Chapter 9 Histology-derived segmentation of ex vivo MRI

Abstract

Background Recent findings have demonstrated that hippocampal subfields can be selectively affected in different disease states, which has led to efforts to segment the human hippocampus with in vivo magnetic resonance imaging (MRI). However, no studies have examined the histological accuracy of subfield segmentation protocols. The presence of MRI-visible anatomical landmarks with known correspondence to histology represents a fundamental prerequisite for in vivo hippocampal subfield segmentation. In the present study, we aimed to: 1) develop a novel method for hippocampal body segmentation, based on two MRI-visible anatomical landmarks (stratum lacunosum moleculare [SLM] & dentate gyrus [DG]), and assess its accuracy in comparison to the gold standard direct histological measurements; 2) quantify the accuracy of two published segmentation strategies in comparison to the histological gold standard; and 3) apply the novel method to ex vivo MRI and correlate the results with histology.

Methods Ultra-high resolution ex vivo MRI was performed on six whole cadaveric hippocampal specimens, which were then divided into 22 blocks and histologically processed. The hippocampal bodies were segmented into subfields based on histological criteria and subfield boundaries and areas were directly measured. A novel method was developed using mean percentage of the total SLM distance to define subfield boundaries. Boundary distances and

subfield areas on histology were then determined using the novel method and compared to the gold standard histological measurements. The novel method was then used to determine ex vivo MRI measures of subfield boundaries and areas, which were compared to histological measurements.

Results For direct histological measurements, the mean percentages of total SLM distance were: Subiculum/CA1 = 9.7%, CA1/CA2 = 78.4%, CA2/CA3 = 97.5%. When applied to histology, the novel method provided accurate measures for CA1/CA2 (ICC = 0.93) and CA2/CA3 (ICC = 0.97) boundaries, but not for the Subiculum/CA1 (ICC = -0.04) boundary. Accuracy was poorer using previous techniques for CA1/CA2 (maximum ICC = 0.85) and CA2/CA3 (maximum ICC = 0.88), with the previously reported techniques also performing poorly in defining the Subiculum/CA1 boundary (maximum ICC = 0.00). Ex vivo MRI measurements using the novel method were linearly related to direct measurements of SLM length ($r^2 = 0.58$), CA1/CA2 boundary ($r^2 = 0.39$) and CA2/CA3 boundary ($r^2 = 0.47$), but not for Subiculum/CA1 boundary ($r^2 = 0.01$). Subfield areas measured with the novel method on histology and ex vivo MRI were linearly related to gold standard histological measures for CA1, CA2, and CA3/CA4/DG.

Conclusions In this initial proof of concept study, we used ex vivo MRI and histology of cadaveric hippocampi to develop a novel segmentation protocol for the hippocampal body. The novel method utilized two anatomical landmarks, SLM & DG, and provided accurate measurements of CA1, CA2, and CA3/CA4/DG subfields in comparison to the gold standard histological measurements. The relationships demonstrated between histology and ex vivo

MRI supports the potential feasibility of applying this method to in vivo MRI studies.

A version of this Chapter was published in
Steve TA, Yasuda CL, Coras R, Lail M, Blumcke I, Livy DJ, Malykhin N,
Gross DW. Development of a histologically validated segmentation protocol
for the hippocampal body. *Neuroimage* 2017;157, 219-232

9.1 Introduction

The hippocampus plays a crucial role in human memory (17) and is prominently affected in both Epilepsy (243) and Alzheimer's disease (244). Hippocampal subfields, which are discrete histological subregions of the hippocampus, are thought to subserve distinct aspects of memory function. The dentate gyrus (DG) has been implicated in discrimination of novel stimuli (pattern separation) during memory encoding (26). Conversely, the CA3 subregion is likely responsible for recall of a memory based on partial cues (pattern completion) during learning (26). Finally, CA1 appears to be critical for autobiographical and episodic memory retrieval (245). In addition to their distinct cognitive functions, hippocampal subfields are differentially involved in several neurological conditions.

Alzheimer's disease (AD) is characterized by the progressive development of neurofibrillary pathology in specific hippocampal subfields. The earliest stages of AD are accompanied by pathology restricted to the transentorhinal and entorhinal cortices of the hippocampal formation (246). When the disease reaches the hippocampus proper, pathology remains strikingly subfield-specific with preferential involvement of Subiculum and CA1 (247). Progression of pathological changes from the entorhinal cortex to the hippocampus is strongly correlated with the development of dementia (248). Measurement of pathology in hippocampal subfields could, therefore, represent a preclinical biomarker for early diagnosis of AD (249).

Hippocampal subfield pathology also has potential direct clinical relevance to the treatment of epilepsy. Hippocampal sclerosis (HS) is the most common pathological finding in drug-resistant epilepsy (217). While pathology

can be seen throughout all hippocampal subfields in HS (235), hippocampal subfields are differentially affected in classical HS, with more severe involvement of the CA1 region and relative sparing of the CA2 subfield (103, 104). While surgery can potentially cure patients who fail medical treatment, recent studies report long-term seizure freedom rates of only 50% (154). However, detection of neuronal loss in CA1 and CA4 subfields with postoperative pathology is consistently associated with a high likelihood of seizure freedom postoperatively (4, 5, 8). Detection of subfield-specific pathology in vivo could therefore potentially allow more accurate preoperative prediction of seizure-free outcomes in patients with epilepsy.

Measurement of hippocampal subfields in vivo has recently become feasible due to advances in magnetic resonance imaging (MRI) spatial resolution. Alterations in hippocampal shape have been used by some investigators to measure subfield-specific atrophy (250, 251), while cortical thickness measurements have been utilized in some protocols to determine subfield locations (252). The majority of published techniques have used a combination of anatomical landmarks and geometric rules to define subfield boundaries (236, 253-256). In total, at least twenty-one distinct methods have been used by different investigators to perform hippocampal subfield segmentation (257).

While previous segmentation protocols have been based on histological references (13), they have not been systematically validated in comparison to histology. Although subfield volumes have been the primary focus of hippocampal segmentation research to date (257), accurate volumetric information is critically dependent upon correct localization of subfield boundaries (232). Hippocampal subfields are defined by transitions in

cytoarchitecture detected with histological analysis (12-14). However, the accuracy of MRI-based subfield boundary delineation in comparison with histology remains unknown (191, 213). Ex vivo MRI has recently been used to allow histologically accurate measurement of the entorhinal cortex (210). In addition, coregistration of hippocampal histology with ex vivo MRI has been described (199, 202, 203), but such techniques have not yet been used to develop a histologically valid segmentation protocol for application to in vivo MRI.

In the present study, we aimed to: 1) develop a novel histology-based method for hippocampal body segmentation, using MRI-visible anatomical landmarks, and assess its accuracy in comparison to the gold standard direct histological measurements; 2) quantify the accuracy of two published segmentation strategies in comparison to the histological gold standard; and 3) apply the novel method to ex vivo MRI and correlate the results with histology.

9.2 Materials and Methods

Six temporal lobes (3 Left / 3 Right) were removed post-mortem from six subjects (age 61-96) with no known history of neuropsychiatric disorders. Brain specimens were fixed in formaldehyde for an average of six months. Surgical cuts were placed in the temporal neocortex to aid coregistration of ex vivo MRI and subsequent histology. Specimens were trimmed to fit into a 50 mL centrifuge tube and submerged in an MRI-compatible liquid fluorocarbon (Fluorinert, 3M). Imaging was performed on a 4.7 T MRI system (Varian, Palo Alto, CA) using a custom-built mouse coil. A T2-weighted (inverted contrast) fast-spin echo technique was used to acquire 40 contiguous 0.5-mm-thick slices, perpendicular to the long axis, across 2 cm of the hippocampal body

[echo time (TE) = 39 ms, repetition time (TR) = 10,000 ms, FOV 40 x 40 mm, in-plane matrix 200 x 200] yielding a native resolution of 0.2 x 0.2 x 0.5 mm³ in nine minutes of total scan time.

Following MRI, each hippocampus (n=6) was dissected from the surrounding temporal lobe and cut, perpendicular to the long axis of the hippocampal body, into four equal 5 mm blocks (n=4x6=24). Previous studies have demonstrated functional differences along the hippocampal long axis (258), while some hippocampal pathologies can also demonstrate variability along the anteroposterior extent of this structure (136). Therefore, the location of the blocks along the anterior-posterior axis of the hippocampus was noted and included in order to allow block-wise analyses along the hippocampal long axis. The blocks were embedded with paraffin and a single 5 µm histological section was taken from each 5 mm block. Two of the blocks contained only tissue from the hippocampal head and were therefore not analyzed. This yielded a final n=22 histological sections for our study.

Gold standard histology measurements

Histological sections (n=22) were stained with cresyl violet / luxol fast blue (Figure 9.1i) as described elsewhere (238). The length of the stratum lacunosum moleculare (SLM) from the superficial hippocampal sulcus to the blades of the DG was measured using the curvilinear measurement tool in ImageJ (259) for each of the histological sections (n=22). Hippocampal subfields were delineated according to histological criteria (12-14) by an experienced neuropathologist (RC), who has substantial experience measuring hippocampal subfields in surgical specimens (Figure 9.1v).

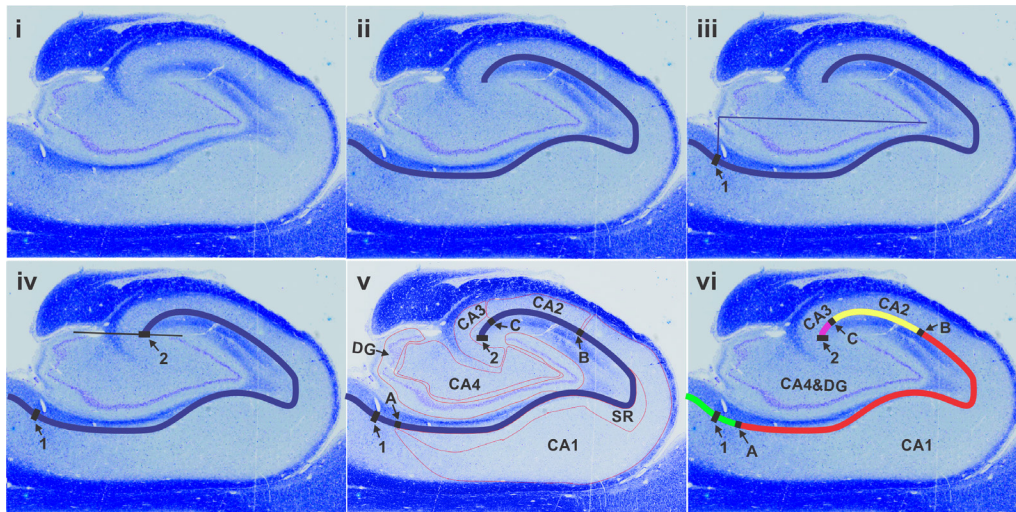


Figure 9.1 - Histology measurements of subfield boundaries and areas

i) Histological sections were stained with cresyl violet / luxol fast blue. ii) The stratum lacunosum moleculare (SLM) was delineated. iii) A line was drawn across the hippocampus connecting the most mesial to the most lateral point of the dentate gyrus (DG). A line was then drawn perpendicular to the first to define the beginning of the SLM (1) at the superficial hippocampal sulcus. iv) A line was then drawn connecting the superior portions of the blades of the DG to define the termination of the SLM (2) at the blades of the DG. v)

Hippocampal subfields (stratum pyramidale) were defined according to histological criteria (12-14) by an experienced neuropathologist. The locations of three hippocampal subfield boundaries: Subiculum/CA1 (A), CA1/CA2 (B), and CA2/CA3 (C) were directly determined. Gold standard measures of hippocampal subfield areas were obtained for CA1-4 & DG. The stratum radiatum (SR) was not included in hippocampal subfield area measurements.

vi) Distances of three hippocampal subfield boundaries [Subiculum/CA1 (A), CA1/CA2 (B), and CA2/CA3 (C)] along a line from the superficial hippocampal sulcus (1) to the blades of the DG (2) were directly measured.

The stratum lacunosum moleculare (SLM) was colour-coded according to histologically defined subfield locations in this specific section (Subiculum, green; CA1, red; CA2, yellow; CA3, pink). In order to allow a direct visual comparison of differences in the different techniques, Figures 9.1 to 9.4 all use the same histological section.

The distances of three hippocampal subfield boundaries (Subiculum/CA1, CA1/CA2, and CA2/CA3) along a line from the superficial hippocampal sulcus to the blades of the DG were directly measured (Figure 9.1vi). The distances to these subfield boundaries were used: i) as the basis for the novel method and ii) as the gold standard to which the novel method and the previously reported methods were compared in the validation study. Gold standard measures of hippocampal subfield areas were also obtained for CA1-4 & DG (Figure 9.1v).

Novel method

The novel method used two anatomical landmarks, SLM & DG, which can be identified on histology and in vivo MRI (180). The SLM was identified on histology as an arcuate structure with increased luxol fast blue staining separating the CA subfields from the DG (Figure 9.2i). The outer boundary of the SLM was chosen for delineation of this structure on histology (Figure 9.2ii). We hypothesized that hippocampal subfields occur at predictable locations as a proportion of SLM length. To develop the novel method, we therefore converted each subfield boundary to a percentage of the total SLM length. The mean value, for all 22 histological sections, was calculated for each of the three subfield boundaries: Subiculum/CA1, 9.7%; CA1/CA2, 78.4%; CA2/CA3, 97.5%.

These mean percentages of the total SLM length were then used to determine the locations of the three subfield boundaries: Subiculum/CA1, CA1/CA2, and CA2/CA3 (Figure 9.2v). For each of the 22 sections, the distance of each subfield boundary from the superficial hippocampal sulcus was measured (Figure 9.2vi). These distances were compared with the gold

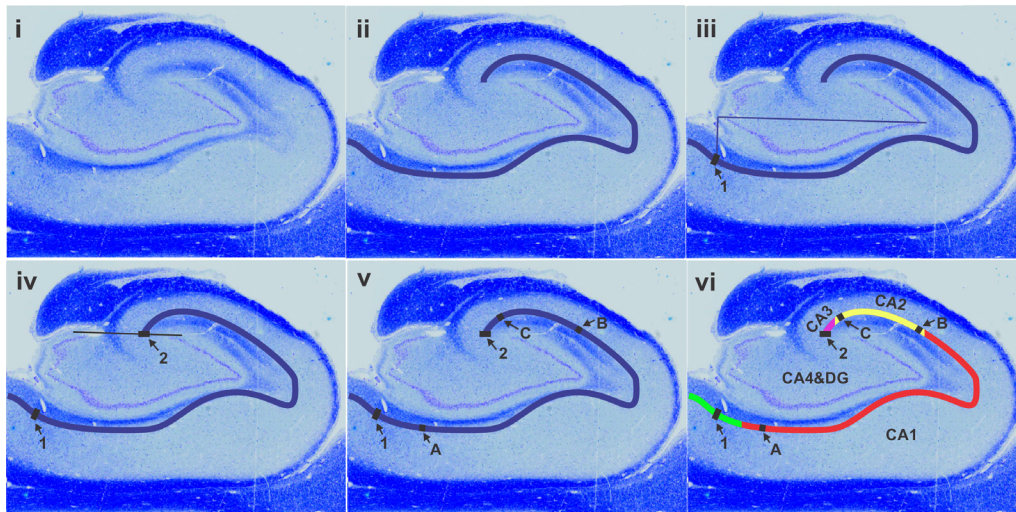


Figure 9.2 - Subfield boundaries according to the novel method

i) Histological sections were stained with cresyl violet / luxol fast blue. ii) The stratum lacunosum moleculare (SLM) was delineated. iii) A line was drawn across the hippocampus connecting the most mesial to the most lateral point of the dentate gyrus (DG). A line was then drawn perpendicular to the first to define the beginning of the SLM (1) at the superficial hippocampal sulcus. iv) A line was then drawn connecting the superior portions of the blades of the DG to define the termination of the SLM (2) at the blades of the DG. v) Mean percentages of the total SLM length were used to determine the locations of three subfield boundaries Subiculum/CA1 (A), CA1/CA2 (B), and CA2/CA3 (C). vi) The SLM was colour-coded according to the gold standard histologically defined subfield locations (Subiculum, green; CA1, red; CA2, yellow; CA3, pink). For this specific section the CA1/CA2 and CA2/CA3 boundaries as determined by the novel method were accurate in comparison with the gold standard whereas the Subiculum/CA1 boundary was less accurate.

standard histology measurements using the Bland-Altman method (260), using linear regression for calculation of coefficient of determination (r^2), and through calculation of intraclass-correlation coefficients (ICCs). The Bland-Altman analysis determines the agreement between two methods of measurement by plotting the difference between measures (dependent variable) against the gold standard (independent variable).

Previous Techniques

We identified two techniques [Technique 1, (254); Technique 2, (190)] from the previous literature with sufficient granularity (providing separate measurements for CA1, CA2, and CA3) to allow comparison with the novel method. For each technique, the locations of three subfield boundaries (Subiculum/CA1, CA1/CA2, and CA2/CA3) were determined according to their respective segmentation protocols (Figures 9.3 & 9.4 and Supplementary Methods). For each of the 22 sections, the distance of each subfield boundary from the superficial hippocampal sulcus was measured. Subfield boundary distances were then compared to the gold standard (directly measured distances) by the Bland-Altman method, using linear regression for calculation of coefficient of determination (r^2), and through calculation of intraclass-correlation coefficients (ICCs).

Intra- and Inter-rater reliability

Segmentation using the novel method was repeated by a single rater (TAS) at an interval of one month for assessment of intra-rater reliability. The same measurements were performed by an additional investigator (CLY) to determine inter-rater reliability. Agreement was determined by calculation of intra-class correlation coefficient (ICC). The entire sample (n=22 histological sections) was used for the reliability analyses. As the novel method involves only one measurement (length of the SLM with the boundaries being percentages of SLM length), reliability is not presented for individual subfields but rather represented by a single ICC.

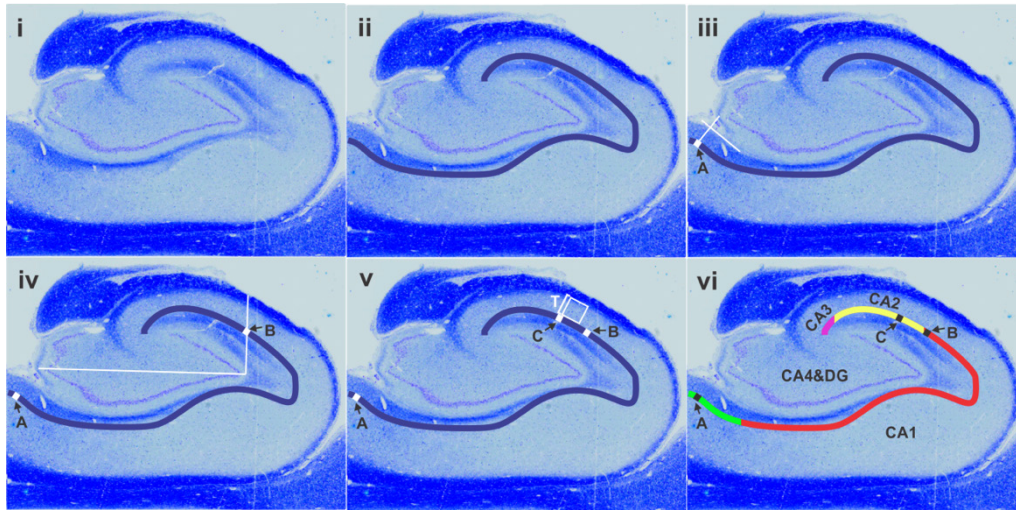


Figure 9.3 - Subfield boundaries according to Technique 1

i) Histological sections were stained with cresyl violet / luxol fast blue. ii) The stratum lacunosum moleculare (SLM) was delineated. iii) Subiculum/CA1: The boundary between CA1 and Subiculum (A) was measured by drawing a straight line parallel to the longitudinal axis of the subiculum, and then drawing a second line perpendicular to the first at the supero-mesial edge of the dentate gyrus (DG). iv) CA1/CA2: A line was drawn connecting the most mesial to the most lateral point of the DG. A second line was then drawn perpendicular to the first at the most lateral point of the DG, to define the boundary between CA1 and CA2 (B). v) CA2/CA3: The boundary between CA2 and CA3 (C) was defined by drawing a virtual square. The four sides of this square had a length equal to the thickness of CA2 at the boundary with CA3 (T). vi) The SLM was colour-coded according to the gold standard histologically defined subfield locations in this specific section (Subiculum, green; CA1, red; CA2, yellow; CA3, pink). In this particular section, the defined CA1 region includes a substantial amount of subiculum and CA3 includes a substantial amount of CA2. In this particular section, the CA1/CA2 boundary was accurately predicted with this method.

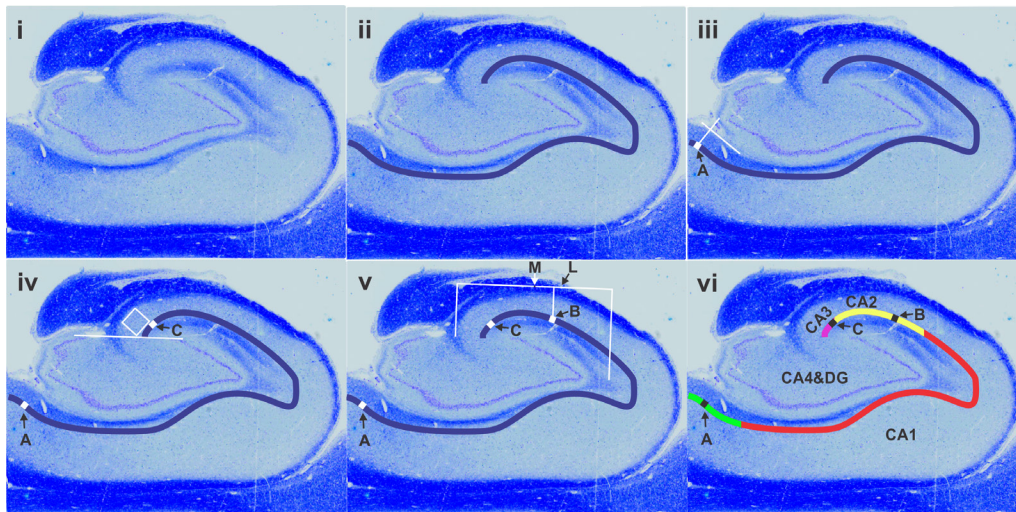


Figure 9.4 - Subfield boundaries according to Technique 2

i) Histological sections were stained with cresyl violet / luxol fast blue. ii) The stratum lacunosum moleculare (SLM) was delineated. iii) Subiculum/CA1: The boundary between CA1 and Subiculum (A) was measured by drawing a straight line along the edge of the dentate gyrus (DG), and then drawing a second line perpendicular to the first at the supero-mesial edge of the DG. iv) CA2/CA3: Based on the segmentation protocol, a voxel was defined as a square measuring 0.4 X 0.4 mm². The boundary between CA2 and CA3 (C) was identified by measuring 0.4 mm (one voxel) above the superior portions of the blades of the DG. v) CA1/CA2: A line (L) was drawn from the medial edge of CA3 to the lateral edge of DG. The midpoint (M) of this line was then defined. The CA1/CA2 boundary (B) was identified by drawing a line perpendicular to the first, one voxel (0.4 mm) lateral to the vertical line. vi) The SLM was colour-coded according to the gold standard histologically defined subfield locations in this specific section (Subiculum, green; CA1, red; CA2, yellow; CA3, pink). In this particular section, the defined CA1 region includes a substantial amount of subiculum and CA2. In this particular section, the CA2/CA3 boundary was accurately predicted with this method.

Application of novel method to ex vivo MRI

We manually coregistered histology sections to ex vivo MRI using surgical cuts in the temporal neocortex as fiducial markers (Figure 9.5). Ex vivo MRI was performed with a slice thickness of 0.5 mm, while each tissue block was 5 mm thick. Therefore, as shown in Figure 9.5, each tissue block was known to correspond to a 10-slice portion of the ex vivo MRI. As described above, a single 5 μm histological section was taken from each 5 mm tissue block. Upon histological examination, we qualitatively analyzed each slice and identified the best matching MRI slice for analysis (Figure 9.5).

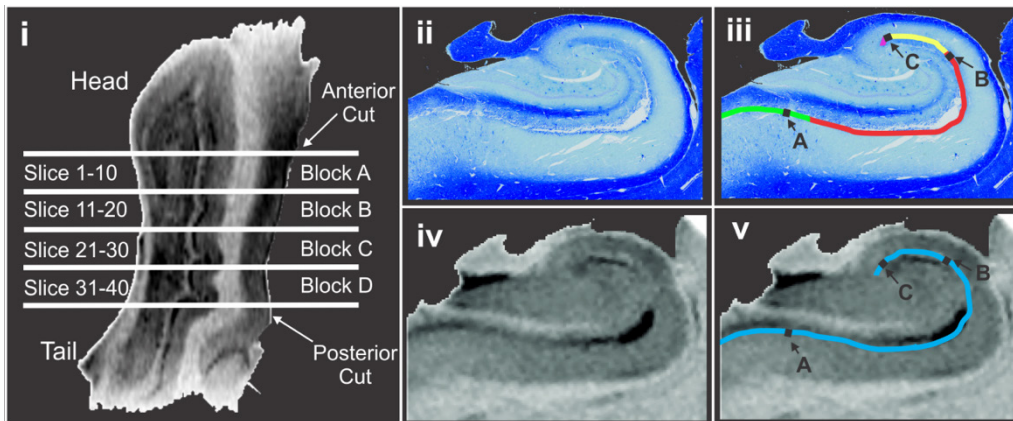


Figure 9.5 - Coregistration of ex vivo MRI with histology

Ultra-high resolution ex vivo MRI (voxel size 0.2 x 0.2 x 0.5 mm³) was performed prior to histological sectioning. i) Anatomical blocks of the hippocampal body (A-D) were coregistered to ex vivo MRI slices (1-40) using fiducial markers (anterior and posterior cuts).

Corresponding histological (ii) and ex vivo MR images (iv) were then identified by qualitatively matching features of the hippocampal architecture. iii) The stratum lacunosum moleculare (SLM) was colour-coded according to histologically defined subfield locations in this specific section (Subiculum, green; CA1, red; CA2, yellow; CA3, pink). v) The SLM was manually traced based on differences in signal intensity between grey and white matter (blue).

iii and v) The novel method was applied to histology (iii) and ex vivo MRI (v): Mean percentages of the total SLM length were used to determine the location of three subfield boundaries: [Subiculum/CA1 (A), CA1/CA2 (B), and CA2/CA3 (C)].

The SLM was identified on our ex vivo MR images as an arcuate structure with increased signal compared with hippocampal grey matter, running from the superficial hippocampal sulcus to the blades of the DG. The SLM was traced by following the boundary of the cornu ammonis grey matter with the adjacent white matter. However, the SLM was not as clearly defined on MRI in comparison to histology in the present study (Figures 9.5 & 9.6). Presumed tissue fixation artifacts, visualized as regions of decreased intensity in the majority of sections (Figures 9.5 & 9.6), represent a partial explanation for the less clear definition of the SLM in the present study.

The length of the SLM was measured on MRI using the curvilinear measurement tool in ImageJ. In order to apply the novel method to MRI, mean percentages of the total SLM length were used to determine the locations of three subfield boundaries: Subiculum/CA1, CA1/CA2, and CA2/CA3 (Figure 9.5v). For each of the 22 sections, the distance of each subfield boundary from the superficial hippocampal sulcus was measured. These distances were compared, using linear regression for calculation of coefficient of determination (r^2), with the histology results as determined 1) by the gold standard (direct measurement) and 2) using the novel method.

Segmentation of ex vivo MRI was repeated by a single rater (Trevor A. Steve) at an interval of one month for assessment of intra-rater reliability. The same measurements were performed by an additional investigator (Clarissa L. Yasuda) to determine inter-rater reliability. Agreement was determined by calculation of ICC. The entire sample (n=22 histological sections) was used for the reliability analyses.

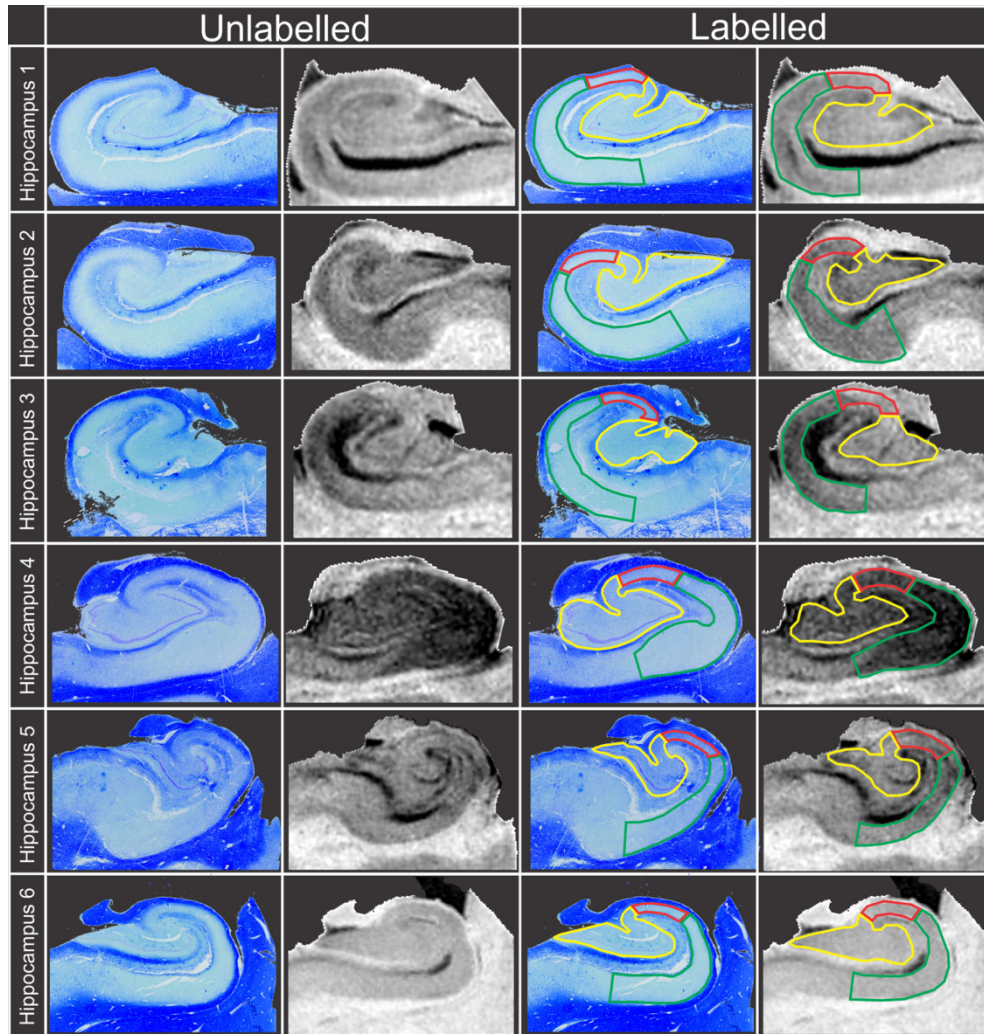


Figure 9.6 - Subfield area measurements

Corresponding histology and ex vivo MRI slices are displayed for each hippocampus ($n=6$), allowing qualitative analysis of coregistration success (Unlabelled panel). In all corresponding sections (Labelled, total $n=21$), the novel method was applied to segment separate areas for three subfields: CA1 (green), CA2 (red), and CA3/CA4/DG (yellow). Subfield areas measured on histology and ex vivo MRI were compared to each other, and to the direct (gold standard) histology measurements, using linear regression for calculation of coefficient of determination (r^2). The SLM was partially obscured by tissue fixation artifact, represented by a region of decreased intensity, which was present on the majority of sections.

Subfield area measurements

We used the novel method to measure subfield areas in corresponding histological sections and ex vivo MRI slices. The CA3/CA4/DG subfields in one of the blocks could not be analyzed due to artifacts induced by tissue sectioning, yielding a final n=21 for the areas analysis for this subfield area measurement.

The mean percentages of total SLM length were used to determine the locations of the CA1/CA2 (78.4%) and CA2/CA3 (97.5%) subfield boundaries. Given the poor performance of the mean in predicting individual Subiculum/CA1 boundary distances (Figures 9.9 & 9.10, Table 9.1), we instead chose to use the limit (26.2% of the total SLM distance, the maximum value from the gold standard histology data) to define the boundary for the CA1 subfield area. The rationale behind this decision was that in using the limit, the CA1 region defined would not include any Subiculum and would therefore be a “pure” CA1 measurement. For each of the 21 sections, separate area measurements were made for the CA1 and CA2 subfields (Figure 9.6). As the boundary between CA3 and CA4 was located within the blades of the DG in the vast majority of sections, we combined all subfields within the end folium into a single area measurement: CA3/CA4/DG (Yellow, Figure 9.6). Subfield areas (CA1, CA2, and CA3/CA4/ DG) measured using the novel method on histology and ex vivo MRI were compared to each other, and to the direct (gold standard) histology measurements using linear regression for calculation of coefficient of determination (r^2).

Segmentation of subfield areas on histology and ex vivo MRI was repeated by a single rater (TAS) at an interval of one month for assessment of intra-rater reliability. The same measurements were performed by an additional

investigator (ML) to determine inter-rater reliability. Agreement was determined by calculation of ICC. The entire sample (n=21 histological sections for subfield area measurements) was used for the reliability analyses.

9.3 Results

Direct measurements

The mean total SLM length (Figure 9.7) was 16.17 mm (95% confidence interval = 15.38 to 16.95 mm; range = 13.89 to 19.57 mm). The mean distance of the Subiculum/CA1 boundary from the superficial hippocampal sulcus was 1.55 mm (95% confidence interval = 1.03 to 2.07 mm; range = -0.42 to 4.60 mm). The mean distance for the CA1/CA2 boundary was 12.66 mm (95% confidence interval = 12.04 to 13.29 mm; range = 10.36 to 15.50 mm). The average distance for the CA2/CA3 boundary was 15.74 mm (95% confidence interval = 15.03 to 16.45 mm; range = 13.79 to 18.73 mm). The mean percentage of total SLM distance for the Subiculum/CA1 boundary from the superficial hippocampal sulcus was 9.7% (95% confidence interval = 6.6 to 12.8%; range = -2.1 to 26.2%). The mean percentage of total SLM distance for the CA1/CA2 boundary was 78.4% (95% confidence interval = 76.8 to 80.0%; range = 69.8 to 83.0%). The mean percentage of total SLM distance for the CA2/CA3 boundary was 97.5% (95% confidence interval = 96.5 to 98.4%; range = 92.1 to 100.7%).

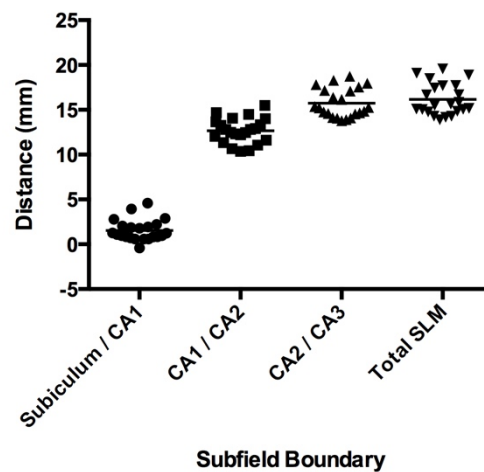


Figure 9.7 - Descriptive statistics

Distances from the hippocampal sulcus as determined by direct measurement (gold standard histology) are displayed for three subfield boundaries (Subiculum/CA1, CA1/CA2, and CA2/CA3) and for the total length of the stratum lacunosum moleculare (SLM).

Agreement between novel method and direct measurements

Segmentations of individual histological sections from each hippocampus (n=6) according to the novel method and gold standard histology are displayed in Figure 9.8. For CA1/CA2 and CA2/CA3 subfield boundaries, the novel method demonstrated excellent accuracy and Bland-Altman analysis revealed no systematic bias in comparison with directly measured boundaries (Figure 9.9). Proportional bias, defined as greater difference between measures with higher gold standard measurements, was observed for the Subiculum/CA1 boundary. The novel method demonstrated poor correlation ($r^2=0.01$, $p=0.76$; ICC = -0.04) with direct measurements at the Subiculum/CA1 boundary (Figure 9.10 and Table 9.1).

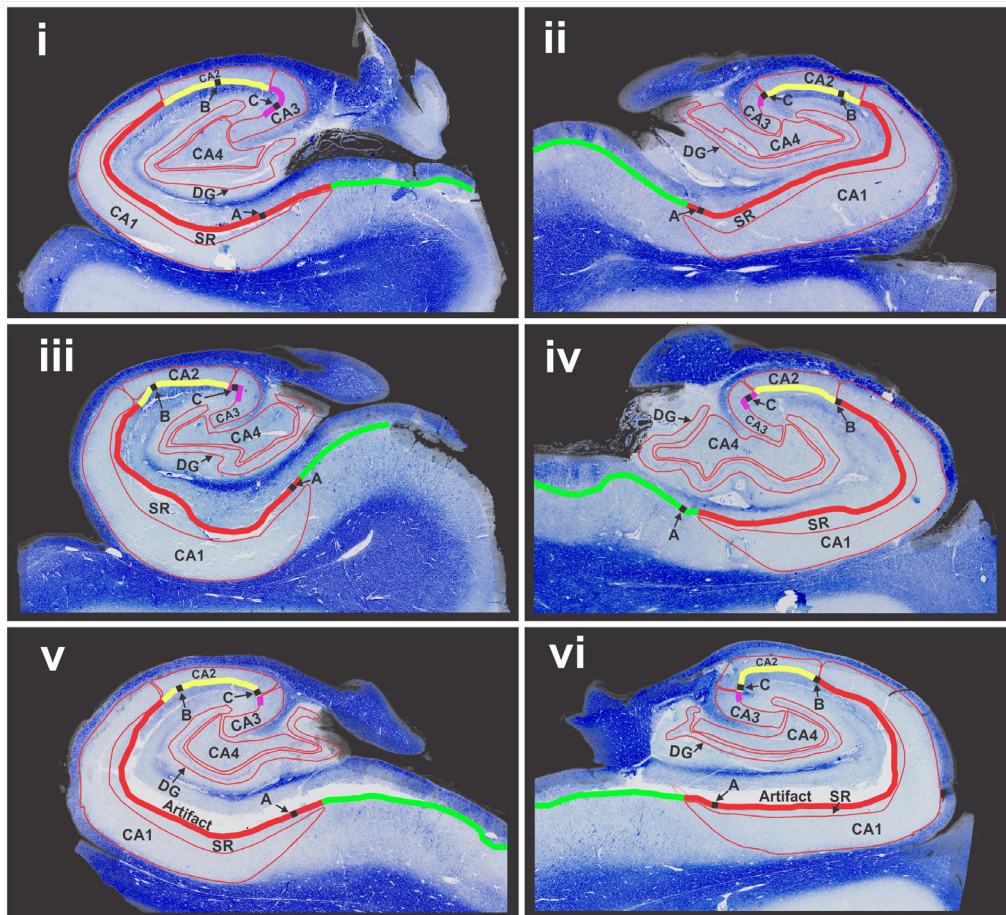


Figure 9.8 - Segmentation according to the novel method

Segmentations of individual histological sections are displayed for each hippocampus (i-vi), allowing qualitative evaluation of the novel method in comparison to gold standard histology measurements. Hippocampal subfields (CA1-4, Dentate Gyrus [DG], and Stratum Radiatum [SR]) were defined according to histological criteria by an experienced neuropathologist. The stratum lacunosum moleculare (SLM) was colour-coded according to histologically defined subfield locations in each specific section (Subiculum, green; CA1, red; CA2, yellow; CA3, pink). Parcellation according to the novel method (using mean percentages of the total SLM length) was then applied to determine the locations of three subfield boundaries: Subiculum/CA1 (A), CA1/CA2 (B), and CA2/CA3 (C).

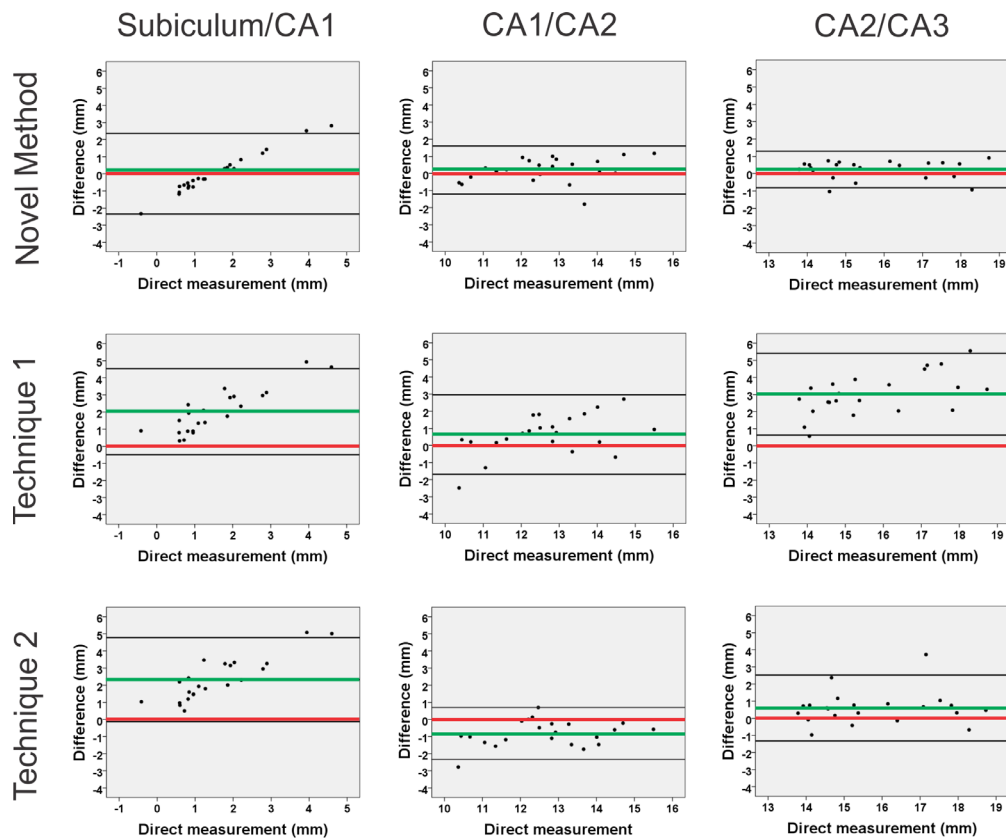


Figure 9.9 - Accuracy of novel method versus previous techniques

Agreement with direct measurements at three subfield boundaries (Subiculum/CA1, CA1/CA2, and CA2/CA3) was assessed by the Bland-Altman method. Perfect agreement (no difference from direct measurements) is indicated by the red line. Mean error (green line) and Bland-Altman limits of agreement (black lines) are also shown. In comparison to Technique 1, the novel method demonstrated reduced systematic bias (distance between red and green lines) and narrower Bland-Altman limits of agreement (distance between black lines) for the CA1/CA2 and CA2/CA3 boundaries. In comparison to Technique 2, the novel method demonstrated reduced systematic bias with similar Bland-Altman limits of agreement at the CA1/CA2 boundary. For the CA2/CA3 boundary, the novel method demonstrated reduced systematic bias and narrower Bland-Altman limits of agreement in comparison with Technique 2. Proportional bias was noted for all techniques (including the novel method) at the Subiculum/CA1 boundary, suggesting limitations for each method in predicting this subfield location.

In contrast, the boundary distance measurements according to the novel method were strongly correlated with gold standard histological distances at CA1/CA2 ($r^2=0.75$, $p=1.7 \times 10^{-7}$; ICC = 0.93) and CA2/CA3 ($r^2=0.90$, $p=2.0 \times 10^{-11}$; ICC = 0.97) boundaries (Figure 9.10 and Table 9.1).

Agreement between previous techniques and direct measurements

In comparison to the novel method, the previous techniques demonstrated poorer agreement with direct measurements (Figures 9.9 & 9.10, Table 9.1). As with the novel method, the previous techniques demonstrated proportional bias at the Subiculum/CA1 boundary. For Technique 1, greater systematic bias and wider Bland-Altman limits of agreement was demonstrated at the CA1/CA2 and CA2/CA3 boundaries. At the CA1/CA2 boundary, Technique 2 demonstrated greater systematic bias with similar Bland-Altman limits of agreement. For the CA2/CA3 boundary Technique 2 demonstrated greater systematic bias and wider Bland-Altman limits of agreement.

As seen for the novel method, poor correlation ($r^2 < 0.1$, $p > 0.5$; ICC = 0.00) with the gold standard at the Subiculum/CA1 boundary was demonstrated for both previous techniques (Figure 9.10 and Table 9.1). At the CA1/CA2 boundary, strongest correlations ($r^2=0.73$, $p=4.7 \times 10^{-7}$; ICC = 0.85) with gold standard measurements were demonstrated for Technique 2. For the CA2/CA3 boundary distances, correlations with gold standard measurements were also strongest ($r^2=0.70$, $p=1.0 \times 10^{-6}$; ICC = 0.88) for Technique 2.

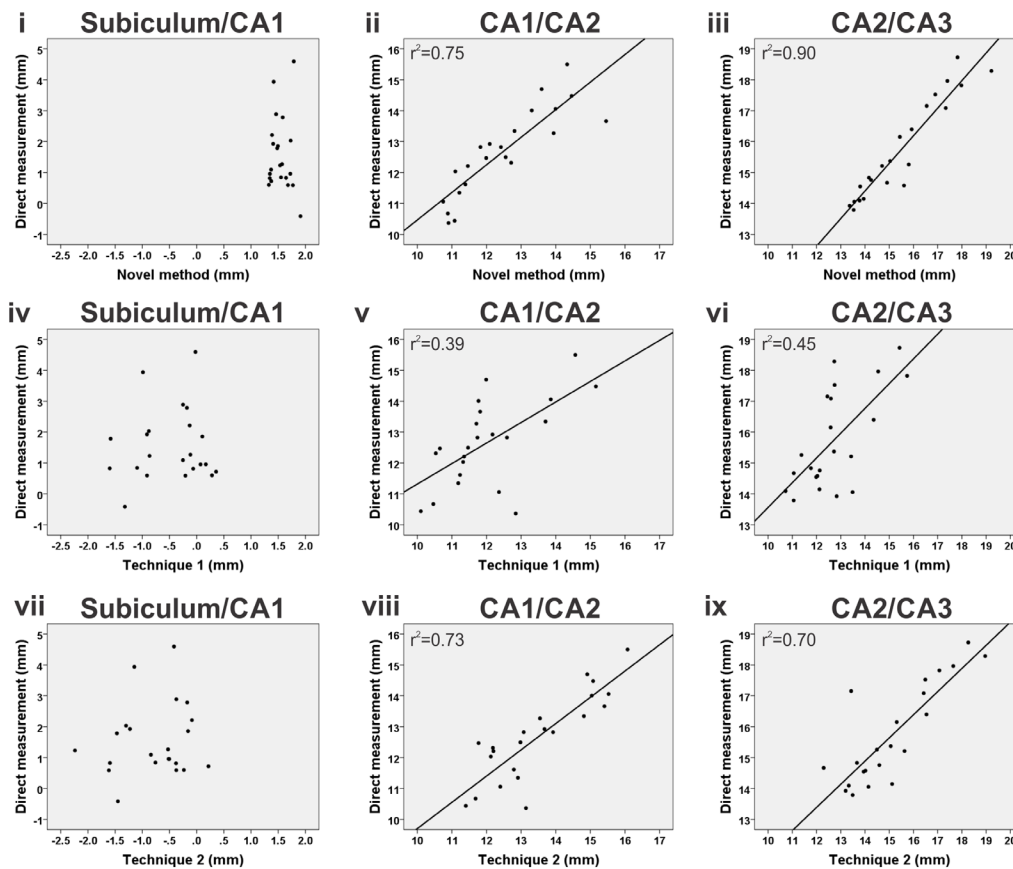


Figure 9.10 - Histological measurement of subfield boundary distances

Distances of three subfield boundaries (Subiculum/CA1, CA1/CA2, and CA2/CA3) from the superficial hippocampal sulcus were measured on histology according to the novel method (i-iii), Technique 1 (iv-vi) and Technique 2 (vii-ix). These measurements were compared with the direct (gold standard histology) measurements using linear regression.

Intra- and Inter-rater reliability of histology distances

Intra-rater (ICC=0.97, $p=7.0 \times 10^{-12}$) and inter-rater (ICC=0.97, $p=5.0 \times 10^{-13}$) reliability was excellent for the novel method.

Segmentation technique	Subfield Boundary		
	Subiculum/CA1 ICC (r ²)	CA1/CA2 ICC (r ²)	CA2/CA3 ICC (r ²)
Novel method	-0.04 (0.01)	0.93 (0.75)	0.97 (0.90)
Technique 1	0.00 (0.01)	0.73 (0.39)	0.35 (0.45)
Technique 2	0.00 (0.02)	0.85 (0.73)	0.88 (0.70)

Table 9.1 - Accuracy of novel method versus previous techniques

Intra-Class Correlation Coefficients (ICCs) and coefficients of determination (r²) were calculated for three segmentation techniques in reference to the gold standard at three hippocampal subfield boundaries. Poor correlation (ICC ≤ 0.00) with the gold standard was seen at the Subiculum/CA1 boundary for all methods. At the CA1/CA2 boundary, the novel method demonstrated greater correlation (ICC = 0.93) with gold standard measurements in comparison with previous techniques (maximum ICC = 0.85, Technique 2). Similarly, for the CA2/CA3 boundary, the novel method demonstrated superior correlation (ICC = 0.97) with gold standard measurements compared to previous methods (maximum ICC = 0.88, Technique 2).

Direct measurements of subfield boundaries in relation to block position and hippocampus

Despite variability of total SLM length according to block position, direct measurements of subfield boundaries as a percentage of the total SLM length were strongly consistent along the longitudinal axis of the hippocampus (Figure 9.11).

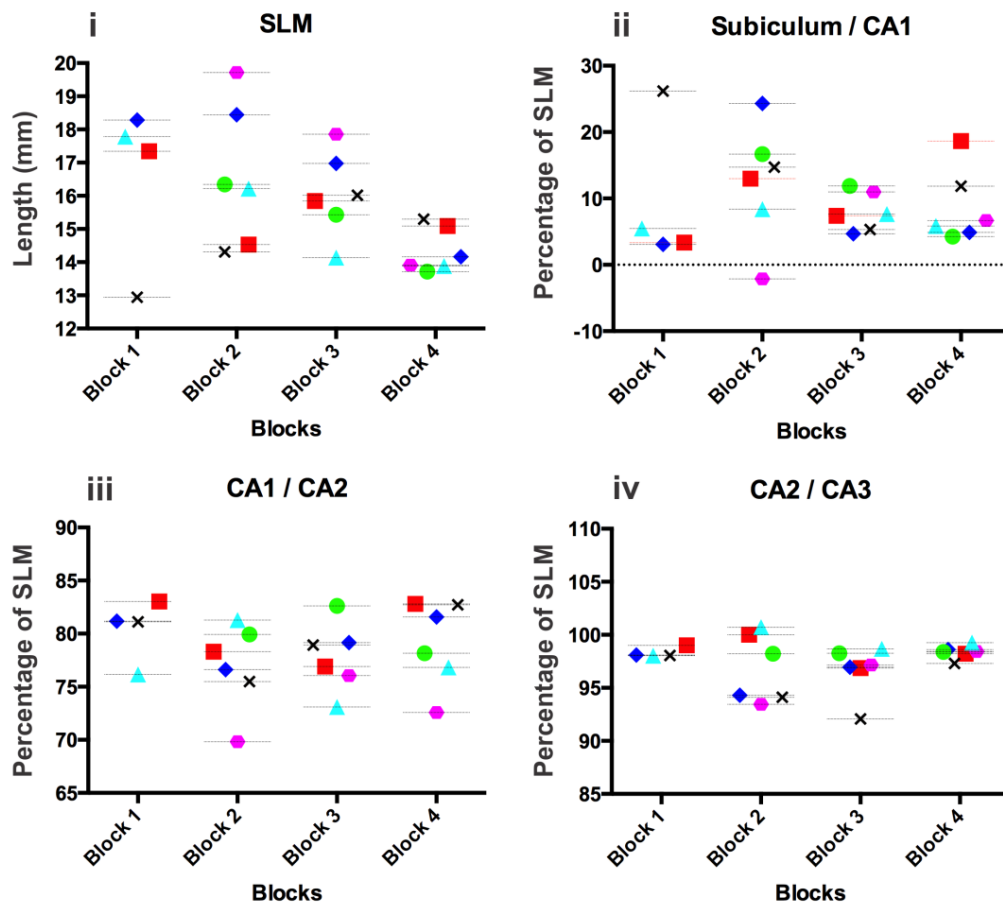


Figure 9.11 - Direct measurements along the longitudinal axis

Data are displayed according to location of blocks (Block 1, most anterior; Block 4, most posterior). All blocks from a given hippocampus are represented by the same shape and colour. i) Length of the stratum lacunosum moleculare (SLM). Variability is demonstrated along the longitudinal axis, with more posterior blocks demonstrating shorter total SLM length. ii-iv) Percentages of SLM length are displayed for three subfield boundaries: Subiculum/CA1, CA1/CA2, and CA2/CA3. Block-wise analysis indicates that while the total SLM length showed differences (lowest for the most posterior block [block 4]), the percentage of SLM length remained consistent along the longitudinal hippocampal axis for each subfield boundary.

Subfield boundary locations according to hippocampus (1-6) are shown in Figure 9.12. The distance of Subiculum/CA1, CA1/CA2, and CA2/CA3 boundaries as a percentage of the total SLM length were consistent between the six hippocampi.

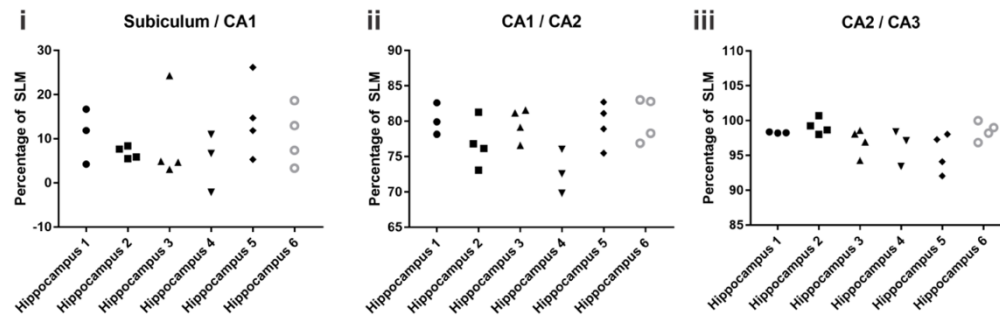


Figure 9.12 - Effect of hippocampus on direct measurements

Subfield boundary locations (mean and standard deviation) including all hippocampi versus deletion of a single hippocampus (1-6) are shown in Figure 9.13. The distance of Subiculum/CA1, CA1/CA2, and CA2/CA3 boundaries as a percentage of the total SLM length were not altered by deletion of any single hippocampus.

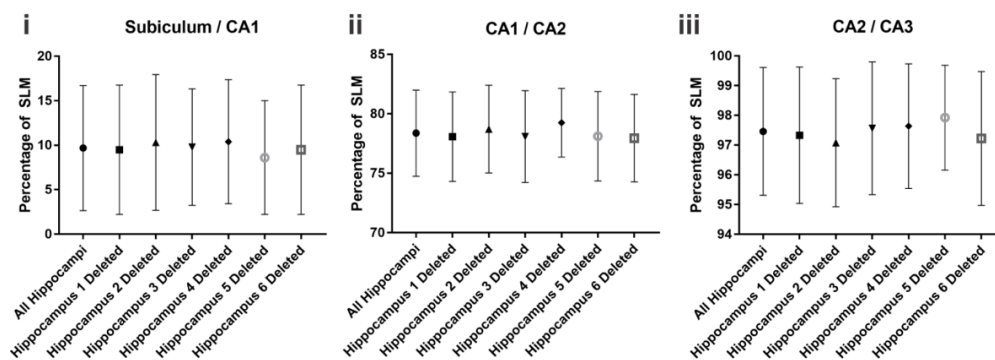


Figure 9.13 - Effect of hippocampus deletion on direct measurements

MRI measurements of hippocampal subfield boundary distances

A statistically significant linear relationship was demonstrated between SLM measurements with ex vivo MRI and histology ($r^2=0.58$, $p=4.0 \times 10^{-5}$). The relationships between ex vivo MRI subfield boundary distances using the novel method and direct histological measurements were: Subiculum/CA1 ($r^2=0.01$, $p=0.66$), CA1/CA2 boundary ($r^2=0.39$, $p=0.002$) and CA2/CA3 boundary ($r^2=0.47$, $p=4.0 \times 10^{-4}$). Intra-rater reliability ($ICC=0.97$, $p=2.2 \times 10^{-11}$) was higher in comparison to inter-rater reliability ($ICC=0.75$, $p=6.6 \times 10^{-7}$) for ex vivo MRI measurements.

Histological and MRI measurements of subfield areas

Linear regression of histological and MRI measures of subfield areas are shown in Figure 9.14. Subfield areas measured using the novel method on histology were linearly related to direct (gold standard) histological measurements at the CA1 ($r^2=0.45$, $p=0.001$), CA2 ($r^2=0.60$, $p=2.6 \times 10^{-5}$), and CA3/CA4/DG ($r^2=0.84$, $p=5.5 \times 10^{-9}$) subfield areas (Figure 9.14 i-iii). The novel method provided comparable area measurements when applied to ex vivo MRI and histology for CA1 ($r^2=0.48$, $p=3.8 \times 10^{-4}$); CA2 ($r^2=0.42$, $p=0.001$); CA3/CA4/DG ($r^2=0.72$, $p=1.0 \times 10^{-6}$) (Figure 9.14 iv-vi). Finally, ex vivo MRI measures using the novel method were linearly related to direct histological measurements of CA1 ($r^2=0.26$, $p=0.02$); CA2 ($r^2=0.23$, $p=0.02$); CA3/CA4/DG ($r^2=0.61$, $p=2.8 \times 10^{-5}$) subfields (Figure 9.14 vii-ix).

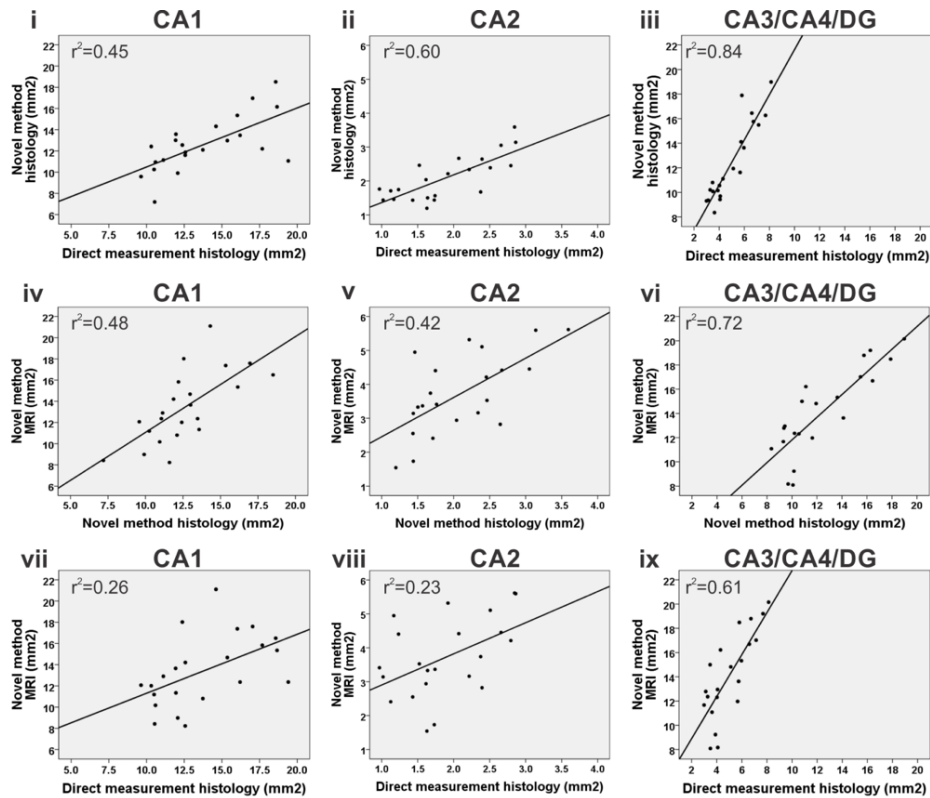


Figure 9.14 - Histological and MRI measurements

Linear regression is displayed comparing subfield areas (CA1, CA2, and CA3/CA4/DG) measured using the novel method on histology with direct (gold standard) histology measurements (i-iii). Ex vivo MRI measurements using the novel method are compared with both novel method histology (iv-vi) and direct histological measurements (vii-ix).

Reliability of subfield area measurements

Intra- and inter-rater reliabilities for each subfield measurement (CA1, CA2, and CA3/CA4/DG) on histology and MRI are shown in Table 9.2. Reliability on histology (ICC 0.76 - 0.99) was higher in comparison to MRI (ICC 0.66 - 0.95).

Modality	Reliability Type	Subfield		
		CA1	CA2	CA3/CA4/DG
Histology	Intra-rater	0.99	0.96	0.99
	Inter-rater	0.76	0.81	0.92
MRI	Intra-rater	0.95	0.82	0.89
	Inter-rater	0.87	0.75	0.66

Table 9.2 - Intra- and inter-rater reliability of hippocampal subfield areas

Intra-class correlation coefficients are shown for intra- and inter-rater reliability of each subfield measurement (CA1, CA2, and CA3/CA4/DG) on histology and MRI.

9.4 Discussion

The presence of MRI-visible anatomical landmarks with known correspondence to histology represents a fundamental prerequisite for in vivo hippocampal subfield segmentation (232). The goal of the present study was to develop a histologically validated approach to subfield segmentation based on two MRI-visible anatomical landmarks, the SLM & DG. These structures were chosen as they are readily visualized with in vivo MRI (180). Based on these landmarks, we used histology of cadaveric specimens to develop and validate a method to localize subfield boundaries in the hippocampal body. The novel method used mean percentage of the total SLM distance to define three subfield boundaries. Our novel method, applied to histology, demonstrated improved accuracy at the CA1/CA2 and CA2/CA3 boundaries in comparison with previously reported MRI based protocols, which were also evaluated. However, none of the methods evaluated performed well in determining the Subiculum/CA1 boundary.

Based on these results, we then applied the novel method of boundary determination to analyze subfield areas in order to develop a histologically validated subfield segmentation protocol. Given the poor performance of our novel method (as well as the two previously reported protocols) in determining the Subiculum/CA1 boundary, we used 26.2% of the total SLM distance (the maximum value from our gold standard histology data) to define the Subiculum/CA1 boundary. The rationale behind using the limit for the Subiculum/CA1 boundary from the histological data was to generate a pure CA1 area that did not include any of the Subiculum/CA1 transition zone. As discussed below, however, we acknowledge that by using the limit for the Subiculum/CA1 boundary, the method for subfield area segmentation described is expected to underestimate true CA1 subfield volumes. Future studies will be required to explore alternative approaches to accurately defining the Subiculum/CA1 boundary.

Furthermore, we combined all subfields within the end folium into a single subfield measurement (CA3/CA4/DG). Subfield areas (CA1, CA2, and CA3/CA4/DG) measured with the novel method on histology were linearly related to gold standard histological measures. Finally, we applied the novel method to ex vivo MRI and compared subfield boundary distances and areas with those measured on histology. MRI distance measurements using the novel method were linearly related to histological distance measures for the CA1/CA2 and CA2/CA3 boundaries. Ex vivo MRI measures of subfield areas (CA1, CA2, and CA3/CA4/DG) using the novel method were also linearly related to direct (gold standard) histological measurements.

To the best of our knowledge, this is the first study to examine the histological accuracy of MRI-based hippocampal segmentation protocols.

While previous investigators have performed hippocampal subfield volumetry on ex vivo MRI (191, 213), these results have not been histologically validated. Our study builds on previous work demonstrating the feasibility of applying histology-based hippocampal subfield delineation to ex vivo MRI (199, 202, 203). In comparison with previous studies, ours is the first to develop histology-based segmentation rules for potential application to in vivo MRI. Our method is based on anatomical landmarks, SLM & DG, which can be clearly delineated on in vivo MRI (257), supporting the potential feasibility of applying this technique in vivo.

Limitations

While the novel method was successful when applied to histology, linear relationships were not as strong when the method was adapted to ex vivo MRI. There are several potential explanations for this discrepancy. First, the novel method relies upon adequate visualization of the SLM in order to determine subfield boundary locations. Ex vivo MRI measurements of the SLM in the present study were linearly related to gold standard histological measurements of this structure. However, in the present study the SLM was often not as clearly defined on MR Images in comparison with histology (Figure 9.6), which is a potential explanation for poorer relationships seen between ex vivo MRI and histology in our study. Secondly, coregistration in our study was performed manually without use of computer-based coregistration techniques. Imperfect coregistration is therefore a second potential explanation for the poorer agreement between ex vivo MRI and histological measurements demonstrated in our study.

In addition to these considerations, our study has a number of further limitations. Importantly, we were unable to accurately determine the Subiculum/CA1 boundary with the novel method. As such, the novel method developed for subfield areas described in the present study used the limit to define the Subiculum/CA1 boundary. Therefore, the technique described herein would be expected to underestimate CA1 subfield measurements. This discrepancy may not have been detected in our analyses, as linear relationships may remain significant when a measurement consistently underestimates the gold standard. However, the magnitude of this underestimation when applied to in vivo MRI is expected to be small but potentially important. For example, using typical high-resolution in vivo MRI with an in-plane resolution of 0.7 mm, the difference between the limit (4.60 mm) and the mean (1.55 mm) distance from the superficial hippocampal sulcus would represent approximately 4 voxels ($[4.6 \text{ mm} - 1.55 \text{ mm}] \div 0.7 \text{ mm per voxel} = 4.35 \text{ voxels}$). Further studies will be required in order to develop a histologically valid method to locate the Subiculum/CA1 boundary.

Furthermore, we used a single sample (n=6) of cadaveric hippocampi to develop and validate the novel method. It remains possible that there is additional variability in the population which was not captured in the present study. For example, as discussed below, previous studies have described a different location for the CA2 subfield compared with that seen in our study (261). While our results provide initial evidence for histological accuracy, external validation in a separate independent data set will thus be required in order to reaffirm these preliminary findings. In addition, inter- and intra- rater reliability of hippocampal subfield delineations on histology remains a critical unanswered question in the literature.

Relatedly, we utilized a practical cytoarchitectonic definition for hippocampal subfields CA1-CA4 and DG. We chose this nomenclature as it is in common usage in clinical neuropathology, is widely accepted by neuroanatomists (12-14), and has been the basis of essentially all previously described segmentation protocols (257). However, further subdivision of the structures delineated in our study could potentially be performed with more sophisticated histological methods. For instance, recent studies have described further subdivision of hippocampal subfields using molecular markers (261, 262). The application of such markers could result in substantial inter-rater variability for histological definitions of hippocampal subfield boundaries, as discussed above. Further studies will be required to determine if these more discrete subdivisions can be accurately measured on histology and MRI.

In addition, data were acquired from subjects without a history of neurological disease and whether our method is valid in patients with known hippocampal pathology, such as temporal lobe epilepsy and Alzheimer's disease, remains uncertain. Similarly, the present study was performed in an elderly cohort (age range 61-96), and the generalizability of our findings to younger subjects remains to be proven. Furthermore, our analysis was restricted to the hippocampal body. We did not analyze the hippocampal head / tail, entorhinal cortex, or adjacent subregions of the parahippocampal gyrus. However, our methodology could be applied in future studies to develop histology-based segmentation protocols for these regions.

Finally, our method is dependent upon visualization of the SLM & DG as these structures are known to be readily visualized with in vivo MRI. However, the spatial resolution of histology (on the order of microns) is much higher than that of even the ex vivo MRI used in our study (voxel size 0.2 x 0.2

x 0.5 mm³). This results in imperfect correspondence between structures visualized in the histology samples as compared with the ex vivo MRI. For example, while the stratum radiatum (SR) could be delineated from the stratum lacunosum moleculare (SLM) and stratum pyramidale on histology (Figures 9.1v and 9.8), this distinction could not be made in our ex vivo MR images (Figures 9.5 and 9.6). Furthermore, we used the granule cell layer of the DG to determine the beginning and end of the SLM for our histological segmentations (Figures 9.1iii and 9.1iv). However, the granule cell layer could not be directly visualized in our ex vivo MR Images, and the grey matter of the DG was therefore used as a surrogate marker for these boundaries on MRI. These difficulties represent potential explanations for the poorer correspondence between histology and MRI measures seen in our study, and these differences are likely to be even greater when applied to in vivo MRI. However, as visualization of the SLM and DG is required for all subfield segmentation protocols (257) these limitations would apply to any attempt at subfield segmentation. Future studies are required to determine the accuracy of our method when applied to in vivo MRI.

9.5 Conclusions

In this initial proof-of-concept study, we used ex vivo MRI and histology of cadaveric hippocampi to develop a novel segmentation protocol for the hippocampal body. We used two anatomical landmarks, SLM & DG, which are known to be readily visualized with high resolution in vivo MRI, as the basis for this method. The novel method provided accurate measurements of CA1, CA2, and CA3/CA4/DG subfield areas in comparison to the gold standard histological measurements. The relationships demonstrated between

histology and ex vivo MRI supports the potential feasibility of applying this method to in vivo MRI studies. However, these are preliminary findings which require validation in an independent data set, as well as in subjects with hippocampal pathology.

9.6 Appendix

Bland-Altman Method

The purpose of this section is to provide further details regarding the Bland-Altman analyses presented in this thesis (Figure 9.9). The Bland-Altman method is used to determine the level of agreement between measurements of a given variable made using two methods (260). In a conventional Bland-Altman analysis, neither method is considered the gold standard for the measurement of the variable of interest. The difference between the two methods (on the y axis) is therefore plotted against *the average* of the two methods (on the x axis). However, as direct histological distances represent *a gold standard measurement* this variable was plotted on the x axis in our analysis (Figure 9.9).

The Bland-Altman method can be used to estimate the *systematic error* (mean error) of one method in comparison to another (260). In Figure 9.9, the mean error for each measurement is shown as the distance between the green line (the mean difference between measurements) and the red line (the line of equality) as measured along the y axis. In this analysis, Technique 1 demonstrated systematic error in comparison to direct measurements at the CA2/CA3 boundary (Figure 9.9). However, as the novel method *utilized the mean* to estimate subfield boundaries - this technique was *guaranteed to demonstrate no systematic error* at each subfield transition in our Bland-Altman analysis (top panels, Figure 9.9).

The *random error* between two methods of measurement can also be determined using a Bland-Altman plot (260). In Figure 9.9, the 95% limits of agreement (black lines) were determined according to the following formula:

Limits = $d \pm 1.96s$; where Limits: 95% limits of agreement, d: mean error between the two measurements, and s: standard deviation of the differences between measurements. The distance between the black lines, as measured along the y axis, provides an estimate of the *random error* between the two measurements (Figure 9.9).

Finally, the Bland-Altman method is unique as it allows for the evaluation of *proportional error* between two methods of measurement (260). Proportional error is detected when the *differences between two methods* of measurement (y axis, Figure 9.9) demonstrate a linear relationship with *gold standard measurements* (x axis, Figure 9.9). In our analysis, each measurement technique demonstrated proportional error in comparison to the gold standard at the Subiculum/CA1 boundary (Figure 9.9). This finding highlights the poor performance of each method at this boundary, which was confirmed with linear regression (Figure 9.10) and by calculation of intra-class correlation coefficients (ICCs, Table 9.1).

Segmentation protocols

In this section, the detailed segmentation protocols for the previous techniques are reproduced verbatim from the original publications:

Technique 1 [Figure 9.3 , (254)] "The border between the subiculum and CA1 was constructed by drawing a line perpendicular to the longitudinal axis of the subiculum at the most medial point of the dentate gyrus. The most lateral point of the dentate gyrus formed the border between CA1 and CA2. The border was constructed by drawing a straight, vertical line to the superior border of the hippocampus. The border between CA2 and CA3 was defined as the medial

side of a virtual square. This square was positioned with its lateral side contacting the border of CA1 and with its superior side along the superior border of CA2. The length of the superior side of the square was modified until it was equal to the thickness of CA2 at the border with CA3."

Technique 2 [Figure 9.4, (190)] "The voxels of the immediate entry point of CA are considered CA3 (that is, penetrating one voxel deep into the dentate gyrus), as are adjacent voxels in the superior direction, extending one voxel superior to the dentate gyrus. CA2 is segmented by drawing a line from the medial edge of CA3 to the lateral edge of the dentate gyrus. Then a second line is drawn orthogonal to the first at its mid-point. The medial boundary of CA2 is CA3, and the lateral boundary is one voxel past the vertical line. CA1 extends from (the) end of CA2 to the most medial point of the dentate gyrus. A line was drawn along the inferior-medial edge of the dentate gyrus, and another line was drawn orthogonal to this at the cornu ammonis / dentate gyrus boundary. This edge formed the CA1 / Subiculum boundary."

Technique 3

In this section, histological validation results are presented for a third previously described technique [Technique 3, (255), Figure 9.15]. The detailed segmentation protocol for this technique is reproduced verbatim below from the original publication:

Technique 3 [Figure 9.15, (255)] "The boundary between CA1 and subiculum is measured by drawing a straight line along the edge of the dentate gyrus, and drawing a second line perpendicular to the first at the edge of the most medial,

most superior voxel of the dentate gyrus. To segment CA2 and CA3, begin by using the annotation tool to draw a line across the longest length of the

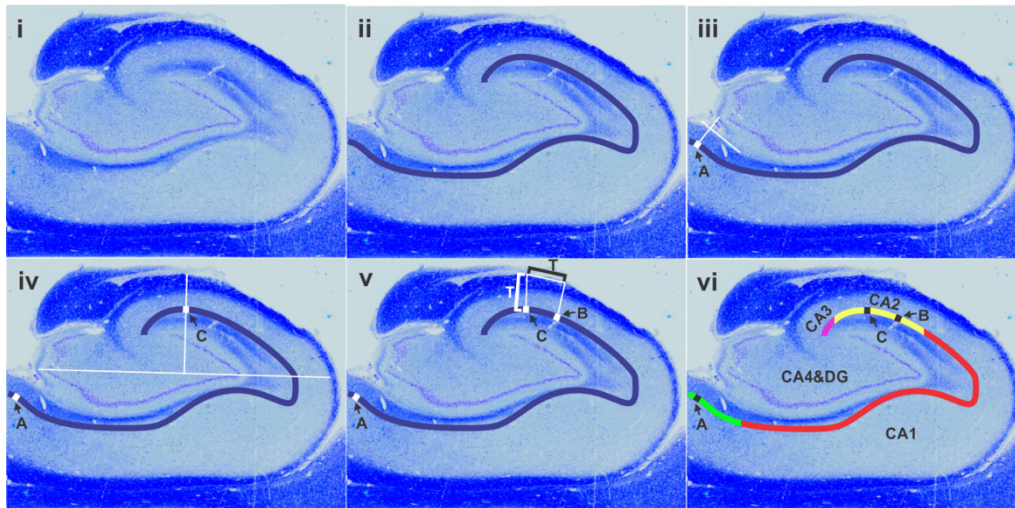


Figure 9.15 - Subfield boundaries according to Technique 3

- i) Histological sections were stained with cresyl violet / luxol fast blue.
- ii) The stratum lacunosum moleculare (SLM) was delineated.
- iii) Subiculum/CA1: The boundary between CA1 and Subiculum (A) was measured by drawing a straight line along the edge of the dentate gyrus (DG), and then drawing a second line perpendicular to the first at the supero-mesial edge of the DG.
- iv) CA2/CA3: A line was drawn from the most medial point of the DG to the furthest point on CA1, as measured across the longest distance of the DG. From the midpoint of that line, a second line was drawn perpendicular to the first extending to the superior edge of the cornu ammonis. This line separated CA2 from CA3 (C).
- v) CA1/CA2: The thickness (T, white) of the cornu ammonis at the CA2/CA3 boundary was measured. This measurement (T, black) was then used to determine the width of the CA2 subfield. The CA1/CA2 boundary (B) was then drawn normal to the outer surface of the cornu ammonis, as measured at the most lateral point of CA2.
- vi) The SLM was colour-coded according to the gold standard histologically defined subfield locations in this specific section (Subiculum, green; CA1, red; CA2, yellow; CA3, pink). In this particular section, the defined CA1 region includes a substantial amount of subiculum and CA2, while CA3 includes a substantial amount of CA2.

hippocampal body. This should extend from the end of the most medial point of the dentate gyrus to the furthest point on CA1, as measured across the longest distance of the dentate gyrus. From the midpoint of the first line, draw a second line perpendicular to the first that extends to the edge of CA1. This line separates CA2 from CA3. The thickness of the cornu ammonis at this point is used to determine the width of the CA2 subfield. Measure the thickness using the annotation tool, and draw a line of that length from the edge of the second line. This determines the CA1/CA2 boundary. Finally, the CA1/CA2 boundary should be normal to the outer surface of the cornu ammonis, measured at the most lateral point of CA2."

Agreement with direct measurements In comparison to the novel method, Technique 3 demonstrated poorer agreement with direct measurements (Figures 9.16 & 9.17, Table 9.3). As with the novel method, Technique 3 demonstrated proportional bias at the Subiculum/CA1 boundary (Figure 9.16). At the CA1/CA2 boundary, Technique 3 demonstrated similar systematic bias with wider Bland-Altman limits of agreement. For the CA2/CA3 boundary Technique 3 demonstrated greater systematic bias and wider Bland-Altman limits of agreement.

As seen for the novel method, poor correlation ($r^2 < 0.1$, $p > 0.5$; ICC = 0.00) with the gold standard at the Subiculum/CA1 boundary was seen for Technique 3 (Figure 9.17 & Table 9.3). At the CA1/CA2 boundary, the novel method demonstrated stronger correlations ($r^2 = 0.75$, ICC = 0.93) with gold standard measurements than Technique 3 ($r^2 = 0.46$, ICC = 0.81). For the CA2/CA3 boundary distances, correlations with gold standard measurements were also greater for the novel method ($r^2 = 0.90$, ICC = 0.97) in comparison to Technique 3 ($r^2 = 0.45$, ICC = 0.61).

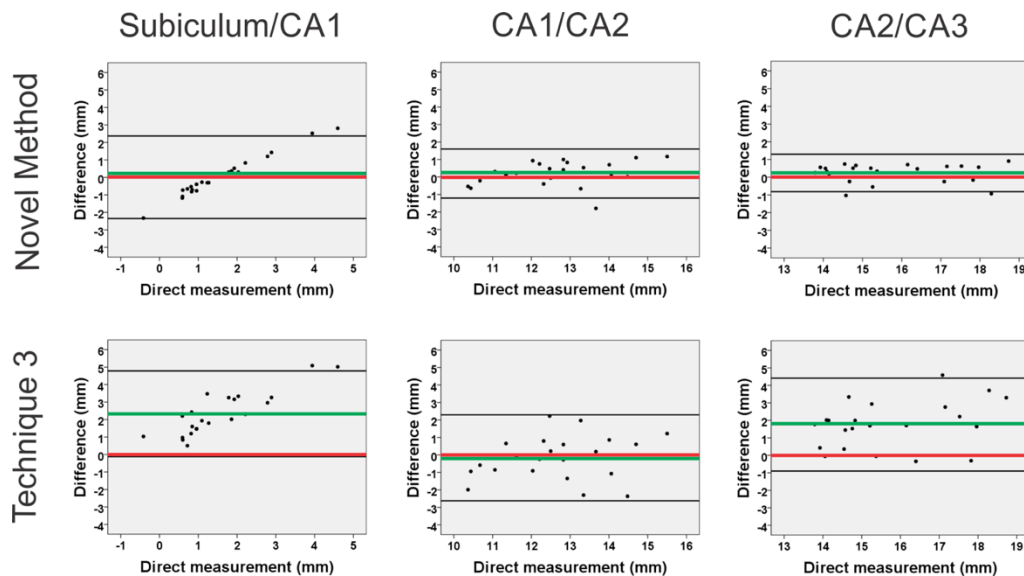


Figure 9.16 - Accuracy of novel method versus Technique 3

Agreement with direct measurements at three subfield boundaries (Subiculum/CA1, CA1/CA2, and CA2/CA3) was assessed by the Bland-Altman method. Perfect agreement (no difference from direct measurements) is indicated by the red line. Mean error (green line) and Bland-Altman limits of agreement (black lines) are also shown. At the CA1/CA2 boundary, the novel method demonstrated similar systematic bias (distance between red and green lines), but narrower Bland-Altman limits of agreement (distance between black lines). For the CA2/CA3 boundary, the novel method demonstrated reduced systematic bias and narrower Bland-Altman limits of agreement. Proportional bias was noted for both techniques at the Subiculum/CA1 boundary, suggesting limitations for each method in predicting this subfield location.

Segmentation technique	Subfield Boundary		
	Subiculum/CA1 ICC (r^2)	CA1/CA2 ICC (r^2)	CA2/CA3 ICC (r^2)
Novel method	-0.04 (0.01)	0.93 (0.75)	0.97 (0.90)
Technique 3	0.00 (0.02)	0.81 (0.46)	0.61 (0.45)

Table 9.3 - Accuracy of novel method versus Technique 3

Intra-Class Correlation Coefficients (ICCs) and coefficients of determination (r^2) were calculated for the novel method and Technique 3 in reference to the gold standard at three hippocampal subfield boundaries. Poor correlation ($ICC \leq 0.00$, $r^2 < 0.1$) with the gold standard was seen at the Subiculum/CA1 boundary for both methods. At the CA1/CA2 boundary, the novel method demonstrated greater correlation ($ICC = 0.93$, $r^2 = 0.75$) with gold standard measurements in comparison with Technique 3 ($ICC = 0.81$, $r^2 = 0.46$). Similarly, for the CA2/CA3 boundary, the novel method demonstrated superior correlation ($ICC = 0.97$, $r^2 = 0.90$) with gold standard measurements compared to Technique 3 ($ICC = 0.61$, $r^2 = 0.45$).

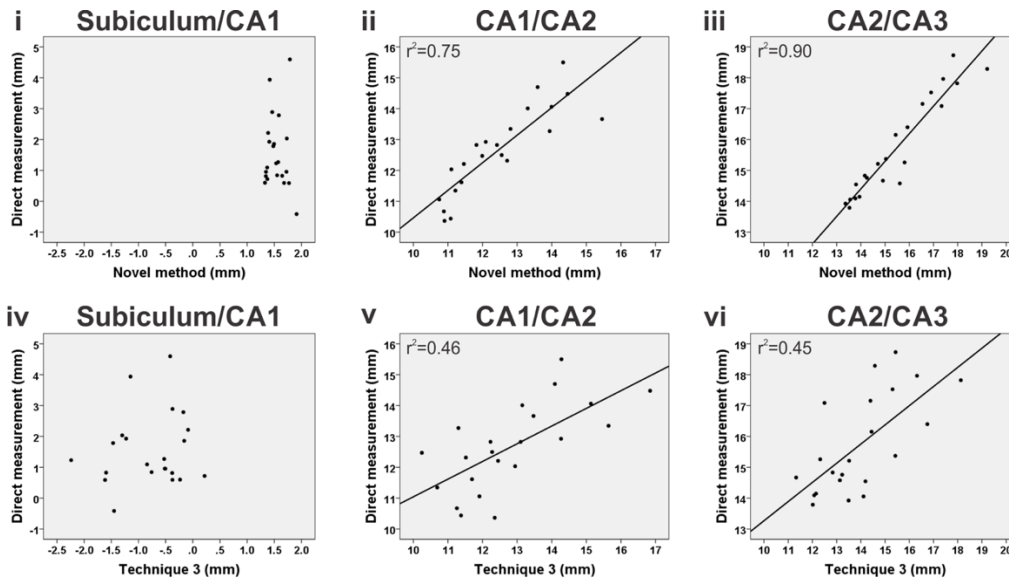


Figure 9.17 - Histological measures with novel method and Technique 3

Distances of three subfield boundaries (Subiculum/CA1, CA1/CA2, and CA2/CA3) from the superficial hippocampal sulcus were measured on histology according to the novel method (i-iii) and Technique 3 (iv-vi). These measurements were compared with the direct (gold standard histology) measurements using linear regression.

Subiculum/CA1 boundary

In this section, we examine potential explanations for the failure of the mean to accurately predict the Subiculum/CA1 boundary.

Range of measurements The range between the lowest and highest distance of the Subiculum/CA1 boundary from the superficial hippocampal sulcus in our study was: (range = -0.42 to 4.60 mm = 5.02 mm); while the mean distance of the Subiculum/CA1 boundary from the superficial hippocampal sulcus was 1.55 mm. Thus, the range for Subiculum/CA1 as a proportion of the mean was very large = 5.02 mm / 1.55 mm = 323%. In contrast, for CA1/CA2 (range =

10.36 to 15.50 mm = 5.14 mm) and (mean = 12.66 mm) the range as a proportion of the mean was much smaller = $5.14 \text{ mm} / 12.66 \text{ mm} = 40.6\%$. Similarly, for CA2/CA3 (range = 13.79 to 18.73 mm = 4.94 mm) and (mean = 15.74 mm) the range as a proportion of the mean was = $4.94 \text{ mm} / 15.74 \text{ mm} = 31.4\%$.

We further evaluated the ability of this larger range to explain the poor performance of the mean in determining the Subiculum/CA1 boundary. This was done by applying the novel method in reverse, measuring the length of the SLM in the opposite direction (i.e. from the blades of the DG to the superficial hippocampal sulcus). The gold standard distances of the Subiculum/CA1 boundaries were also measured in the opposite direction, as distance from the blades of the DG, which yielded a mean distance of the Subiculum/CA1 boundary of 14.3 mm, or 90.0% of the total SLM length. This was then used to determine the location of the Subiculum/CA1 boundaries in each section according to the reverse of the novel method.

In this analysis, the range between the lowest and highest distance of the Subiculum/CA1 boundary from the blades of the DG according to the gold standard histology was (range = 9.00 to 20.13 mm = 11.13 mm) and (mean = 14.28 mm) so that the range as a proportion of the mean was much smaller compared with measurement in the forward direction = $11.13 \text{ mm} / 14.28 \text{ mm} = 77.9\%$. The range for the reverse Subiculum/CA1 measurements as a proportion of the mean (77.9%) according to this analysis, however, were still nearly double that for CA1/CA2 (40.6%) and CA2/CA3 (31.4%).

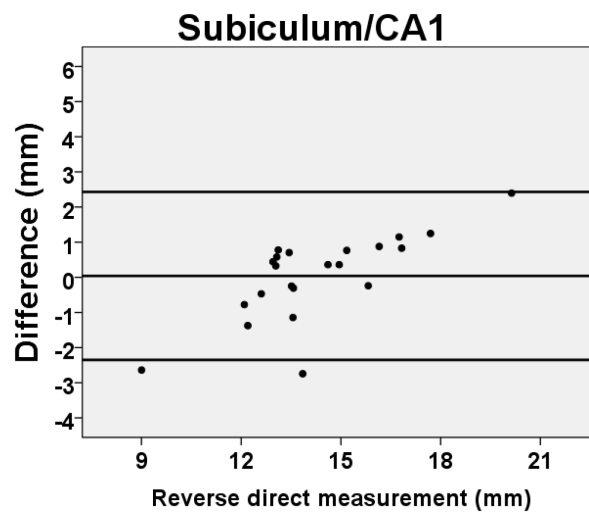


Figure 9.18 - Subiculum/CA1 boundaries measured in reverse direction.

Proportional bias remains strongly statistically significant ($p < 0.0001$) with measurement in the reverse direction

However, this analysis failed to eliminate the proportional bias detected for the Subiculum/CA1 boundary, which remained strongly statistically significant ($p = 0.000093$, Figure 9.18). As measurement in reverse resulted in a dramatically lower range as a proportion of the mean but did not affect the finding of proportional bias, we do not believe that this is an adequate explanation for the finding of proportional bias.

Non-normal distribution As an alternative explanation, we postulated that the Subiculum/CA1 boundary measurements could be non-normally distributed, and that this may represent a cause for poor performance at the Subiculum/CA1 boundary. To test this, the statistical distribution of the gold standard measurements for each hippocampal subfield boundary was evaluated using the Shapiro-Wilk test, which tests the null hypothesis that the data are

normally distributed. The distances of the Subiculum/CA1 boundary from the superficial hippocampal sulcus were non-normally distributed (Shapiro-Wilk test, $p = 0.033$). The distances of the CA1/CA2 boundary from the superficial hippocampal sulcus were normally distributed (Shapiro-Wilk test, $p = 0.904$). The distances of the CA2/CA3 boundary from the superficial hippocampal sulcus were non-normally distributed (Shapiro-Wilk test, $p = 0.029$). As the CA2/CA3 boundary was also non-normally distributed yet did not show proportional bias, the distribution of the data was thus excluded as a potential etiology for the poor performance of the novel method at the Subiculum/CA1 boundary.

Chapter 10 In vivo diagnosis of MTLE subtypes

Abstract

Objective Neuropathological studies have shown that hippocampal sclerosis (HS) consists of four distinct subtypes (ILAE Types 1-3 HS and No HS). However, HS subtypes currently can only be diagnosed by pathological analysis of hippocampal tissue resected during epilepsy surgery. In vivo diagnosis of HS subtypes holds potential to improve our understanding of these variants and enable prognostic information to be used for surgical decision-making. In the present study, we aimed to develop a method to characterize HS subtypes using in vivo MRI.

Methods Five subjects with TLE and unilateral HS (ILAE type 1 HS based on surgical pathology in all five cases) were compared with five healthy controls. We used a 4.7 T MRI system to acquire high resolution ($0.26 \times 0.34 \times 1 \text{ mm}^3$) MR Images of the hippocampus in each subject. In vivo-MRI diagnosis of ILAE HS subtypes was then determined in each patient by two methods: volumetric analysis and subfield area analysis along the hippocampal long axis.

Results Subfield volumetry demonstrated abnormalities in all five patients with three subjects demonstrating findings consistent with ILAE type 1 HS and two subjects with volumetry-defined atypical HS (one ILAE type 2 HS & one ILAE type 3 HS). Subfield area analyses demonstrated variability in ILAE HS subtype along the hippocampal long axis in several subjects.

Significance In the present study, hippocampal subfield volume abnormalities were observed for all subjects with agreement in ILAE subtype between histology and MRI observed in three out of five cases. The discrepancy of ILAE HS subtype observed for the remaining two subjects could be related to heterogeneity of HS subtypes along the long axis of the hippocampus. However, our results provide preliminary evidence that determining HS Subtype using high resolution in vivo MRI may allow preoperative diagnosis of ILAE HS subtypes. The heterogeneity of abnormalities observed with hippocampal subfield areas along the long axis of the hippocampus is consistent with previous autopsy studies and highlights the importance of studying the entire hippocampus in TLE patients.

10.1 Introduction

While hippocampal sclerosis (HS) is the most common lesion associated with intractable epilepsy (18), several studies have demonstrated considerable heterogeneity regarding pathological involvement of different hippocampal subfields (4, 8, 157, 164, 168, 171, 263). Surgical specimens from individual patients can demonstrate classical involvement of both CA1 and CA4 (ILAE Type 1 HS), CA1 predominant disease (ILAE Type 2 HS), or end folium (CA4) sclerosis (ILAE Type 3 HS) (5). Patients with medically intractable temporal lobe epilepsy (TLE) and HS can have an excellent surgical outcome. However, long term follow up demonstrates that only around 50% of patients remain seizure-free 10 years postoperatively (154). Classification of the HS subtypes described above (5) based on subfield analysis of postoperative pathology has been shown to provide important prognostic information regarding expected surgical outcomes, with ILAE Type 1 HS having the best prognosis (4, 8). However, a reliable method to determine HS subtype preoperatively has not yet been established. Along with heterogeneity of subfield involvement between subjects with HS, variability of pathological changes in subfields has also been demonstrated along the long axis of the hippocampus for individual subjects which has emphasized the importance of obtaining and examining large surgical specimens in order to obtain a more complete assessment of hippocampal pathology (136).

Magnetic Resonance Imaging (MRI) was the first technology to demonstrate HS noninvasively (142-144, 147), and MRI evidence of HS is associated with better surgical outcomes (149). With increasing MRI magnetic field strength, the spatial resolution of MRI continues to improve, to the point where it has now become feasible to study individual hippocampal subregions

(180, 236). CA1 and CA4 subfields can now be measured in patients with HS (10), which provides the potential opportunity to more accurately predict surgical outcome with HS subtype diagnosis prior to surgery (7).

However, hippocampal subfields are defined according to cytoarchitectonic features which are not discernible with MRI (232). While existing protocols have been based on a standard anatomical reference (13), the relationships between in vivo segmentation rules and histology have not been analyzed. As a direct result, a large number of methods using different rules have been described for hippocampal subfield segmentation (257). While harmonization of such protocols will reduce variability between labs (264), this approach will not address the unknown correspondence between in vivo MRI and ground truth measures (histological subfield definitions). The development of histologically validated in vivo MRI segmentation methods holds potential to address these current limitations. To date the hippocampal subfield imaging literature has, for the most part, focused on volumes. While volumes would be expected to provide a global assessment of the hippocampus as a whole, volume assessment has limitations in studying the subfield variability that has been demonstrated along the long axis of the hippocampus in autopsy studies of patients with HS (136).

We have recently developed a method for hippocampal body segmentation based on histology and ex vivo MRI of the human hippocampus (237). However, ex vivo MRI of cadaveric hippocampi provides much higher spatial resolution (voxel size $0.2 \times 0.2 \times 0.5 \text{ mm}^3$) than can currently be achieved in vivo. This greater spatial resolution provides superior visualization of anatomical landmarks than is possible with in vivo MRI. Therefore, whether our segmentation method can be implemented reliably with in vivo MRI has

not been determined. Furthermore, whether reliability of this method is affected by the presence of hippocampal pathology remains unknown.

In the present study, we aimed to: 1) Determine the intra-rater reliability *for in vivo application* of our hippocampal segmentation protocol - in control subjects and TLE patients with unilateral HS; and 2) Correlate hippocampal subfield *areas and volumes* with surgical pathology in TLE patients with unilateral HS undergoing surgery.

10.2 Materials and Methods

Five healthy subjects served as controls and were compared with five patients with TLE. The project received research ethics approval from the University of Alberta Research Ethics Board. Each of the patients had unilateral (three right) HS detected with 1.5 tesla clinical MRI scans, and all underwent unilateral resection of the hippocampus for treatment of epilepsy with postoperative *pathology revealing ILAE type 1 HS in each patient*. Preoperatively, high resolution MR Imaging was performed in all subjects on a 4.7 T MRI system (Varian, Palo Alto, CA). A T2-weighted (inverted contrast) fast-spin echo technique was used to acquire 90 contiguous 1.0-mm-thick coronal slices, perpendicular to the anterior commissure - posterior commissure line (AC-PC line), including the entire hippocampal formation [echo time (TE) = 39 ms, repetition time (TR) = 11,000 ms, FOV 20 x 20 cm, in-plane matrix 384 x 296] yielding a native resolution of 0.52 x 0.68 x 1.0 mm³ in 13.5 minutes of total scan time. Images were then interpolated in-plane by a factor of 2, yielding a final resolution of 0.26 x 0.34 x 1.0 mm³ as previously described (256).

Segmentation of hippocampal subfields using in vivo MRI

Delineation of the hippocampal body from the head and tail The landmarks used for segmentation of the hippocampal body are shown in Figure 10.1. The presence of uncal tissue was used to define the most posterior slice of the hippocampal head (1, Figure 10.1A) (265). Hippocampal body segmentation began on the most anterior slice where uncal tissue was absent (2, Figure 10.1B) (265). The boundary between the hippocampal body and the hippocampal tail was determined by measuring 15 mm posteriorly from the head-body junction (Figure 10.1E). The hippocampal body was therefore delineated on 15 slices (1 mm slice thickness). The hippocampal head and tail were excluded from the analysis (Figure 10.1F). Subfield volumes for the hippocampal body were derived from the 15 1mm slices.

Hippocampal subfield segmentation In vivo subfield segmentation of the hippocampal body according to histology-derived rules is described in Figure 10.2. Segmentation was performed on each of the 15 coronal slices of the hippocampal body (Figure 10.2A), while the sagittal and axial planes were systematically checked to confirm anatomical landmarks.

The method was based on two MRI-visible anatomical landmarks: the stratum lacunosum moleculare (SLM) and the dentate gyrus (DG). The beginning (1, Figure 10.2B) of the SLM was identified at the superficial hippocampal sulcus (237). The termination of the SLM (2, Figure 10.2C) was identified visually at the blades of the DG. A curvilinear line (blue, Figure 10.2D) was then drawn at the tissue interface between the SLM and the cornu ammonis. The length of this line was measured using the curvilinear measurement tool in ImageJ (259) to determine the total SLM length.

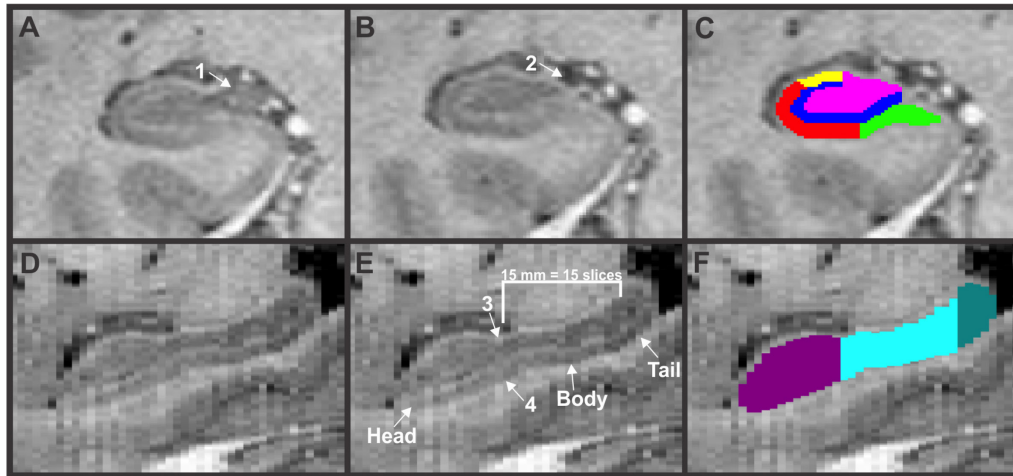


Figure 10.1 - Delineation of the hippocampal body from the head and tail

A) The most posterior slice of the hippocampal head was defined as the most posterior slice containing uncal tissue (1) (265). B) The most anterior slice of the hippocampal body was defined as the most anterior slice where uncal tissue was absent (2) (265). Hippocampal subfield segmentation began on the most anterior (first) slice of the hippocampal body. C) Hippocampal subfields [(Subiculum, green); (CA1, red); (CA2, yellow); (CA3/CA4/DG, magenta)] were delineated on the first slice of the hippocampal body in this subject. D) Unlabelled sagittal MR Image showing the hippocampal head, body, and tail along the longitudinal axis of the hippocampus in the same subject. E) The most posterior slice of the hippocampal head (3, panel A from this figure) and the most anterior slice of the hippocampal body (4, panel B from this figure) were used to define the head-body junction. The body-tail junction was determined by measuring 15 mm posterior from the head-body junction. The hippocampal body thus comprised 15 slices (1 mm slice thickness) and the 16th slice posterior to the head-body junction was labelled as hippocampal tail. F) Labelled sagittal MR Image is shown from the same subject. Hippocampal head (purple) and tail (teal) were excluded from the subfield segmentation protocol. Hippocampal subfield segmentation (as shown in panel C) was restricted to the hippocampal body (turquoise).

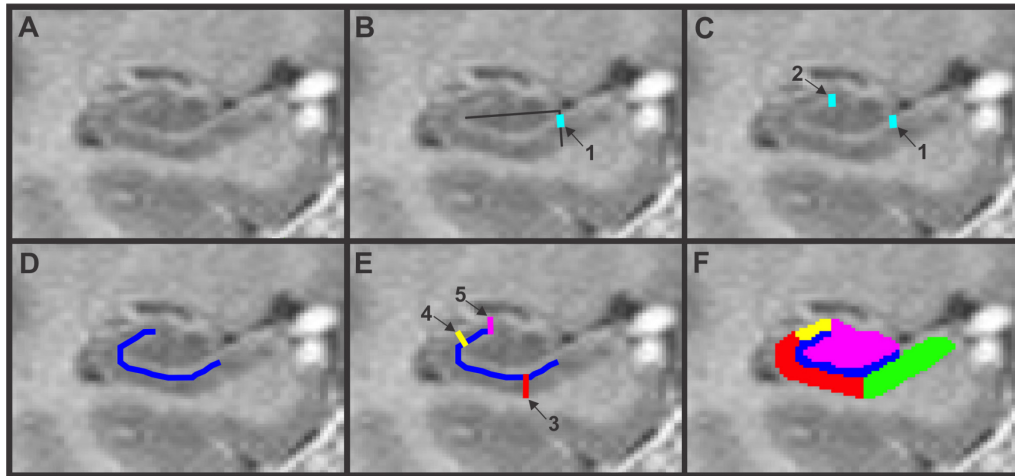


Figure 10.2 - Segmentation of hippocampal subfields using in vivo MRI

A) Unlabelled coronal MR Image of the hippocampal body. Segmentation was performed in the coronal plane (sagittal and axial planes were systematically checked to confirm anatomical landmarks). B) A line was drawn across the longest diameter of the dentate gyrus. A second line was then drawn perpendicular to the first (237) to define the beginning (1) of the stratum lacunosum moleculare (SLM) at the superficial hippocampal sulcus. C) The termination of the SLM (2) was identified visually at the blades of the dentate gyrus. D) A curvilinear line (blue) was drawn at the tissue interface between the SLM and the cornu ammonis. The length of this line was measured using the curvilinear measurement tool in ImageJ to determine the total SLM length. E) Hippocampal subfield transitions were determined as a proportion of the total SLM length (237): Subiculum/CA1 (3, 26% of SLM); CA1/CA2 (4, 78% of SLM); and CA2/CA3 (5, 98% of SLM). At each transition, a line was drawn perpendicular to the SLM to define the subfield boundaries: Subiculum/CA1 (red), CA1/CA2 (yellow), and CA2/CA3 (magenta). F) Subfields were delineated using tissue contrast between grey and white matter. The mesial boundary of the subiculum was defined by a loss of grey matter signal intensity at the superomesial aspect of the parahippocampal gyrus. The cortical mantle was followed from the subiculum laterally over the cornu ammonis and dentate gyrus, with the alveus being excluded from subfield measurements. The SLM (blue) was also excluded. The segmentation protocol yielded four hippocampal subfield measurements: Subiculum (green), CA1 (red), CA2 (yellow), and CA3/CA4/DG (magenta).

Hippocampal subfield transitions (Figure 10.2E) were then determined as a proportion of the total SLM length (237): Subiculum/CA1 (26% of SLM); CA1/CA2 (78% of SLM); and CA2/CA3 (98% of SLM). At each transition, a line was drawn perpendicular to the SLM to define the subfield boundaries (Figure 10.2E). Subfields were then delineated using tissue contrast between grey and white matter. The mesial boundary of the subiculum was defined by a loss of grey matter signal intensity at the superomesial aspect of the parahippocampal gyrus (Figure 10.2F). The cortical mantle was then followed from the subiculum laterally over the cornu ammonis and DG, with the alveus and SLM being excluded from subfield measurements. The segmentation protocol thus yielded four hippocampal subfield measurements: Subiculum, CA1, CA2, and CA3/CA4/DG (Figure 10.3).

Evaluation of Intra-rater Reliability

Reliability of the segmentation protocol was evaluated in controls (n=5 bilaterally, 10 hippocampi) and patients with HS (n=5 bilaterally, 10 hippocampi). Segmentation was performed by a single investigator (TAS, 5 years of manual segmentation experience) on the same subjects twice at an interval of 1 week for evaluation of intra-rater reliability. Agreement was determined by measurement of Intra-Class correlation Coefficients (ICCs) and Dice Similarity Coefficients (DSCs). The DSC determines the amount of spatial overlap between two segmentations ($Dice = \frac{2TP}{2TP+FP+FN}$, where TP: true positive, FP: false positive, FN: false negative). The value ranges from 0 (no overlap) to 1 (full overlap). Calculation of DSCs was performed using Matlab R2017b (Mathworks Inc., Natick, MA, USA).

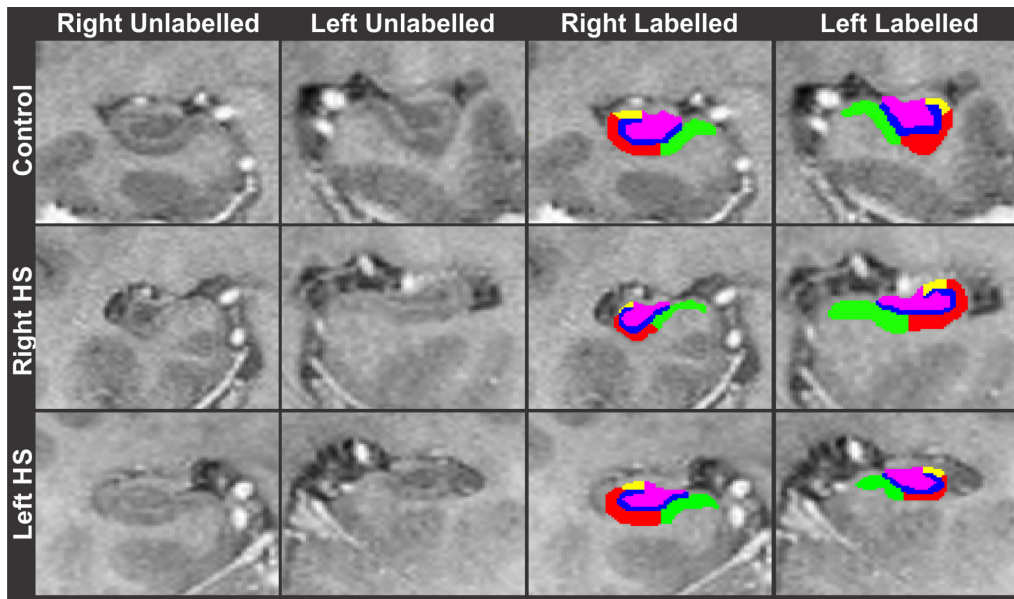


Figure 10.3 - Hippocampal subfield measurements

Left panels: High resolution unlabelled in vivo MR Images of the hippocampus are shown bilaterally from a normal control (top row), a subject with pathologically confirmed right hippocampal sclerosis (HS, middle row), and a subject with pathologically confirmed left HS (bottom row).

Right panels: Hippocampal subfields [(Subiculum, green); (CA1, red); (CA2, yellow); (CA3/CA4/DG, magenta)] were delineated on the same slices as shown on the left. While the hippocampal internal architecture in HS subjects was not as clearly visualized in comparison to controls, the internal architecture was clear enough for subfield segmentation in each subject.

Comparison of hippocampal subfield volumes in controls and patients with HS

Subfield volumes from 5 controls bilaterally (10 hippocampi) were compared with subfield volumes from 5 subjects with pathologically confirmed HS. In

subjects with HS, the hippocampus with qualitatively evident sclerosis was defined as the "ipsilateral" hippocampus, while the other hippocampus was defined as the "contralateral" hippocampus. A normal range was constructed by determining the 10th to 90th percentiles from the control group. Volume measurements falling within the normal range were defined as normal while measurements falling below the normal range were defined as abnormal. In HS subjects, each hippocampus was then given an ***HS subtype classification based on the subfield volume measurements***: No HS (CA1 and CA3/CA4/DG normal); Type 1 HS (CA1 and CA3/CA4/DG abnormal); Type 2 HS (CA1 abnormal but CA3/CA4/DG normal); Type 3 HS (CA1 normal but CA3/CA4/DG abnormal) following the ILAE classification scheme (5).

Characterizing HS Subtype atrophy patterns along hippocampal long axis

Methodology of HS Subtype slice classification CA1 and CA3/CA4/DG subfield areas at each of 15 slices along the hippocampal long axis were used to determine HS subtype atrophy patterns (Figure 10.4). Control subfield areas were measured from 5 subjects bilaterally (10 hippocampi) at 15 slices each, for a total of 150 control slices. A normal range was constructed by determining the 10th to 90th percentiles from the control group. An individual slice area measurement was defined as normal if it was above the lower limit of normal and abnormal if it fell below the lower limit of normal. In subjects with HS, ***each slice*** was then classified as an HS subtype pattern ***based on evaluation of subfield areas***: No HS (CA1 and CA3/CA4/DG normal); Type 1 HS (CA1 and CA3/CA4/DG abnormal); Type 2 HS (CA1 abnormal but CA3/CA4/DG normal); Type 3 HS (CA1 normal but CA3/CA4/DG abnormal) (5).

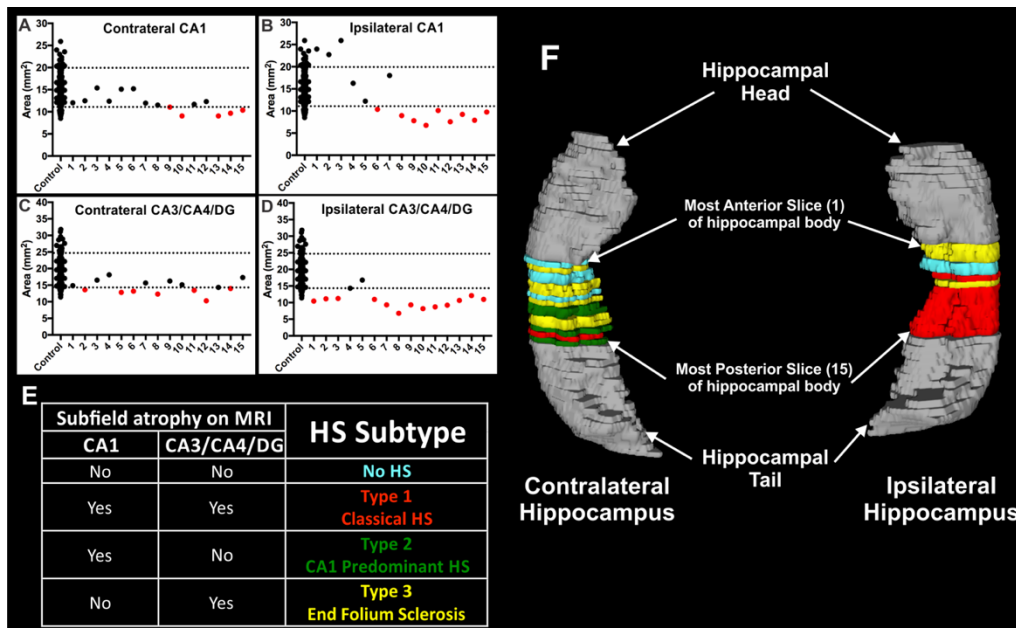


Figure 10.4 - Subtype atrophy patterns along the hippocampal long axis

A-D) Subfield areas (mm^2) at each of 15 slices from a single subject with right HS (Subject 2) are shown for CA1 (A & B) and CA3/CA4/DG (C&D) bilaterally. Control subfield areas were measured from 5 subjects bilaterally (10 hippocampi) at 15 slices each, for a total of 150 control slices. The normal range (dotted lines) was constructed by determining the 10th to 90th percentiles from the control group. An individual slice area measurement was defined as normal (black) if it was above the lower limit of normal and abnormal (red) if it fell below the lower limit of normal.

E) The presence or absence of subfield atrophy on MRI at CA1 versus CA3/CA4/DG was used to determine the ILAE HS Subtype classification for each slice (5).

F) Volume rendering depicting HS Subtypes [(No HS, turquoise); (Type 1 Classical HS, red); (Type 2 CA1 Predominant HS, green); (Type 3 End Folium Sclerosis, yellow)] at each of 15 slices along the longitudinal axis (slices 1-15) in the contralateral (left) and ipsilateral (right) hippocampi for a single subject (Subject 2).

10.3 Results

Hippocampal subfield measurements

Subfield segmentations from a control subject and two patients with HS are shown in Figure 10.3. Control subjects demonstrated bilaterally symmetric hippocampal volume and visualization of the SLM. In contrast, subjects with HS demonstrated qualitatively evident hippocampal atrophy and less obvious visualization of the SLM in the sclerotic hippocampus, while the contralateral hippocampus appeared similar to controls. While the internal architecture of HS hippocampi was less clear, the internal architecture was adequate to perform segmentation in all subjects (Figure 10.3). In patients with HS, qualitative evaluation of segmentations revealed reduced size of all subfields in sclerotic hippocampi when compared with controls. In contrast, contralateral hippocampi from subjects with HS demonstrated similar size of all subfields compared with normal controls.

Intra-rater reliability

Controls Intra-rater reliability data from controls are shown in Table 10.1. Intra-rater reliability revealed $DSC \geq 0.75$ in 8/8 subfields and $ICC \geq 0.75$ in 8/8 subfields.

Hippocampal sclerosis Intra-rater reliability data from patients with HS are shown in Table 10.2. Intra-rater reliability with DSC was ≥ 0.75 in 7/8 subfields and $ICC \geq 0.75$ in 7/8 subfields.

	DSC (mean \pm SD)			ICC		
	Left	Right	Combined	Left	Right	Combined
CA1	0.87 \pm 0.02	0.86 \pm 0.04	0.87 \pm 0.03	0.99	0.99	0.99
CA2	0.78 \pm 0.05	0.78 \pm 0.06	0.78 \pm 0.05	0.81	0.87	0.82
CA3/CA4/DG	0.91 \pm 0.02	0.90 \pm 0.05	0.90 \pm 0.04	0.98	0.92	0.96
Subiculum	0.87 \pm 0.03	0.86 \pm 0.04	0.86 \pm 0.03	0.92	0.85	0.88

Table 10.1 - Intra-rater reliability in controls

Dice similarity coefficient (DSC) and Intra-Class Correlation coefficient (ICC) data are shown from controls for subfields CA1, CA2, CA3/CA4/DG, and Subiculum bilaterally - for a total of 8 subfields. Intra-rater reliability with DSC was ≥ 0.75 in 8/8 subfields and ICC ≥ 0.75 in 8/8 subfields. Reliability data combining left and right hippocampi are also shown.

	DSC (mean \pm SD)			ICC		
	Ipsi-lateral	Contra-lateral	Combined	Ipsi-lateral	Contra-lateral	Combined
CA1	0.79 \pm 0.05	0.84 \pm 0.03	0.82 \pm 0.05	0.99	0.94	0.98
CA2	0.68 \pm 0.09	0.75 \pm 0.04	0.72 \pm 0.07	0.73	0.98	0.92
CA3/ CA4/ DG	0.85 \pm 0.03	0.87 \pm 0.04	0.86 \pm 0.04	0.90	0.99	0.98
SUB	0.79 \pm 0.04	0.82 \pm 0.05	0.80 \pm 0.04	0.95	0.89	0.94

Table 10.2 - Intra-rater reliability in hippocampal sclerosis

Dice similarity coefficient (DSC) and Intra-Class Correlation coefficient (ICC) data are shown for subfields CA1, CA2, CA3/CA4/DG, and Subiculum ipsilateral and contralateral to known hippocampal sclerosis - for a total of 8 subfields. Intra-rater reliability with DSC was ≥ 0.75 in 7/8 subfields and ICC ≥ 0.75 in 7/8 subfields. Reliability data combining ipsilateral and contralateral hippocampi are also shown.

Subfield-specific volume loss in patients with hippocampal sclerosis

Hippocampal subfield volumes from controls and patients with HS are shown in Figure 10.5. Individual patients demonstrated different patterns of subfield-specific volume loss in the ipsilateral hippocampus. Based on volumetric analysis, three subjects (subjects 1, 3 and 4) demonstrated findings consistent with ILAE type 1 HS (involvement of both CA1 and CA4). Subject 2 demonstrated findings consistent with ILAE type 3 HS (involvement of CA4). Subject 5 demonstrated findings consistent with ILAE type 2 HS (involvement of CA1).

Volume loss was also subject-specific in the contralateral hippocampus. Two subjects (subjects 2 and 4) demonstrated atrophy of the CA3/CA4/DG subfields, consistent with an ILAE type 3 HS pattern. Three subjects (subjects 1, 3, and 5) did not have appreciable abnormalities of the contralateral hippocampus with volumetric analysis.

Individualized assessment of ILAE HS subtypes along the hippocampal longitudinal axis in 5 subjects with pathologically confirmed hippocampal sclerosis

Volume renderings from five subjects with HS, colour-coded according to HS subtype classification at each slice along the hippocampal long axis, are shown in Figure 10.6. Assessment of volumetry data and longitudinal axis analyses provided complementary information regarding ILAE HS subtype classification in each patient.

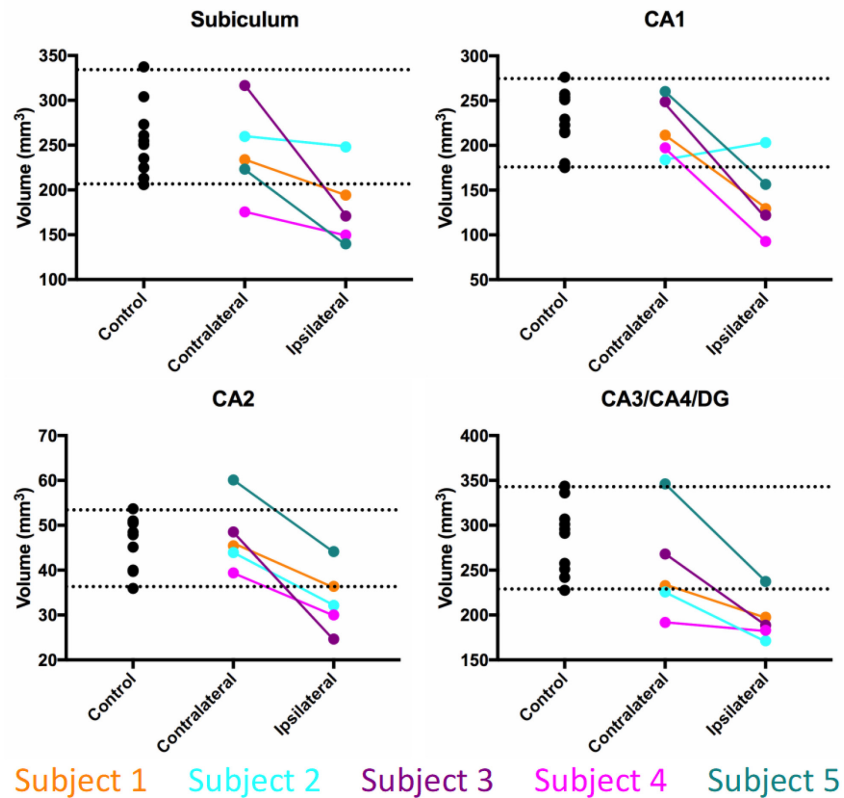


Figure 10.5 - Subfield-specific volume loss in patients with HS

Subfield volumes (mm³) for Subiculum, CA1, CA2, and CA3/CA4/DG are shown from 5 controls bilaterally (10 hippocampi) and 5 subjects with pathologically confirmed HS. Individual subjects demonstrated different patterns of subfield-specific volume loss in the ipsilateral hippocampus. Based on volumetric analysis, three subjects (subjects 1, 3 and 4) demonstrated findings consistent with ILAE type 1 HS (involvement of both CA1 and CA4). Subject 2 demonstrated findings consistent with ILAE type 3 HS (involvement of CA4). Subject 5 demonstrated findings consistent with ILAE type 2 HS (involvement of CA1). Volume loss was also subject-specific in the contralateral hippocampus. Two subjects (subjects 2 and 4) demonstrated atrophy of the CA3/CA4/DG subfields. Three subjects (subjects 1, 3, and 5) did not have appreciable abnormalities of the contralateral hippocampus with volumetric analysis.

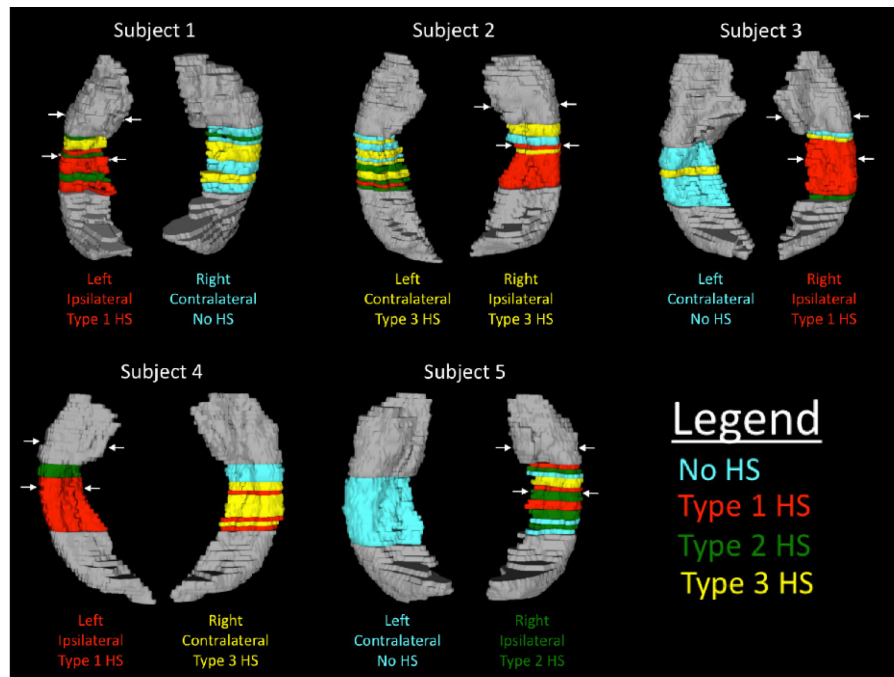


Figure 10.6 - Assessment of HS subtypes along the hippocampal long axis

Volume renderings are shown from five subjects with pathologically confirmed hippocampal sclerosis (HS), with the location of surgical biopsy indicated by white arrows. HS subtype classifications based on hippocampal subfield volume measurements (derived from Figure 10.5) are listed below each hippocampus. Individual slices were colour-coded according to HS subtype [(No HS, turquoise); (Type 1 Classical HS, red); (Type 2 CA1 Predominant HS, green); (Type 3 End Folium Sclerosis, yellow)] using the methodology described in Figure 10.4. Three subjects (Subject 1, 3, and 4) were defined as having Type 1 HS in the ipsilateral hippocampus based on subfield volumetry. Each of these hippocampi demonstrated at least 3 slices showing an HS subtype discordant with the overall volume-based classification. Subject 2 was classified as Type 3 HS on volumetric analysis, but the majority of slices (9/15) in this hippocampus were Type 1 based on subfield areas. Subject 5, defined as Type 2 HS based on volume, demonstrated remarkable variability of HS subtypes along the long axis – with at least two slices of each of the different subfield atrophy patterns. Three subjects (subject 1, 3 and 5) were defined as No HS in the contralateral hippocampus based on subfield volumetry. In subject 5 this finding was confirmed on subfield areas – with no HS found at any of the 15 slices. However, subject 3 was found to have 2 slices with subfield pathology and subject 1 had 7 slices with subfield atrophy patterns. Subject 2 and 4 both had Type 3 HS as defined by the subfield volumes analysis. Subject 4 had 7 slices showing discordant results with the volumetry data. Subject 2 demonstrated remarkable variability of HS subtype along the long axis, with the majority of slices (9/15) showing a different atrophy pattern than suggested by volumetry.

As described above, three subjects (subjects 1, 3 and 4) demonstrated findings consistent with ILAE type 1 HS (involvement of both CA1 and CA4) in the ipsilateral hippocampus on volumetric analysis. Subject 1 demonstrated Type 1 HS in the ipsilateral hippocampus in 8/15 slices on area-based subtype analysis along the long axis. However, for the remaining 7 slices, Type 2 HS was found in 4/15 slices and Type 3 HS was found in 3/15 slices. Volumetric and longitudinal axis data were strongly concordant for Subject 3, both indicating a diagnosis of ILAE Type 1 HS. Similarly, Subject 4 demonstrated primarily Type 1 HS in the ipsilateral hippocampus, although three slices of Type 2 HS were also detected anteriorly.

Subject 2 demonstrated findings consistent with ILAE type 3 HS (involvement of CA4 only) on volumetry analysis. Subtype analysis along the long axis in Subject 2 corroborated a Type 3 HS pattern in 4 anterior slices of the ipsilateral hippocampus, while Type 1 HS patterns were seen in 9 slices posteriorly - suggesting significant involvement of CA1. This was not detected on volumetric analysis, as CA1 volume from subject 2 for the ipsilateral hippocampus was normal. Subject 5 demonstrated findings consistent with ILAE type 2 HS (involvement of CA1 only) on volumetric analysis. However, analysis of subtype patterns along the longitudinal axis revealed remarkable variability in this patient. Although six slices of Type 2 HS were seen, this was accompanied by three slices of No HS, four slices of Type 1 HS, and two slices of Type 3 HS.

Contralateral hippocampal volumes were in the normal range for 3 of 5 subjects (subjects 1, 3, and 5). However, 2 of 3 subjects with normal contralateral hippocampal volumes demonstrated abnormalities on long axis subtype analysis. In Subject 1, the contralateral hippocampus demonstrated

multiple regions of abnormality, including one slice with subfield abnormalities consistent with Type 2 HS and six slices of Type 3 HS. For subject 3, two slices of Type 3 HS were detected in the contralateral hippocampus.

Contralateral hippocampal volumes were reduced in the CA3/CA4/DG subregions for subjects 2 and 4, suggesting a Type 3 HS pattern contralaterally in these subjects. Subtype analysis in subject 2 revealed primarily Type 3 HS (6 slices) in the contralateral hippocampus, while four slices of Type 2 HS and one slice of Type 1 HS were also detected. Subject 4 demonstrated eight slices of Type 3 HS (concordant with the volumetry data) and three slices of Type 1 HS (discordant with the volumetry data).

Histopathologic Classification of HS Subtypes

Hippocampal biopsy specimens were obtained intra-operatively from the anterior portion of the hippocampal body (white arrows, Figure 10.6). The hippocampal surgical specimen has as its anterior border the junction of the hippocampal body as it turns medially to become the head of the hippocampus. The posterior border of the hippocampal surgical specimen is usually 1.5–2.0 cm posterior to the anterior resection margin. The remainder of the hippocampal resection is carried out with the ultrasonic aspirator to a point which aligns with the lateral mesencephalic sulcus. This posterior portion is not available for pathological analysis.

Specimens were sectioned at 5 mcm and stained for Neuronal nuclear antigen (NeuN) (Figure 10.7). Neuropathological classification was performed by a board-certified neuropathologist (Laura Schmitt) based on ILAE criteria

(5): No HS (CA1 and CA4 normal); Type 1 HS (CA1 and CA4 abnormal);
Type 2 HS (CA1

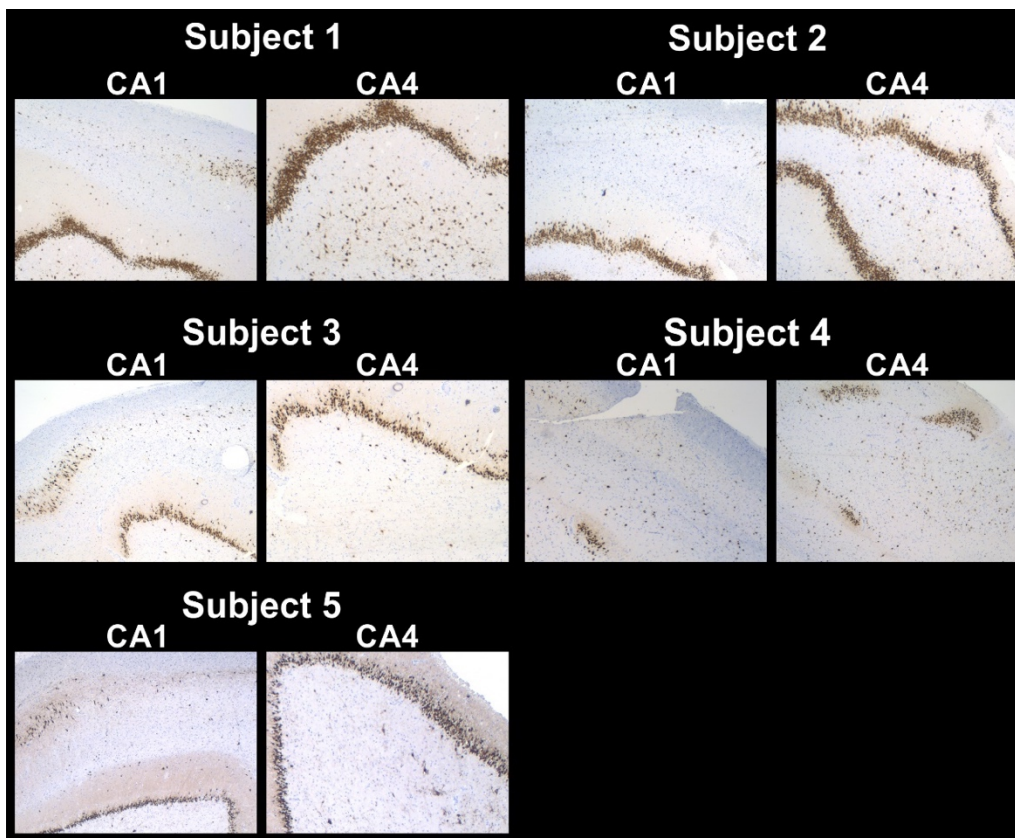


Figure 10.7 - Histopathologic classification of ILAE HS subtypes

Photomicrographs are displayed showing Neuronal nuclear antigen (NeuN) immunostaining in CA1 and CA4 subfields for each subject.

Neuropathological classification was performed by a board-certified neuropathologist (Laura Schmitt) (5): No HS (CA1 and CA4 normal); Type 1 HS (CA1 and CA4 abnormal); Type 2 HS (CA1 abnormal but CA4 normal); Type 3 HS (CA1 normal but CA4 abnormal). Each specimen demonstrated neuronal loss in both CA1 and CA4 and was therefore classified as Type 1 HS.

abnormal but CA4 normal); Type 3 HS (CA1 normal but CA4 abnormal). Each specimen demonstrated neuronal loss in both CA1 and CA4 and was therefore classified as Type 1 HS (Figure 10.7).

10.4 Discussion

In the present study, we applied our histology-derived hippocampal subfield segmentation protocol to in vivo MRI. Our method demonstrated similar intra-rater reliability for *subfield volume measurements* in controls and subjects with HS in comparison with previous protocols. Previous investigators used 4 tesla MRI (10) to measure the entorhinal cortex, subiculum, CA1, CA2, and CA3/CA4/DG across 5 slices (10 mm) of the anterior hippocampal body. Intra-rater reliability data (ICCs) *in controls* (236) (CA1 = 0.99, CA2 = 0.87, CA3/CA4/DG = 0.99, Subiculum = 0.99) were similar to our *control* intra-rater reliability results (CA1 = 0.99, CA2 = 0.82, CA3/CA4/DG = 0.96, Subiculum = 0.88). In another study CA1, CA2/CA3, and CA4/DG were measured with 3 tesla MRI across the entire hippocampal body (9). The intra-rater reliability results (ICCs) *in TLE* (9) (CA1 = 0.91, CA2/CA3 = 0.88, CA4/DG = 0.93) were similar to the intra-rater reliability data for the application of our protocol in *sclerotic hippocampi* (CA1 = 0.98, CA2 = 0.92, CA3/CA4/DG = 0.98).

We then used our method to characterize ILAE HS Subtypes in five subjects with TLE and unilateral HS according to *volumetric analysis*. For three of five subjects, HS subtype diagnosis as predicted by *subfield volumetry* was consistent with the histopathologic diagnosis (Type 1 HS). This finding is consistent with previous studies which have demonstrated a significant correlation between hippocampal volumes and neuronal densities in hippocampal subfields (9, 168, 240, 241). These results suggest that

determining HS Subtype using *hippocampal subfield volumetry* (9, 10) may allow preoperative diagnosis of *histopathological HS subtypes* (5). However, in two of five subjects, subfield volumetry suggested atypical HS (one ILAE type 2 HS & one ILAE type 3 HS) while histopathology in each of these patients demonstrated Type 1 HS. There are several potential explanations for this discrepancy. Firstly, the hippocampal biopsy margins in each subject (white arrows, Figure 10.6) included a portion of the hippocampal head (grey, Figure 10.6) which we did not analyze with in vivo MRI. However, this explanation for the aforementioned discrepancy is unlikely as pathological specimens from each subject demonstrated morphology typical of the hippocampal body. Our subfield area analyses across the hippocampal long axis provide a second potential explanation for the discordance between subfield volumes and histopathology findings. As shown in Figure 10.6, each subject with atypical HS based on subfield volumetry demonstrated several slices of Type 1 HS based on subfield area analyses. Pathological analysis at any of these locations would be expected to demonstrate Type 1 HS, which could potentially explain our results.

Relatedly, our results demonstrate that in some patients HS subtype diagnoses based on *subfield volumetry* measurements do not appear to adequately reflect *HS subtype atrophy patterns along the entire hippocampal long axis*. In the present study, the degree of concordance observed between volumetric and longitudinal axis analyses differed between patients. In some subjects, HS patterns were relatively homogenous along the long axis and were therefore predicted accurately by the analysis of subfield volumes. Remarkable variability was demonstrated for HS patterns along the long axis in other patients, which could not be adequately captured by the volumetric method. The variability of HS along the long axis demonstrated in the present study

adds to an existing literature suggesting that in order to adequately define HS in patients with TLE, the entire long axis must be examined. Previous MRI studies have shown that sclerosis can be seen at specific locations along the hippocampal long axis, while some segments of the hippocampus can appear normal on MRI (266). Furthermore, pathological analysis often reveals significant heterogeneity of HS subtype classification along the hippocampal long axis (136).

In vivo MRI-based diagnoses of HS subtypes could potentially be incorporated with pathology into future ILAE classification systems (5). While individual surgical pathology series have suggested prognostic significance of HS subtype diagnoses (8), surgical outcomes for HS subtypes ***have not been consistent across studies*** (4). For example, in one study (8), Type 2 HS patients had a similar likelihood (67%) of seizure freedom compared with Type 1 HS patients (72%). In another study, however, Type 2 HS patients had a much poorer prognosis (33% seizure-free) than those with Type 1 HS (69% seizure-free) (4). Similarly, Type 3 HS was shown to be associated with a very low (28%) chance of seizure freedom (8), while another study found that Type 3 HS was associated with an excellent prognosis (100% seizure free) (4). These discordant findings are potentially due to the variability of pathological HS subtype classification across the hippocampal long axis described above (136) and demonstrated in the present study. As in our study, biopsies of the hippocampus obtained during epilepsy surgery often represent only a small portion of the entire structure - and therefore cannot accurately reflect subtype pathology across the entire long axis (136). In vivo MRI-based methods hold promise to address this current limitation by allowing determination of HS subtypes along the entire longitudinal axis, which may eventually allow more accurate prediction of surgical outcomes.

Our data emphasize the remarkable *inter-subject variability* of specific subfield involvement *between individual patients* with TLE, both ipsilateral and contralateral to pathologically confirmed HS. Subfield pathology in the ipsilateral hippocampus was variable, for example, with some subjects identified with nearly uniform Type 1 HS that contrasted with other patients demonstrating a variety of HS subtypes along the hippocampal long axis. This finding is consistent with the neuropathology literature demonstrating *patient-specific* involvement of hippocampal subfields in TLE (4, 8, 157, 164, 168, 171, 263).

Our results also demonstrate heterogeneous abnormalities in the contralateral hippocampus in subjects with unilateral HS. One subject demonstrated a completely normal contralateral hippocampus, suggesting that bilateral neuronal loss (174) is not ubiquitous in patients with TLE. In contrast, three subjects demonstrated Type 3 HS in the contralateral hippocampus *on subfield area analysis*, which is consistent with the 'end folium sclerosis' described in previous autopsy series (15). These subfield abnormalities were not detected with *volumetric analysis* in two of these three subjects, both of whom demonstrated normal contralateral hippocampal subfield *volumes*. This finding further emphasizes the importance of characterizing the entire hippocampus along the long axis in patients with TLE.

The remarkable inter-subject variability demonstrated in TLE strongly suggests that HS subtypes should be characterized bilaterally along the entire hippocampal long axis and *assessed independently in individual patients* with TLE. While neuroimaging methods that pool patients together will detect group differences (267), such techniques would be expected to miss these important *differences between patients*.

Limitations

In the present study, we analyzed a small sample of controls (n=5) and subjects with HS (n=5). Further studies with a larger sample size will be important to confirm these preliminary results. We were unable to correct for total intracranial volume (ICV) due to an error resulting in incomplete whole-brain coverage of the volumetric T1 scans acquired in the control group. It is possible that correction for differences in ICV might result in slightly different subfield volumes in the TLE patients, which could potentially change the volumetry-based classification of HS subtype for some patients. However, the subfield area-based HS subtype analyses along the hippocampal long axis would not be affected by the absence of an ICV control in our study.

Future Directions

Future studies are required to determine if our method is able to predict surgical outcomes in patients with TLE. As our method can be performed preoperatively, it could be used to inform surgical decision-making in patients with TLE. Further experiments are also required to determine if our method is able to detect subtle HS in patients with nonlesional TLE. Approximately 20% of patients with pathologically confirmed HS cannot be diagnosed with currently available MRI techniques (150). In the present study, analysis of HS subtypes along the long axis detected subtle abnormalities in two hippocampi (both 'contralateral' to known HS) which were characterized as normal based on volumetric analysis.

Finally, the 'ground truth' for diagnosis of HS subtypes remains a critical unanswered question in the neuropathological literature. The current ILAE classification system is based on analysis of hippocampal biopsies obtained during epilepsy surgery (5), which typically represent only a small portion of the entire hippocampus. However, autopsy studies have demonstrated significant heterogeneity of HS along the long axis in patients with epilepsy (136). Therefore, whether biopsies obtained during epilepsy surgery can be considered representative for the entire hippocampus remains unclear. Our data provide MRI evidence that HS subtypes vary substantially along the long axis in some TLE patients, as described in previous autopsy studies in patients with chronic epilepsy (136).

10.5 Conclusions

In the present study, we describe a novel method to characterize HS subtypes using in vivo MRI. Hippocampal subfield volumetry using this method was predictive of histopathological HS subtype in 3/5 patients with TLE and unilateral HS. Subfield area analyses demonstrated substantial variability of HS subtypes along the longitudinal axis in several subjects. Our results suggest that determining HS subtype using high resolution in vivo MRI may allow preoperative diagnosis of histopathological HS subtypes in some patients.

III Discussion

Chapter 11 Conclusion

The purpose of this section is to consider our experimental results in the context of the current literature. This chapter is therefore organized to mirror the Experiments portion of this thesis (Chapters 7-10). For each of these chapters, we provide a brief overview of requisite background information, highlight the knowledge gaps that we addressed, and emphasize the contributions of our experimental findings to current knowledge.

11.1 Neuronal densities in MTLE (Chapter 7)

Background

There is a strong scientific rationale for the study of hippocampal subfields in patients with mesial temporal lobe epilepsy (MTLE). Animal models have demonstrated subfield-specific neuronal loss following status epilepticus (36) and classical neuropathological studies have revealed selective involvement of discrete subregions in patients with chronic epilepsy (103). Qualitative analysis of hippocampal specimens resected from patients with MTLE has demonstrated severe neuronal loss in CA1 and CA4 subfields (103). In contrast, area CA2 appears to be relatively spared in patients with MTLE (156).

Knowledge gaps

The classical neuropathology literature was based on qualitative examination of hippocampal specimens. However, the current neuropathological

classification of MTLE is based on quantitative measurement of neuronal densities (5). Whether neuronal density measurements demonstrate subfield-specific neuronal loss in subjects with MTLE remains unknown.

Contributions

We performed a meta-analysis of previous studies reporting neuronal densities from autopsy controls and patients with MTLE. This analysis revealed a greater severity of neuronal loss in CA1 in comparison to all other subfields. Furthermore, CA2 was found to have the lowest magnitude of cell loss. These findings are consistent with the qualitative neuropathological literature and confirm our current understanding of MTLE as a subfield-specific disorder.

11.2 Neuronal density and subfield areas (Chapter 8)

Background

The neuropathological classification of MTLE is based on measurement of neuronal densities in the CA1 and CA4 sectors of the hippocampus (5). Recent studies have shown that these subregions can be reliably delineated with in vivo MRI. However, despite increases in spatial resolution, neuronal densities cannot be directly measured with in vivo MRI. Classification of MTLE subtypes using MRI-based hippocampal subfield volumetry is based on the hypothesis that subfield area (or volume) measurements are correlated with neuronal densities in these regions.

Knowledge gaps

Whether a relationship exists between neuronal densities and subfield areas in specific hippocampal subregions remains unclear from the previous literature. We therefore examined the correlation between these two variables in our cohort of autopsy controls.

Contributions

Interestingly, our analyses did not identify a significant relationship between neuronal densities and subfield areas in healthy controls. These results are concordant with a recent ex vivo MRI study performed in subjects with MTLE (203). Collectively, these findings suggest a complex relationship between neuronal number and tissue volume in healthy controls and subjects with MTLE.

11.3 Histology-derived segmentation of ex vivo MRI (Chapter 9)

Background

The relationships between anatomical landmarks (gyri and sulci) and histologically-defined brain regions (Brodmann areas) have been established for many cortical areas (268). Recent work has shown that the entorhinal (210) and perirhinal (209) cortices can also be accurately localized in relation to gyral patterns.

Knowledge gaps

The relationships between internal landmarks and histologically-defined subfield transitions in the hippocampus remain unclear. Furthermore, the correlation between MRI-based measurements of hippocampal subfield areas and ground truth histological measures remains unknown.

Contributions

In this chapter, we describe the development of a new method to measure hippocampal subfields with ex vivo MRI. Our method is based on two anatomical landmarks, the stratum lacunosum moleculare (SLM) and the dentate gyrus (DG). In this technique, subfield areas are segmented in the hippocampal body by determining subfield transitions as a proportion of the total SLM length. We found that subfield areas measured with MRI were strongly correlated with histologically defined measurements. Furthermore, we found that our method could be applied with good intra- and inter-rater reliability.

Our results suggest that histologically-defined hippocampal subfield areas can be accurately measured with ex vivo MRI. This represents a significant contribution to the literature as the only previous study to utilize histology-derived subfield definitions to segment ex vivo MRI was performed in a single subject (202). In addition, our method can potentially be directly applied to preoperative MRI in subjects with MTLE as it is based on anatomical landmarks which are readily visualized on in vivo MR Images.

11.4 In vivo diagnosis of MTLE subtypes (Chapter 10)

Background

MTLE subtypes currently can only be diagnosed postoperatively following hippocampal resection. As a result, our current knowledge of MTLE subtypes remains limited and prognostic information cannot be used to inform surgical decision-making. Furthermore, recent autopsy studies have shown that MTLE subtypes vary along the hippocampal long axis in the majority of patients with chronic epilepsy (136).

Knowledge gaps

It remains unknown whether it is possible to characterize MTLE subtypes preoperatively using in vivo MRI.

Contributions

We determined MTLE subtypes with in vivo MRI using two methods: *hippocampal subfield volumetry* and *subfield area measurements along the hippocampal long axis*. We found that the volumetry results were consistent with neuropathological findings in three out of five patients. This result suggests that MTLE subtypes can be characterized using in vivo hippocampal subfield volumetry in some patients.

However, we also found that MRI-defined MTLE subtypes demonstrated significant variability along the hippocampal long axis in some patients. This finding in our cohort of patients with MTLE provides support for previous autopsy results from patients with chronic epilepsy (136). These results are important as they emphasize the limitations of both surgical biopsies (which do not evaluate the entire hippocampus) and subfield volume measurements (which combine measurements across the entire hippocampal body) in the assessment of MTLE subtypes. As discussed in chapter 4, these findings represent a potential explanation for the discordant results obtained across prior clinico-pathologic series of patients with MTLE.

Our data also demonstrate the potential for in vivo MRI to characterize subfield involvement in the "contralateral" hippocampus in patients with MTLE, which is currently only possible in autopsy studies (15, 136). Interestingly, our results provide preliminary support for Margerison and Corsellis' seminal finding that Type 3 HS is commonly identified contralateral to the seizure focus (15). However, further studies in a larger number of patients are required to determine the clinical relevance and prognostic significance of these findings.

Finally, our in vivo data demonstrated significant variability of subregional atrophy patterns between patients. We identified some subjects with relatively uniform MTLE subtype diagnoses along the hippocampal long axis. In contrast, other patients were found to have a combination of several subtype atrophy patterns throughout the hippocampus. This finding emphasizes the importance of evaluating MTLE subtypes in individual subjects as pooling patients together would be expected to miss potentially important patient-specific characteristics.

Chapter 12 Limitations

The purpose of this chapter is to review the limitations of our experimental work described in chapters 7-10 of this thesis. For each of our experiments, we discuss important limitations and consider their importance to the interpretation of our results. These caveats will be used to inform the design of future studies to further test our hypothesis.

Neuronal densities in MTLE (Chapter 7)

Qualitative examination of hippocampal specimens typically reveals severe neuronal loss in the CA1 and CA4 subregions. Interestingly, however, our data did not demonstrate greater neuronal loss in CA4 when compared with CA3. This discrepancy may relate to significant variability (termed heterogeneity) in subfield-specific neuronal loss between the individual studies included in our meta-analysis. As discussed in chapter 7, there are several potential reasons for the heterogeneity demonstrated in our study. Firstly, some of the studies reported neuronal densities from a small sample of controls and patients with mesial temporal lobe epilepsy (MTLE). Secondly, all included studies utilized a two-dimensional cell counting technique which (as discussed further below) may not provide an accurate assessment of true neuronal loss. Therefore, while our study provides evidence for greatest neuronal loss in CA1 and relative sparing of CA2, whether more subtle quantitative differences exist for CA3 and CA4 remains unknown.

Neuronal density and subfield areas (Chapter 8)

Previous studies have produced discordant results regarding the correlation between neuronal densities and hippocampal subfield volumes. As shown in table 8.1, some studies have demonstrated a positive correlation between these variables while others have not found such a relationship. As discussed in chapter 8, our data also suggest a complex relationship between neuronal densities and histologically-defined subfield areas. However, our study (and nearly all previous reports) utilized a two-dimensional cell counting technique which may underestimate true neuronal loss in MTLE. While three-dimensional cell counting methods would provide more accurate measurements of total neuronal loss, such methods are not straightforward to incorporate into the clinical workflow of neuropathology departments. However, future studies could potentially use stereological methods to determine the relationships between neuronal numbers and subfield volumes in cadaveric hippocampi.

Histology-derived segmentation of ex vivo MRI (Chapter 9)

Our ex vivo MRI study has several important limitations. Firstly, we developed our segmentation rules in a single sample of cadaveric hippocampi and then validated the method in these same hippocampi. In chapter 9, we present data (figures 9.12 & 9.13) to support the validity of our approach. However, external validation in a separate sample of cadaveric hippocampi will be required to confirm the accuracy of our method across a range of hippocampal specimens from healthy controls.

The application of segmentation rules developed in healthy controls to map the diseased hippocampus represents a second important limitation. It is possible that the presence of hippocampal pathology in patients with MTLE results in an altered location of hippocampal subfield boundaries in comparison to health controls. This hypothesis could be further evaluated in anatomically intact hippocampal specimens resected from patients with MTLE, which were not available for the work described in this thesis.

In vivo diagnosis of MTLE subtypes (Chapter 10)

There are several important limitations for the in vivo application of our method to determine MTLE subtypes. Due to an error in the acquisition of volumetric T1 images in control subjects, we were unable to correct for intracranial volume (ICV) in this study. ICV-corrected subfield volumes could potentially result in different volumetry-based MTLE diagnoses for some subjects. In future studies, we therefore plan to ensure whole-brain coverage of volumetric T1 images in order to allow correction of subfield volumes for ICV. Finally, due to the significant learning curve for hippocampal subfield segmentation we were only able to document the intra-rater reliability of our method. We plan to determine the inter-rater reliability of our method in a subsequent study of a larger cohort of controls and patients with MTLE.

Bibliography

1. Epilepsy fact sheet: World Health Organization; 2018 [Available from: <http://www.who.int/mediacentre/factsheets/fs999/en/>].
2. Kwan P, Brodie MJ. Early identification of refractory epilepsy. *New England Journal of Medicine*. 2000;342(5):314-9.
3. Semah F, Picot MC, Adam C, Broglin D, Arzimanoglou A, Bazin B, et al. Is the underlying cause of epilepsy a major prognostic factor for recurrence? *Neurology*. 1998;51(5):1256-62.
4. Thom M, Liagkouras I, Elliot KJ, Martinian L, Harkness W, McEvoy A, et al. Reliability of patterns of hippocampal sclerosis as predictors of postsurgical outcome. *Epilepsia*. 2010;51:1801-8.
5. Blumcke I, Thom M, Aronica E, Armstrong DD, Bartolomei F, Bernasconi A, et al. International consensus classification of hippocampal sclerosis in temporal lobe epilepsy: a Task Force report from the ILAE Commission on Diagnostic Methods. *Epilepsia*. 2013;54(7):1315-29.
6. Thom M, Mathern GW, Cross JH, Bertram EH. Mesial temporal lobe epilepsy: How do we improve surgical outcome? *Annals of Neurology*. 2010;68:424-34.
7. Eriksson SH, Thom M, Bartlett PA, Symms MR, McEvoy AW, Sisodiya SM, et al. PROPELLER MRI visualizes detailed pathology of hippocampal sclerosis. *Epilepsia*. 2008;49(1):33-9.
8. Blumcke I, Pauli E, Clusmann H, Schramm J, Becker A, Elger C, et al. A new clinico-pathological classification system for mesial temporal sclerosis. *Acta Neuropathologica*. 2007;113(3):235-44.
9. Goubran M, Bernhardt BC, Cantor-Rivera D, Lau JC, Blinston C, Hammond RR, et al. In vivo MRI signatures of hippocampal subfield pathology in intractable epilepsy. *Hum Brain Mapp*. 2016;37(3):1103-19.
10. Mueller SG, Laxer KD, Barakos J, Cheong I, Garcia P, Weiner MW. Subfield atrophy pattern in temporal lobe epilepsy with and without mesial

sclerosis detected by high-resolution MRI at 4 Tesla: preliminary results. *Epilepsia*. 2009;50(6):1474-83.

11. Insausti R, Amaral DG. Hippocampal Formation. In: Mai JK, Paxinos G, editors. *The Human Nervous System* 2012. p. 869-942.
12. Braak H. *Architectonics of the Human Telencephalic Cortex*. Berlin: 1980; 1980.
13. Duvernoy HM. *The Human Hippocampus: Functional Anatomy, Vascularization and Serial Sections with MRI*. 3 ed. Germany: Springer; 2005. 232 p.
14. Lorente de No R. Studies on the structure of the cerebral cortex, II: continuation of the study of the ammonic system. *J Psychol Neurol (Leipzig)*. 1934;46:113-77.
15. Margerison JH, Corsellis JA. Epilepsy and the temporal lobes. A clinical, electroencephalographic and neuropathological study of the brain in epilepsy, with particular reference to the temporal lobes. *Brain*. 1966;89(3):499-530.
16. Amaral DG, Witter MP. The 3-Dimensional Organization of the Hippocampal-Formation - a Review of Anatomical Data. *Neuroscience*. 1989;31(3):571-91.
17. Scoville WB, Milner B. Loss of Recent Memory After Bilateral Hippocampal Lesions. *Journal of Neurology Neurosurgery and Psychiatry*. 1957;20(1):11-21.
18. Blumcke I, Spreafico R, Haaker G, Coras R, Kobow K, Bien CG, et al. Histopathological Findings in Brain Tissue Obtained during Epilepsy Surgery. *N Engl J Med*. 2017;377(17):1648-56.
19. Concha L, Beaulieu C, Gross DW. Bilateral limbic diffusion abnormalities in unilateral temporal lobe epilepsy. *Annals of Neurology*. 2005;57(2):188-96.
20. Liu M, Chen Z, Beaulieu C, Gross DW. Disrupted anatomic white matter network in left mesial temporal lobe epilepsy. *Epilepsia*. 2014;55(5):674-82.

21. Walker MC. Hippocampus and Human Disease. In: Andersen P, editor. *The Hippocampus Book*. New York: Oxford University Press; 2007. p. 769-812.
22. Ewell LA, Jones MV. Frequency-tuned distribution of inhibition in the dentate gyrus. *J Neurosci*. 2010;30(38):12597-607.
23. Traub RD, Jefferys JG. Simulations of epileptiform activity in the hippocampal CA3 region in vitro. *Hippocampus*. 1994;4(3):281-5.
24. Wong RK, Prince DA, Basbaum AI. Intradendritic recordings from hippocampal neurons. *Proc Natl Acad Sci U S A*. 1979;76(2):986-90.
25. Miles R, Wong RK. Single neurones can initiate synchronized population discharge in the hippocampus. *Nature*. 1983;306(5941):371-3.
26. Neunuebel JP, Knierim JJ. CA3 Retrieves Coherent Representations from Degraded Input: Direct Evidence for CA3 Pattern Completion and Dentate Gyrus Pattern Separation. *Neuron*. 2014;81(2):416-27.
27. Vazdarjanova A, Guzowski JF. Differences in hippocampal neuronal population responses to modifications of an environmental context: Evidence for distinct, yet complementary, functions of CA3 and CA1 ensembles. *Journal of Neuroscience*. 2004;24(29):6489-96.
28. Leutgeb S, Leutgeb JK, Treves A, Moser MB, Moser EI. Distinct ensemble codes in hippocampal areas CA3 and CA1. *Science*. 2004;305(5688):1295-8.
29. Lee I, Yoganarasimha D, Rao G, Knierim JJ. Comparison of population coherence of place cells in hippocampal subfields CA1 and CA3. *Nature*. 2004;430(6998):456-9.
30. Marr D. Simple Memory - Theory for Archicortex. *Philosophical Transactions of the Royal Society of London Series B-Biological Sciences*. 1971;262(841).
31. Su H, Alroy G, Kirson ED, Yaari Y. Extracellular calcium modulates persistent sodium current-dependent burst-firing in hippocampal pyramidal neurons. *J Neurosci*. 2001;21(12):4173-82.

32. Karnup S, Stelzer A. Seizure-like activity in the disinhibited CA1 minislice of adult guinea-pigs. *J Physiol.* 2001;532(Pt 3):713-30.
33. Goldberg EM, Coulter DA. Mechanisms of epileptogenesis: a convergence on neural circuit dysfunction. *Nature Reviews Neuroscience.* 2013;14:337-49.
34. Yu EP, Dengler CG, Frausto SF, Putt ME, Yue C, Takano H, et al. Protracted postnatal development of sparse, specific dentate granule cell activation in the mouse hippocampus. *J Neurosci.* 2013;33(7):2947-60.
35. Goddard GV. Development of epileptic seizures through brain stimulation at low intensity. *Nature.* 1967;214(5092):1020-1.
36. Cavazos JE, Das I, Sutula TP. Neuronal loss induced in limbic pathways by kindling: evidence for induction of hippocampal sclerosis by repeated brief seizures. *J Neurosci.* 1994;14(5 Pt 2):3106-21.
37. Bengzon J, Kokaia Z, Elmer E, Nanobashvili A, Kokaia M, Lindvall O. Apoptosis and proliferation of dentate gyrus neurons after single and intermittent limbic seizures. *Proc Natl Acad Sci U S A.* 1997;94(19):10432-7.
38. Ben-Ari Y. Limbic seizure and brain damage produced by kainic acid: mechanisms and relevance to human temporal lobe epilepsy. *Neuroscience.* 1985;14(2):375-403.
39. Meldrum BS. First Alfred Meyer Memorial Lecture. Epileptic brain damage: a consequence and a cause of seizures. *Neuropathol Appl Neurobiol.* 1997;23(3):185-201; discussion -2.
40. Eriksson PS, Perfilieva E, Bjork-Eriksson T, Alborn AM, Nordborg C, Peterson DA, et al. Neurogenesis in the adult human hippocampus. *Nature medicine.* 1998;4(11):1313-7.
41. Parent JM, Yu TW, Leibowitz RT, Geschwind DH, Sloviter RS, Lowenstein DH. Dentate granule cell neurogenesis is increased by seizures and contributes to aberrant network reorganization in the adult rat hippocampus. *J Neurosci.* 1997;17(10):3727-38.
42. Houser CR. Granule cell dispersion in the dentate gyrus of humans with temporal lobe epilepsy. *Brain Res.* 1990;535(2):195-204.

43. Dietrich D, Clusmann H, Kral T, Steinhauser C, Blumcke I, Heinemann U, et al. Two electrophysiologically distinct types of granule cells in epileptic human hippocampus. *Neuroscience*. 1999;90(4):197-206.
44. Magloczky Z, Wittner L, Borhegyi Z, Halasz P, Vajda J, Czirjak S, et al. Changes in the distribution and connectivity of interneurons in the epileptic human dentate gyrus. *Neuroscience*. 2000;96(1):7-25.
45. Sutula T, He XX, Cavazos J, Scott G. Synaptic reorganization in the hippocampus induced by abnormal functional activity. *Science*. 1988;239(4844):1147-50.
46. Tauck DL, Nadler JV. Evidence of functional mossy fiber sprouting in hippocampal formation of kainic acid-treated rats. *J Neurosci*. 1985;5(4):1016-22.
47. Sutula T, Cascino G, Cavazos J, Parada I, Ramirez L. Mossy fiber synaptic reorganization in the epileptic human temporal lobe. *Ann Neurol*. 1989;26(3):321-30.
48. Scheibel ME, Crandall PH, Scheibel AB. The hippocampal-dentate complex in temporal lobe epilepsy. A Golgi study. *Epilepsia*. 1974;15(1):55-80.
49. Cronin J, Obenaus A, Houser CR, Dudek FE. Electrophysiology of dentate granule cells after kainate-induced synaptic reorganization of the mossy fibers. *Brain Res*. 1992;573(2):305-10.
50. Jones RS. Ictal epileptiform events induced by removal of extracellular magnesium in slices of entorhinal cortex are blocked by baclofen. *Exp Neurol*. 1989;104(2):155-61.
51. Thom M, Eriksson S, Martinian L, Caboclo LO, McEvoy AW, Duncan JS, et al. Temporal lobe sclerosis associated with hippocampal sclerosis in temporal lobe epilepsy: neuropathological features. *Journal of neuropathology and experimental neurology*. 2009;68:928-38.
52. Yilmazer-Hanke DM, Wolf HK, Schramm J, Elger CE, Wiestler OD, Blumcke I. Subregional pathology of the amygdala complex and entorhinal region in surgical specimens from patients with pharmaco-resistant temporal lobe epilepsy. *J Neuropathol Exp Neurol*. 2000;59(10):907-20.

53. Du F, Whetsell WO, Jr., Abou-Khalil B, Blumenkopf B, Lothman EW, Schwarcz R. Preferential neuronal loss in layer III of the entorhinal cortex in patients with temporal lobe epilepsy. *Epilepsy Res.* 1993;16(3):223-33.
54. Stafstrom CE. The role of the subiculum in epilepsy and epileptogenesis. *Epilepsy Curr.* 2005;5(4):121-9.
55. Mattia D, Kawasaki H, Avoli M. In vitro electrophysiology of rat subicular bursting neurons. *Hippocampus.* 1997;7(1):48-57.
56. Wellmer J, Su H, Beck H, Yaari Y. Long-lasting modification of intrinsic discharge properties in subicular neurons following status epilepticus. *Eur J Neurosci.* 2002;16(2):259-66.
57. Menendez de la Prida L, Gal B. Synaptic contributions to focal and widespread spatiotemporal dynamics in the isolated rat subiculum in vitro. *J Neurosci.* 2004;24(24):5525-36.
58. Wozny C, Gabriel S, Jandova K, Schulze K, Heinemann U, Behr J. Entorhinal cortex entrains epileptiform activity in CA1 in pilocarpine-treated rats. *Neurobiol Dis.* 2005;19(3):451-60.
59. Ang CW, Carlson GC, Coulter DA. Massive and specific dysregulation of direct cortical input to the hippocampus in temporal lobe epilepsy. *J Neurosci.* 2006;26(46):11850-6.
60. Fisher RS, Van EB, Blume W, Elger C, Genton P, Lee P, et al. Epileptic seizures and epilepsy: Definitions proposed by the International League Against Epilepsy (ILAE) and the International Bureau for Epilepsy (IBE). *Epilepsia.* 2005;46(4):470-2.
61. Fisher RS, Cross JH, French JA, Higurashi N, Hirsch E, Jansen FE, et al. Operational classification of seizure types by the International League Against Epilepsy. 2016:1-9.
62. Berg AT, Berkovic SF, Brodie MJ, Buchhalter J, Cross JH, Van EB, et al. Revised terminology and concepts for organization of seizures and epilepsies: Report of the ILAE Commission on Classification and Terminology, 2005-2009. *Epilepsia.* 2010;51(4):676-85.
63. McCormick DA, Contreras D. On the cellular and network bases of epileptic seizures. *Annu Rev Physiol.* 2001;63:815-46.

64. Beghi E, Carpio A, Forsgren L, Hesdorffer DC, Malmgren K, Sander JW, et al. Recommendation for a definition of acute symptomatic seizure. *Epilepsia*. 2010;51(4):671-5.
65. Annegers JF, Hauser WA, Lee JR, Rocca WA. Incidence of acute symptomatic seizures in Rochester, Minnesota, 1935-1984. *Epilepsia*. 1995;36(4):327-33.
66. Hesdorffer DC, Benn EK, Cascino GD, Hauser WA. Is a first acute symptomatic seizure epilepsy? Mortality and risk for recurrent seizure. *Epilepsia*. 2009;50(5):1102-8.
67. Hauser WA, Annegers JF, Kurland LT. Incidence of epilepsy and unprovoked seizures in Rochester, Minnesota: 1935-1984. *Epilepsia*. 1993;34(3):453-68.
68. Hauser WA, Rich SS, Lee JR, Annegers JF, Anderson VE. Risk of recurrent seizures after two unprovoked seizures. *N Engl J Med*. 1998;338(7):429-34.
69. Krumholz A, Wiebe S, Gronseth GS, Gloss DS, Sanchez AM, Kabir AA, et al. Evidence-based guideline: Management of an unprovoked first seizure in adults: Report of the Guideline Development Subcommittee of the American Academy of Neurology and the American Epilepsy Society. *Neurology*. 2015;84(16):1705-13.
70. Fisher RS, Acevedo C, Arzimanoglou A, Bogacz A, Cross JH, Elger CE, et al. ILAE Official Report: A practical clinical definition of epilepsy. *Epilepsia*. 2014;55(4):475-82.
71. Gilmour HR-M, Pamela; Wong, Suzie L. Epilepsy in Canada: Prevalence and impact [Webpage]. Statistics Canada; 2016 [Available from: <https://www.statcan.gc.ca/pub/82-003-x/2016009/article/14654-eng.htm>].
72. Fazel S, Wolf A, Langstrom N, Newton CR, Lichtenstein P. Premature mortality in epilepsy and the role of psychiatric comorbidity: a total population study. *Lancet*. 2013;382(9905):1646-54.
73. Scheffer IE, Berkovic S, Capovilla G, Connolly MB, French J, Guilhoto L, et al. ILAE classification of the epilepsies: Position paper of the ILAE Commission for Classification and Terminology. *Epilepsia*. 2017:1-10.

74. Ohtahara S, Yamatogi Y. Epileptic encephalopathies in early infancy with suppression-burst. *J Clin Neurophysiol.* 2003;20(6):398-407.
75. Ramsay RE, Rowan AJ, Pryor FM. Special considerations in treating the elderly patient with epilepsy. *Neurology.* 2004;62(5 Suppl 2):S24-9.
76. Misulis KE. Basic electronics for clinical neurophysiology. *J Clin Neurophysiol.* 1989;6(1):41-74.
77. Lesser RP, Luders H, Dinner DS, Morris H. An introduction to the basic concepts of polarity and localization. *J Clin Neurophysiol.* 1985;2(1):45-61.
78. Knott JR. Further thoughts on polarity, montages, and localization. *J Clin Neurophysiol.* 1985;2(1):63-75.
79. Olejniczak P. Neurophysiologic basis of EEG. *J Clin Neurophysiol.* 2006;23(3):186-9.
80. Gloor P. Neuronal generators and the problem of localization in electroencephalography: application of volume conductor theory to electroencephalography. *J Clin Neurophysiol.* 1985;2(4):327-54.
81. Lothman EW. Basic mechanisms of the epilepsies. *Curr Opin Neurol Neurosurg.* 1992;5(2):216-23.
82. Hrachovy RA, Frost JD, Jr. The EEG in selected generalized seizures. *J Clin Neurophysiol.* 2006;23(4):312-32.
83. Verma A, Radtke R. EEG of partial seizures. *J Clin Neurophysiol.* 2006;23(4):333-9.
84. Blume WT. Invited review: clinical and basic neurophysiology of generalised epilepsies. *Can J Neurol Sci.* 2002;29(1):6-18.
85. Salinsky M, Kanter R, Dasheiff RM. Effectiveness of Multiple EEGs in Supporting the Diagnosis of Epilepsy: An Operational Curve. *Epilepsia.* 1987;28(4):331-4.
86. King MA, Newton MR, Jackson GD, Fitt GJ, Mitchell LA, Silvapulle MJ, et al. Epileptology of the first-seizure presentation: a clinical, electroencephalographic, and magnetic resonance imaging study of 300 consecutive patients. *Lancet.* 1998;352(9133):1007-11.

87. Staley K. Molecular mechanisms of epilepsy. *Nature neuroscience*. 2015;18(3):367-72.
88. Kwan P, Sills GJ, Brodie MJ. The mechanisms of action of commonly used antiepileptic drugs. *Pharmacol Ther*. 2001;90(1):21-34.
89. Lynch BA, Lambeng N, Nocka K, Kensel-Hammes P, Bajjalieh SM, Matagne A, et al. The synaptic vesicle protein SV2A is the binding site for the antiepileptic drug levetiracetam. *Proc Natl Acad Sci U S A*. 2004;101(26):9861-6.
90. Marson AG, Al-Kharusi AM, Alwaidh M, Appleton R, Baker GA, Chadwick DW, et al. The SANAD study of effectiveness of carbamazepine, gabapentin, lamotrigine, oxcarbazepine, or topiramate for treatment of partial epilepsy: an unblinded randomised controlled trial. *Lancet*. 2007;369(9566):1000-15.
91. Marson AG, Al-Kharusi AM, Alwaidh M, Appleton R, Baker GA, Chadwick DW, et al. The SANAD study of effectiveness of valproate, lamotrigine, or topiramate for generalised and unclassifiable epilepsy: an unblinded randomised controlled trial. *Lancet*. 2007;369(9566):1016-26.
92. Kwan P, Brodie MJ. Effectiveness of first antiepileptic drug. *Epilepsia*. 2001;42(10):1255-60.
93. Kwan P, Arzimanoglou A, Berg AT, Brodie MJ, Allen Hauser W, Mathern G, et al. Definition of drug resistant epilepsy: consensus proposal by the ad hoc Task Force of the ILAE Commission on Therapeutic Strategies. *Epilepsia*. 2010;51(6):1069-77.
94. Begley CE, Annegers JF, Lairson DR, Reynolds TF, Hauser WA. Cost of epilepsy in the United States: a model based on incidence and prognosis. *Epilepsia*. 1994;35(6):1230-43.
95. Sander JW, Bell GS. Reducing mortality: an important aim of epilepsy management. *Journal of Neurology Neurosurgery and Psychiatry*. 2004;75(3):349-51.
96. Hughlings Jackson J. Case of epilepsy with tasting movements and 'dreamy state' - very small patch of softening in the left uncinat gyrus. *Brain*. 1898;21:580-90.

97. Taylor DC, Marsh SM. Hughlings Jackson's Dr Z: the paradigm of temporal lobe epilepsy revealed. *J Neurol Neurosurg Psychiatry*. 1980;43(9):758-67.
98. Berg aT. The natural history of mesial temporal lobe epilepsy. *Curr Opin Neurol*. 2008;21(2):173-8.
99. French JA, Williamson PD, Thadani VM, Darcey TM, Mattson RH, Spencer SS, et al. Characteristics of medial temporal lobe epilepsy: I. Results of history and physical examination. *Annals of Neurology*. 1993;34:774-80.
100. Berg AT, Langfitt J, Shinnar S, Vickrey BG, Sperling MR, Walczak T, et al. How long does it take for partial epilepsy to become intractable? *Neurology*. 2003;60(2):186-90.
101. Mathern GW, Babb TL, Vickrey BG, Melendez M, Pretorius JK. The clinical-pathogenic mechanisms of hippocampal neuron loss and surgical outcomes in temporal lobe epilepsy. *Brain*. 1995;118(1):105-18.
102. Mathern GW, Adelson PD, Cahan LD, Leite JP. Hippocampal neuron damage in human epilepsy: Meyer's hypothesis revisited. *Prog Brain Res*. 2002;135:237-51.
103. Sommer W. Erkrankung des Ammonshorns als aetiologisches Moment der Epilepsie. *Arch Psychiatr Nervenkr*. 1880;10:631-75.
104. Spielmeyer W. Die Pathogenese des epileptischen Krampfes. *Z Ges Neurol Psychiat*. 1927;109:501-20.
105. Dudek SM, Alexander GM, Farris S. Rediscovering area CA2: unique properties and functions. *Nature Reviews Neuroscience*. 2016;17(2):89-102.
106. Meyer A, Falconer MA, Beck E. Pathological findings in temporal lobe epilepsy. *J Neurol Neurosurg Psychiatry*. 1954;17(4):276-85.
107. Dawodu S, Thom M. Quantitative neuropathology of the entorhinal cortex region in patients with hippocampal sclerosis and temporal lobe epilepsy. *Epilepsia*. 2005;46(1):23-30.
108. Thom M, Blumcke I, Aronica E. Long-term epilepsy-associated tumors. *Brain Pathol*. 2012;22(3):350-79.

109. Blumcke I, Thom M, Aronica E, Armstrong DD, Vinters HV, Palmini A, et al. The clinicopathologic spectrum of focal cortical dysplasias: a consensus classification proposed by an ad hoc Task Force of the ILAE Diagnostic Methods Commission. *Epilepsia*. 2011;52(1):158-74.
110. Rosenow F, Alonso-Vanegas MA, Baumgartner C, Blumcke I, Carreno M, Gizewski ER, et al. Cavernoma-related epilepsy: review and recommendations for management--report of the Surgical Task Force of the ILAE Commission on Therapeutic Strategies. *Epilepsia*. 2013;54(12):2025-35.
111. Stapleton CJ, Barker FG, 2nd. Cranial Cavernous Malformations: Natural History and Treatment. *Stroke*. 2018;49(4):1029-35.
112. Lévesque MF, Nakasato N, Vinters HV, Babb TL, Levesque MF, Nakasato N, et al. Surgical treatment of limbic epilepsy associated with extrahippocampal lesions: the problem of dual pathology. *Journal of neurosurgery*. 1991;75:364-70.
113. Cendes F, Cook MJ, Watson C, Andermann F, Fish DR, Shorvon SD, et al. Frequency and characteristics of dual pathology in patients with lesional epilepsy. *Neurology*. 1995;45(11):2058-64.
114. Li LM, Cendes F, Andermann F, Watson C, Fish DR, Cook MJ, et al. Surgical outcome in patients with epilepsy and dual pathology. *Brain*. 1999;122 (Pt 5):799-805.
115. Rosenow F, Luders H. Presurgical evaluation of epilepsy. *Brain*. 2001;124(Pt 9):1683-700.
116. Gibbs FA. Electroencephalography. *Am J Psychiatry*. 1946;102:527-35.
117. Jasper HH, Carmichael L. Electrical Potentials from the Intact Human Brain. *Science*. 1935;81(2089):51-3.
118. Penfield W. The Radical Treatment of Traumatic Epilepsy and Its Rationale. *Can Med Assoc J*. 1930;23(2):189-97.
119. Penfield W, Steelman H. The treatment of focal epilepsy by cortical excision. *Ann Surg*. 1947;126(5):740-62.
120. Penfield W, Flanigin H. Surgical therapy of temporal lobe seizures. *AMA Arch Neurol Psychiatry*. 1950;64(4):491-500.

121. Bailey P, Gibbs FA. The surgical treatment of psychomotor epilepsy. *J Am Med Assoc.* 1951;145(6):365-70.
122. Falconer MA, Meyer A, Hill D, Mitchell W, Pond DA. Treatment of temporal-lobe epilepsy by temporal lobectomy; a survey of findings and results. *Lancet.* 1955;268(6869):827-35.
123. Talairach J, Bancaud J, Bonis A, Szikla G, Tournoux P. Functional stereotaxic exploration of epilepsy. *Confin Neurol.* 1962;22:328-31.
124. Crandall PH, Walter RD, Rand RW. Clinical Applications of Studies on Stereotactically Implanted Electrodes in Temporal-Lobe Epilepsy. *J Neurosurg.* 1963;20:827-40.
125. Falconer M. MESIAL TEMPORAL (AMMON'S HORN) SCLEROSIS AS A COMMON CAUSE OF EPILEPSY: ETIOLOGY, TREATMENT, AND PREVENTION. *The Lancet.* 1974;304:767-70.
126. Nelson KB, Ellenberg JH. Predictors of epilepsy in children who have experienced febrile seizures. *N Engl J Med.* 1976;295(19):1029-33.
127. Annegers JF, Hauser WA, Shirts SB, Kurland LT. Factors prognostic of unprovoked seizures after febrile convulsions. *N Engl J Med.* 1987;316(9):493-8.
128. Lewis DV, Shinnar S, Hesdorffer DC, Bagiella E, Bello JA, Chan S, et al. Hippocampal sclerosis after febrile status epilepticus: The FEBSTAT study. *Annals of Neurology.* 2014;75(2):178-85.
129. Hardiman O, Burke T, Phillips J, Murphy S, O'Moore B, Staunton H, et al. Microdysgenesis in resected temporal neocortex: incidence and clinical significance in focal epilepsy. *Neurology.* 1988;38(7):1041-7.
130. Thom M, Sisodiya S, Harkness W, Scaravilli F. Microdysgenesis in temporal lobe epilepsy. A quantitative and immunohistochemical study of white matter neurones. *Brain.* 2001;124(Pt 11):2299-309.
131. Garbelli R, Frassoni C, Ferrario A, Tassi L, Brammerio M, Spreafico R. Cajal-Retzius cell density as marker of type of focal cortical dysplasia. *Neuroreport.* 2001;12(12):2767-71.

132. Blümcke I, Thom M, Wiestler OD. Ammon's horn sclerosis: a maldevelopmental disorder associated with temporal lobe epilepsy. *Brain pathology* (Zurich, Switzerland). 2002;12:199-211.
133. Cendes F, Lopes-Cendes I, Andermann E, Andermann F. Familial temporal lobe epilepsy: a clinically heterogeneous syndrome. *Neurology*. 1998;50(2):554-7.
134. Andrade-Valenca LPA, Valenca MM, Velasco TR, Carlotti Jr. CG, Assirati JA, Galvis-Alonso OY, et al. Mesial temporal lobe epilepsy: clinical and neuropathologic findings of familial and sporadic forms. *Epilepsia*. 2008;49:1046-54.
135. Kasperaviciute D, Catarino CB, Matarin M, Leu C, Novy J, Tostevin A, et al. Epilepsy, hippocampal sclerosis and febrile seizures linked by common genetic variation around SCN1A. *Brain*. 2013;136:3140-50.
136. Thom M, Liagkouras I, Martinian L, Liu J, Catarino CB, Sisodiya SM. Variability of sclerosis along the longitudinal hippocampal axis in epilepsy: A post mortem study. *Epilepsy research*. 2012;102(1-2):45-59.
137. Wolf HK, Aliashkevich AF, Blumcke I, Wiestler OD, Zentner J. Neuronal loss and gliosis of the amygdaloid nucleus in temporal lobe epilepsy. A quantitative analysis of 70 surgical specimens. *Acta Neuropathologica*. 1997;93(6):606-10.
138. Thom M, Eriksson S, Martinian L, Caboclo LO, McEvoy AW, Duncan JS, et al. Temporal lobe sclerosis associated with hippocampal sclerosis in temporal lobe epilepsy: neuropathological features. *J Neuropathol Exp Neurol*. 2009;68(8):928-38.
139. Thom M. Review: Hippocampal sclerosis in epilepsy: a neuropathology review. *Neuropathology and applied neurobiology*. 2014;40(5):520-43.
140. Williamson PD, French JA, Thadani VM, Kim JH, Novelly RA, Spencer SS, et al. Characteristics of medial temporal lobe epilepsy: II. Interictal and ictal scalp electroencephalography, neuropsychological testing, neuroimaging, surgical results, and pathology. *Annals of Neurology*. 1993;34(6):781-7.

141. Gloor P. Long term monitoring of the EEG: the challenge of the future. *Electroencephalography and clinical neurophysiology Supplement*. 1982;36:579-83.
142. Kuzniecky R, Delasayette V, Ethier R, Melanson D, Andermann F, Berkovic S, et al. Magnetic-Resonance-Imaging in Temporal-Lobe Epilepsy - Pathological Correlations. *Annals of Neurology*. 1987;22(3):341-7.
143. Berkovic SF, Andermann F, Olivier A, Ethier R, Melanson D, Robitaille Y, et al. Hippocampal sclerosis in temporal lobe epilepsy demonstrated by magnetic resonance imaging. *Ann Neurol*. 1991;29(2):175-82.
144. Jackson GD, Berkovic SF, Tress BM, Kalnins RM, Fabinyi GC, Bladin PF. Hippocampal sclerosis can be reliably detected by magnetic resonance imaging. *Neurology*. 1990;40(12):1869-75.
145. von Oertzen J, Urbach H, Jungbluth S, Kurthen M, Reuber M, Fernandez G, et al. Standard magnetic resonance imaging is inadequate for patients with refractory focal epilepsy. *Journal of Neurology Neurosurgery and Psychiatry*. 2002;73(6):643-7.
146. Cascino GD, Jack CR, Jr., Parisi JE, Sharbrough FW, Hirschorn KA, Meyer FB, et al. Magnetic resonance imaging-based volume studies in temporal lobe epilepsy: pathological correlations. *Ann Neurol*. 1991;30(1):31-6.
147. Jackson GD, Connelly A, Duncan JS, Grunewald RA, Gadian DG. Detection of hippocampal pathology in intractable partial epilepsy: increased sensitivity with quantitative magnetic resonance T2 relaxometry. *Neurology*. 1993;43(9):1793-9.
148. Briellmann RS, Kalnins RM, Berkovic SF, Jackson GD. Hippocampal pathology in refractory temporal lobe epilepsy: T2-weighted signal change reflects dentate gliosis. *Neurology*. 2002;58(2):265-71.
149. Berkovic SF, McIntosh AM, Kalnins RM, Jackson GD, Fabinyi GCA, Brazenor GA, et al. Preoperative Mri Predicts Outcome of Temporal Lobectomy - an Actuarial Analysis. *Neurology*. 1995;45(7):1358-63.
150. Bell ML, Rao S, So EL, Trenerry M, Kazemi N, Stead SM, et al. Epilepsy surgery outcomes in temporal lobe epilepsy with a normal MRI. *Epilepsia*. 2009;50(9):2053-60.

151. Spencer S, Huh L. Outcomes of epilepsy surgery in adults and children. *The Lancet Neurology*. 2008;7:525-37.
152. Wiebe S, Blume WT, Girvin JP, Eliasziw M, Effectiveness, Efficiency of Surgery for Temporal Lobe Epilepsy Study G. A randomized, controlled trial of surgery for temporal-lobe epilepsy. *New England Journal of Medicine*. 2001;345(5):311-8.
153. Bell GS, Sinha S, Tisi J, Stephani C, Scott CA, Harkness WF, et al. Premature mortality in refractory partial epilepsy: does surgical treatment make a difference? *J Neurol Neurosurg Psychiatry*. 2010;81(7):716-8.
154. de Tisi J, Bell GS, Peacock JL, McEvoy AW, Harkness WF, Sander JW, et al. The long-term outcome of adult epilepsy surgery, patterns of seizure remission, and relapse: a cohort study. *Lancet*. 2011;378(9800):1388-95.
155. Wolf HK, Buslei R, SchmidtKastner R, SchmidtKastner PK, Pietsch T, Wiestler OD, et al. NeuN: A useful neuronal marker for diagnostic histopathology. *Journal of Histochemistry & Cytochemistry*. 1996;44(10):1167-71.
156. Bratz E. Ammonshornbefunde bei Epileptikern. *Arch Psychiatr Nervenkr*. 1899;32:820-35.
157. De Lanerolle NC, Kim JH, Williamson A, Spencer SS, Zaveri HP, Eid T, et al. A retrospective analysis of hippocampal pathology in human temporal lobe epilepsy: Evidence for distinctive patient subcategories. *Epilepsia*. 2003;44(5):677-87.
158. Sim J, Wright CC. The kappa statistic in reliability studies: use, interpretation, and sample size requirements. *Phys Ther*. 2005;85(3):257-68.
159. Mathon B, Bielle F, Samson S, Plaisant O, Dupont S, Bertrand A, et al. Predictive factors of long-term outcomes of surgery for mesial temporal lobe epilepsy associated with hippocampal sclerosis. *Epilepsia*. 2017;58(8):1473-85.
160. Tezer FI, Xasiyev F, Soylemezoglu F, Bilginer B, Oguz KK, Saygi S. Clinical and electrophysiological findings in mesial temporal lobe epilepsy with hippocampal sclerosis, based on the recent histopathological classifications. *Epilepsy Research*. 2016;127:50-4.

161. Deleo F, Garbelli R, Milesi G, Gozzo F, Bramerio M, Villani F, et al. Short- and long-term surgical outcomes of temporal lobe epilepsy associated with hippocampal sclerosis: Relationships with neuropathology. *Epilepsia*. 2016;57(2):306-15.
162. Sastri BVS, Arivazhagan A, Sinha S, Mahadevan A, Bharath RD, Saini J, et al. Clinico-pathological factors influencing surgical outcome in drug resistant epilepsy secondary to mesial temporal sclerosis. *Journal of the Neurological Sciences*. 2014;340(1-2):183-90.
163. Coras R, Pauli E, Li J, Schwarz M, Roessler K, Buchfelder M, et al. Differential influence of hippocampal subfields to memory formation: insights from patients with temporal lobe epilepsy. *Brain*. 2014;137:1945-57.
164. Davies KG, Hermann BP, Dohan FC, Jr., Foley KT, Bush AJ, Wyler AR. Relationship of hippocampal sclerosis to duration and age of onset of epilepsy, and childhood febrile seizures in temporal lobectomy patients. *Epilepsia research*. 1996;24(2):119-26.
165. Prada Jardim A, Liu J, Baber J, Michalak Z, Reeves C, Ellis M, et al. Characterising subtypes of hippocampal sclerosis and reorganization: correlation with pre and postoperative memory deficit. *Brain Pathol*. 2018;28(2):143-54.
166. Gales JM, Jehi L, Nowacki A, Prayson RA. The role of histopathologic subtype in the setting of hippocampal sclerosis-associated mesial temporal lobe epilepsy. *Human Pathology*. 2017;63:79-88.
167. Jardim AP, Neves RS, Caboclo LO, Lancellotti CL, Marinho MM, Centeno RS, et al. Temporal lobe epilepsy with mesial temporal sclerosis: hippocampal neuronal loss as a predictor of surgical outcome. *Arquivos de Neuro-Psiquiatria*. 2012;70(5):319-24.
168. Van Paesschen W, Revesz T, Duncan JS, King MD, Connelly A. Quantitative neuropathology and quantitative magnetic resonance imaging of the hippocampus in temporal lobe epilepsy. *Ann Neurol*. 1997;42(5):756-66.
169. Labate A, Gambardella A, Andermann E, Aguglia U, Cendes F, Berkovic SF, et al. Benign mesial temporal lobe epilepsy. *Nat Rev Neurol*. 2011;7(4):237-40.

170. Na M, Ge HT, Shi C, Shen H, Wang Y, Pu S, et al. Long-term seizure outcome for international consensus classification of hippocampal sclerosis: A survival analysis. *Seizure-European Journal of Epilepsy*. 2015;25:141-6.
171. Sagar HJ, Oxbury JM. Hippocampal neuron loss in temporal lobe epilepsy: correlation with early childhood convulsions. *Annals of Neurology*. 1987;22(3):334-40.
172. Alvim MK, Coan AC, Campos BM, Yasuda CL, Oliveira MC, Morita ME, et al. Progression of gray matter atrophy in seizure-free patients with temporal lobe epilepsy. *Epilepsia*. 2016;57(4):621-9.
173. Spencer SS, Berg AT, Vickrey BG, Sperling MR, Bazil CW, Shinnar S, et al. Predicting long-term seizure outcome after resective epilepsy surgery - The Multicenter Study. *Neurology*. 2005;65(6):912-8.
174. Babb TL. Bilateral pathological damage in temporal lobe epilepsy. *Canadian Journal of Neurological Sciences*. 1991;18(4 Suppl):645-8.
175. Jack CR, Jr., Sharbrough FW, Cascino GD, Hirschorn KA, O'Brien PC, Marsh WR. Magnetic resonance image-based hippocampal volumetry: correlation with outcome after temporal lobectomy. *Ann Neurol*. 1992;31(2):138-46.
176. Fuerst D, Shah J, Shah A, Watson C. Hippocampal sclerosis is a progressive disorder: A longitudinal volumetric MRI study. *Annals of Neurology*. 2003;53(3):413-6.
177. Bernasconi N, Natsume J, Bernasconi A. Progression in temporal lobe epilepsy: differential atrophy in mesial temporal structures. *Neurology*. 2005;65(2):223-8.
178. Coan AC, Appenzeller S, Li LM, Cendes F. Seizure frequency and lateralization affect progression of atrophy in temporal lobe epilepsy. *Neurology*. 2009;73(11):834-42.
179. Bernhardt BC, Kim H, Bernasconi A, Bernasconi N. Subregional mesiotemporal patterns of disease progression in temporal lobe epilepsy. *Epilepsia*. 2013;54:11-2.

180. Pan JW, Vaughan JT, Kuzniecky RI, Pohost GM, Hetherington HP. High resolution neuroimaging at 4.1 T. *Magnetic resonance imaging*. 1995;13(7):915-21.
181. Na M, Liu YS, Shi C, Gao WP, Ge HT, Wang Y, et al. Prognostic value of CA4/DG volumetry with 3 T magnetic resonance imaging on postoperative outcome of epilepsy patients with dentate gyrus pathology. *Epilepsy Research*. 2014;108(8):1315-25.
182. Henry TR, Chupin M, Lehericy S, Strupp JP, Sikora MA, Sha ZY, et al. Hippocampal Sclerosis in Temporal Lobe Epilepsy: Findings at 7 T. *Radiology*. 2011;261(1):199-209.
183. Shrout PE, Fleiss JL. Intraclass Correlations - Uses in Assessing Rater Reliability. *Psychological bulletin*. 1979;86(2):420-8.
184. Dice LR. Measures of the Amount of Ecologic Association between Species. *Ecology*. 1945;26(3):297-302.
185. Fischl B. FreeSurfer. *Neuroimage*. 2012;62(2):774-81.
186. Jardim AP, Corso JT, Garcia MT, Gaca LB, Comper SM, Lancellotti CL, et al. Hippocampal atrophy on MRI is predictive of histopathological patterns and surgical prognosis in mesial temporal lobe epilepsy with hippocampal sclerosis. *Epilepsy Res*. 2016;128:169-75.
187. Bin Kim J, Suh SI, Kim JH. Volumetric and shape analysis of hippocampal subfields in unilateral mesial temporal lobe epilepsy with hippocampal atrophy. *Epilepsy Research*. 2015;117:74-81.
188. Schoene-Bake JC, Keller SS, Niehusmann P, Volmering E, Elger C, Deppe M, et al. In vivo mapping of hippocampal subfields in mesial temporal lobe epilepsy: relation to histopathology. *Hum Brain Mapp*. 2014;35(9):4718-28.
189. Van Leemput K, Bakkour A, Benner T, Wiggins G, Wald LL, Augustinack J, et al. Automated segmentation of hippocampal subfields from ultra-high resolution in vivo MRI. *Hippocampus*. 2009;19(6):549-57.
190. Yushkevich PA, Pluta JB, Wang H, Xie L, Ding SL, Gertje EC, et al. Automated volumetry and regional thickness analysis of hippocampal subfields

and medial temporal cortical structures in mild cognitive impairment. *Human brain mapping*. 2015;36(1):258-87.

191. Eugenio Iglesias J, Augustinack JC, Khoa N, Player CM, Player A, Wright M, et al. A computational atlas of the hippocampal formation using ex vivo, ultra-high resolution MRI: Application to adaptive segmentation of in vivo MRI. *NeuroImage*. 2015;115:117-37.

192. Sone D, Sato N, Maikusa N, Ota M, Sumida K, Yokoyama K, et al. Automated subfield volumetric analysis of hippocampus in temporal lobe epilepsy using high-resolution T2-weighted MR imaging. *Neuroimage Clin*. 2016;12:57-64.

193. Santyr BG, Goubran M, Lau JC, Kwan BYM, Salehi F, Lee DH, et al. Investigation of hippocampal substructures in focal temporal lobe epilepsy with and without hippocampal sclerosis at 7T. *J Magn Reson Imaging*. 2017;45(5):1359-70.

194. Staba RJ, Ekstrom AD, Suthana NA, Burggren A, Fried I, Engel J, Jr., et al. Gray matter loss correlates with mesial temporal lobe neuronal hyperexcitability inside the human seizure-onset zone. *Epilepsia*. 2012;53(1):25-34.

195. Hermann BP, Seidenberg M, Schoenfeld J, Davies K. Neuropsychological characteristics of the syndrome of mesial temporal lobe epilepsy. *Arch Neurol*. 1997;54(4):369-76.

196. Mueller SG, Laxer KD, Scanlon C, Garcia P, McMullen WJ, Loring DW, et al. Different structural correlates for verbal memory impairment in temporal lobe epilepsy with and without mesial temporal lobe sclerosis. *Human Brain Mapping*. 2012;33(2):489-99.

197. Das SR, Mechanic-Hamilton D, Pluta J, Korczykowski M, Detre JA, Yushkevich PA. Heterogeneity of functional activation during memory encoding across hippocampal subfields in temporal lobe epilepsy. *NeuroImage*. 2011;58(4):1121-30.

198. Kwan BYM, Salehi F, Ohorodnyk P, Lee DH, Burneo JG, Mirsattari SM, et al. Usage of SWI (susceptibility weighted imaging) acquired at 7 T for qualitative evaluation of temporal lobe epilepsy patients with histopathological and clinical correlation: An initial pilot study. *Journal of the Neurological Sciences*. 2016;369:82-7.

199. Goubran M, Crukley C, de Ribaupierre S, Peters TM, Khan AR. Image registration of ex-vivo MRI to sparsely sectioned histology of hippocampal and neocortical temporal lobe specimens. *NeuroImage*. 2013;83:770-81.
200. Stefanits H, Springer E, Patarraia E, Baumgartner C, Hainfellner JA, Prayer D, et al. Seven-Tesla MRI of Hippocampal Sclerosis An In Vivo Feasibility Study With Histological Correlations. *Investigative Radiology*. 2017;52(11):666-71.
201. Wieshmann UC, Symms MR, Mottershead JP, Macmanus DG, Barker GJ, Tofts PS, et al. Hippocampal layers on high resolution magnetic resonance images: real or imaginary? *Journal of anatomy*. 1999;195:131-5.
202. Adler DH, Pluta J, Kadivar S, Craige C, Gee JC, Avants BB, et al. Histology-derived volumetric annotation of the human hippocampal subfields in postmortem MRI. *NeuroImage*. 2014;84:505-23.
203. Coras R, Milesi G, Zucca I, Mastropietro A, Scotti A, Figini M, et al. 7T MRI features in control human hippocampus and hippocampal sclerosis: An ex vivo study with histologic correlations. *Epilepsia*. 2014;55:2003-16.
204. Chakeres DW, Whitaker CD, Dashner RA, Scharre DW, Beversdorf DQ, Raychaudhury A, et al. High-resolution 8 Tesla imaging of the formalin-fixed normal human hippocampus. *Clinical Anatomy*. 2005;18(2):88-91.
205. Fatterpekar GM, Naidich TP, Delman BN, Aguinaldo JG, Gultekin SH, Sherwood CC, et al. Cytoarchitecture of the human cerebral cortex: MR microscopy of excised specimens at 9.4 Tesla. *American Journal of Neuroradiology*. 2002;23:1313-21.
206. Augustinack JC, Helmer K, Huber KE, Kakunoori S, Zollei L, Fischl B. Direct visualization of the perforant pathway in the human brain with ex vivo diffusion tensor imaging. *Frontiers in Human Neuroscience*. 2010;4:42.
207. Shepherd TM, Ozarslan E, Yachnis AT, King MA, Blackband SJ. Diffusion tensor microscopy indicates the cytoarchitectural basis for diffusion anisotropy in the human hippocampus. *Ajnr: American Journal of Neuroradiology*. 2007;28(5):958-64.
208. Conturo TE, Lori NF, Cull TS, Akbudak E, Snyder AZ, Shimony JS, et al. Tracking neuronal fiber pathways in the living human brain. *Proc Natl Acad Sci U S A*. 1999;96(18):10422-7.

209. Augustinack JC, Huber KE, Stevens AA, Roy M, Frosch MP, van der Kouwe AJW, et al. Predicting the location of human perirhinal cortex, Brodmann's area 35, from MRI. *NeuroImage*. 2013;64:32-42.
210. Fischl B, Stevens AA, Rajendran N, Yeo BTT, Greve DN, Van Leemput K, et al. Predicting the location of entorhinal cortex from MRI. *NeuroImage*. 2009;47(1):8-17.
211. Augustinack JC, van der Kouwe AJW, Blackwell ML, Salat DH, Wiggins CJ, Frosch MP, et al. Detection of entorhinal layer II using tesla magnetic resonance imaging. *Annals of Neurology*. 2005;57(4):489-94.
212. Adler DH, Wisse LEM, Ittyerah R, Pluta JB, Ding SL, Xie L, et al. Characterizing the human hippocampus in aging and Alzheimer's disease using a computational atlas derived from ex vivo MRI and histology. *Proc Natl Acad Sci U S A*. 2018;115(16):4252-7.
213. Yushkevich PA, Avants BB, Pluta J, Das S, Minkoff D, Mechanic-Hamilton D, et al. A high-resolution computational atlas of the human hippocampus from postmortem magnetic resonance imaging at 9.4 T. *NeuroImage*. 2009;44:385-98.
214. Wisse LEM, Adler DH, Ittyerah R, Pluta JB, Robinson JL, Schuck T, et al. Comparison of In Vivo and Ex Vivo MRI of the Human Hippocampal Formation in the Same Subjects. *Cerebral Cortex*. 2017;27(11):5185-96.
215. Modo M, Hitchens TK, Liu JR, Richardson RM. Detection of aberrant hippocampal mossy fiber connections: Ex vivo mesoscale diffusion MRI and microtractography with histological validation in a patient with uncontrolled temporal lobe epilepsy. *Hum Brain Mapp*. 2016;37(2):780-95.
216. Thivard L, Lehericy S, Krainik A, Adam C, Dormont D, Chiras J, et al. Diffusion tensor imaging in medial temporal lobe epilepsy with hippocampal sclerosis. *Neuroimage*. 2005;28(3):682-90.
217. Thom M, Sisodiya S, Najm I. Neuropathology of epilepsy. In: Love S, Louis DN, Ellison DW, editors. *Greenfield's Neuropathology*. 8 ed: Hodder Arnold, London; 2008. p. 833-87.
218. Cascino GD. Clinical correlations with hippocampal atrophy. *Magnetic resonance imaging*. 1995;13(8):1133-6.

219. Dam AM. Epilepsy and neuron loss in the hippocampus. *Epilepsia*. 1980;21(6):617-29.
220. Thom M, Zhou J, Martinian L, Sisodiya S. Quantitative post-mortem study of the hippocampus in chronic epilepsy: seizures do not inevitably cause neuronal loss. *Brain*. 2005;128:1344-57.
221. Babb TL, Brown WJ, Pretorius J, Davenport C, Lieb JP, Crandall PH. Temporal lobe volumetric cell densities in temporal lobe epilepsy. *Epilepsia*. 1984;25(6):729-40.
222. Wieser HG. ILAE Commission Report. Mesial temporal lobe epilepsy with hippocampal sclerosis. *Epilepsia*. 2004;45(6):695-714.
223. Andrioli A, Alonso-Nanclares L, Arellano JI, DeFelipe J. Quantitative analysis of parvalbumin-immunoreactive cells in the human epileptic hippocampus. *Neuroscience*. 2007;149(1):131-43.
224. Moher D, Liberati A, Tetzlaff J, Altman DG, Prisma G. Preferred reporting items for systematic reviews and meta-analyses: the PRISMA statement. *PLoS Medicine / Public Library of Science*. 2009;6(7):e1000097.
225. Sterne JAC, Harris RJ, Harbord RM, Steichen TJ. User-written packages for meta-analysis in Stata; <http://www.stata.com/support/faqs/statistics/meta-analysis>. 2011. p. 2.
226. Higgins JP, Thompson SG. Quantifying heterogeneity in a meta-analysis. *Statistics in medicine*. 2002;21(11):1539-58.
227. RevMan. Review Manager; 2012.
228. Foldvary N, Lee N, Hanson MW, Coleman RE, Hulette CM, Friedman AH, et al. Correlation of hippocampal neuronal density and FDG-PET in mesial temporal lobe epilepsy. *Epilepsia*. 1999;40(1):26-9.
229. Mathern GW, Kuhlman PA, Mendoza D, Pretorius JK. Human fascia dentata anatomy and hippocampal neuron densities differ depending on the epileptic syndrome and age at first seizure. *Journal of Neuropathology & Experimental Neurology*. 1997;56(2):199-212.
230. Blumcke I, Beck H, Nitsch R, Eickhoff C, Scheffler B, Celio MR, et al. Preservation of calretinin-immunoreactive neurons in the hippocampus of

- epilepsy patients with Ammon's horn sclerosis. *Journal of Neuropathology & Experimental Neurology*. 1996;55(3):329-41.
231. West MJ, Gundersen HJ. Unbiased stereological estimation of the number of neurons in the human hippocampus. *Journal of Comparative Neurology*. 1990;296(1):1-22.
232. van Strien NM, Wideroe M, van de Berg WDJ, Uylings HBM. Imaging hippocampal subregions with in vivo MRI: advances and limitations. *Nature Reviews Neuroscience*. 2012;13:70.
233. Abercrombi M. The density of neurones in the human hippocampus. *Anat Rec*. 1946;94:239-47.
234. Dam AM. The Density of Neurons in the Human Hippocampus. *Neuropathology and applied neurobiology*. 1979;5:249-64.
235. Steve TA, Jirsch JD, Gross DW. Quantification of subfield pathology in hippocampal sclerosis: a systematic review and meta-analysis. *Epilepsy Res*. 2014;108(8):1279-85.
236. Mueller SG, Stables L, Du AT, Schuff N, Truran D, Cashdollar N, et al. Measurement of hippocampal subfields and age-related changes with high resolution MRI at 4T. *Neurobiology of aging*. 2007;28:719-26.
237. Steve TA, Yasuda CL, Coras R, Lail M, Blumcke I, Livy DJ, et al. Development of a histologically validated segmentation protocol for the hippocampal body. *Neuroimage*. 2017;157:219-32.
238. Blumcke I, Sarnat HB, Coras R. *Surgical neuropathology of focal epilepsies*. Montrouge, France: John Libbey Eurotext; 2015.
239. Bronen RA, Cheung G, Charles JT, Kim JH, Spencer DD, Spencer SS, et al. Imaging findings in hippocampal sclerosis: correlation with pathology. *Ajnr: American Journal of Neuroradiology*. 1991;12(5):933-40.
240. Cascino GD, Jack CR, Jr., Parisi JE, Sharbrough FW, Hirschorn KA, Meyer FB, et al. Magnetic resonance imaging-based volume studies in temporal lobe epilepsy: pathological correlations. *Annals of Neurology*. 1991;30(1):31-6.
241. Lencz T, McCarthy G, Bronen RA, Scott TM, Inserni JA, Sass KJ, et al. Quantitative magnetic resonance imaging in temporal lobe epilepsy:

- relationship to neuropathology and neuropsychological function. *Annals of Neurology*. 1992;31(6):629-37.
242. Lee N, Tien RD, Lewis DV, Friedman AH, Felsberg GJ, Crain B, et al. Fast spin-echo, magnetic resonance imaging-measured hippocampal volume: correlation with neuronal density in anterior temporal lobectomy patients. *Epilepsia*. 1995;36:899-904.
243. Bouchet C, Cazauvieilh. *Epilepsie et l'alienation mentale*. *Arch Gen Med*. 1825;9:510.
244. Braak H, Braak E. Neuropathological staging of Alzheimer-related changes. *Acta Neuropathologica*. 1991;82(4):239-59.
245. Bartsch T, Doehring J, Rohr A, Jansen O, Deuschl G. CA1 neurons in the human hippocampus are critical for autobiographical memory, mental time travel, and auto-noetic consciousness. *Proceedings of the National Academy of Sciences of the United States of America*. 2011;108(42):17562-7.
246. Braak H, Alafuzoff I, Arzberger T, Kretschmar H, Del Tredici K. Staging of Alzheimer disease-associated neurofibrillary pathology using paraffin sections and immunocytochemistry. *Acta Neuropathologica*. 2006;112(4):389-404.
247. West MJ, Coleman PD, Flood DG, Troncoso JC. Differences in the Pattern of Hippocampal Neuronal Loss in Normal Aging and Alzheimer's Disease. *Lancet*. 1994;344(8925):769-72.
248. Thal DR, Holzer M, Rub U, Waldmann G, Gunzel S, Zedlick D, et al. Alzheimer-related tau-pathology in the perforant path target zone and in the hippocampal stratum oriens and radiatum correlates with onset and degree of dementia. *Experimental neurology*. 2000;163(1):98-110.
249. Jack CR, Jr., Knopman DS, Jagust WJ, Shaw LM, Aisen PS, Weiner MW, et al. Hypothetical model of dynamic biomarkers of the Alzheimer's pathological cascade. *Lancet Neurology*. 2010;9(1):119-28.
250. La Joie R, Fouquet M, Mézenge F, Landeau B, Villain N, Mevel K, et al. Differential effect of age on hippocampal subfields assessed using a new high-resolution 3T MR sequence. *NeuroImage*. 2010;53:506-14.

251. Wang L, Swank JS, Glick IE, Gado MH, Miller MI, Morris JC, et al. Changes in hippocampal volume and shape across time distinguish dementia of the Alzheimer type from healthy aging. *NeuroImage*. 2003;20:667-82.
252. Kerchner GA, Deutsch GK, Zeineh M, Dougherty RF, Saranathan M, Rutt BK. Hippocampal CA1 apical neuropil atrophy and memory performance in Alzheimer's disease. *NeuroImage*. 2012;63(1):194-202.
253. Winterburn JL, Pruessner JC, Chavez S, Schira MM, Lobaugh NJ, Voineskos AN, et al. A novel in vivo atlas of human hippocampal subfields using high-resolution 3T magnetic resonance imaging. *NeuroImage*. 2013;74:254-65.
254. Wisse LEM, Gerritsen L, Zwanenburg JJM, Kuijf HJ, Luijten PR, Biessels GJ, et al. Subfields of the hippocampal formation at 7T MRI: In vivo volumetric assessment. *NeuroImage*. 2012;61:1043-9.
255. Yushkevich PA, Wang H, Pluta J, Das SR, Craige C, Avants BB, et al. Nearly automatic segmentation of hippocampal subfields in in vivo focal T2-weighted MRI. *NeuroImage*. 2010;53:1208-24.
256. Malykhin NV, Lebel RM, Coupland NJ, Wilman AH, Carter R. In vivo quantification of hippocampal subfields using 4.7 T fast spin echo imaging. *NeuroImage*. 2010;49:1224-30.
257. Yushkevich PA, Amaral RSC, Augustinack JC, Bender AR, Bernstein JD, Boccardi M, et al. Quantitative comparison of 21 protocols for labeling hippocampal subfields and parahippocampal subregions in in vivo MRI: Towards a harmonized segmentation protocol. *NeuroImage*. 2015;111:526-41.
258. Poppenk J, Evensmoen HR, Moscovitch M, Nadel L. Long-axis specialization of the human hippocampus. *Trends in cognitive sciences*. 2013;17(5):230-40.
259. Schneider CA, Rasband WS, Eliceiri KW. NIH Image to ImageJ: 25 years of image analysis. *Nature Methods*. 2012;9(7):671-5.
260. Bland JM, Altman DG. Statistical methods for assessing agreement between two methods of clinical measurement. *Lancet*. 1986;1(8476):307-10.
261. Ding S-L, Van Hoesen GW. Organization and detailed parcellation of human hippocampal head and body regions based on a combined analysis of

- Cyto- and chemoarchitecture. *Journal of Comparative Neurology*. 2015;523(15):2233-53.
262. Ding S-L. Comparative Anatomy of the Prosubiculum, Subiculum, Presubiculum, Postsubiculum, and Parasubiculum in Human, Monkey, and Rodent. *Journal of Comparative Neurology*. 2013;521(18):4145-62.
263. Bruton CJ. *The neuropathology of temporal lobe epilepsy*: Oxford University Press; 1988.
264. Wisse LEM, Daugherty AM, Olsen RK, Berron D, Carr VA, Stark CEL, et al. A harmonized segmentation protocol for hippocampal and parahippocampal subregions: Why do we need one and what are the key goals? *Hippocampus*. 2017;27(1):3-11.
265. Malykhin NV, Bouchard TP, Ogilvie CJ, Coupland NJ, Seres P, Camicioli R. Three-dimensional volumetric analysis and reconstruction of amygdala and hippocampal head, body and tail. *Psychiatry research*. 2007;155(2):155-65.
266. Bronen RA, Fulbright RK, Kim JH, Spencer SS, Spencer DD, al-Rodhan NR. Regional distribution of MR findings in hippocampal sclerosis. *Ajnr: American Journal of Neuroradiology*. 1995;16(6):1193-200.
267. Bernhardt BC, Bernasconi A, Liu M, Hong S-J, Caldairou B, Goubran M, et al. The spectrum of structural and functional imaging abnormalities in temporal lobe epilepsy. *Annals of Neurology*. 2016:1-12.
268. Fischl B, Rajendran N, Busa E, Augustinack J, Hinds O, Yeo BT, et al. Cortical folding patterns and predicting cytoarchitecture. *Cereb Cortex*. 2008;18(8):1973-80.